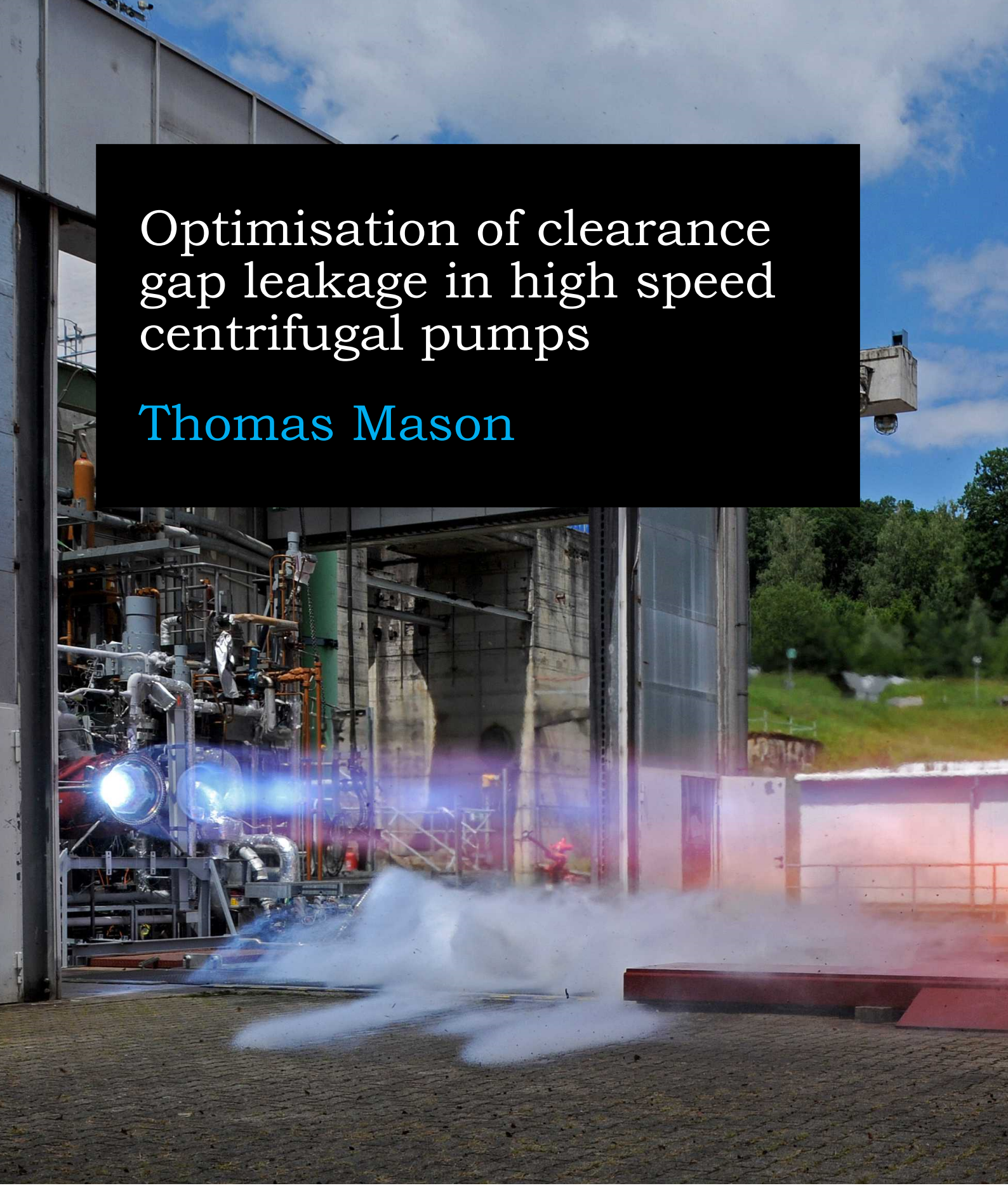

Optimisation of clearance gap leakage in high speed centrifugal pumps

Thomas Mason

TU Delft Delft University of Technology

Cover image taken from www.dlr.de

Optimisation of clearance gap leakage in high speed centrifugal pumps

A multi-model approach to the development of the DLR LUMEN fuel turbopump impeller

For the degree of Master of Science in Space Engineering at Delft University of Technology

Thomas Mason
The Netherlands
24/05/2019

Preface

This thesis was completed as partial fulfilment of a Master of Science in Aerospace Engineering at the Delft University of Technology, The Netherlands. The work detailed here was completed at the Space Propulsion Institute of the Deutsches Zentrum für Luft- und Raumfahrt e.V. in Lampoldshausen, Germany. All fluid visualisation figures were produced using Ansys CFD Post unless noted otherwise.

Acknowledgements

Firstly I would like to thanks my thesis supervisors Assistant Professor Angelo Cervone (TU Delft) and Tobias Traudt (DLR) for their guidance throughout the thesis. I would also like to thank my fellow students at the DLR Lampoldshausen and the TU Delft for the welcome distractions and sharing a passion for rocketry as well as the people of The Netherlands and Germany for welcoming a foreigner with open arms. Lastly, I am endlessly grateful for the support and encouragement I received from my parents, family and friends back in Australia.

T. Mason
15/05/2019
Heilbronn, Germany

Summary

High performance liquid rocket engines utilise complex turbomachinery to convert low pressure stored propellants into high pressure working fluids required to operate powerful and efficient launch vehicles. The emergence of small scale microlaunchers is pushing the limits of mass saving and by association the limits of turbomachinery in these applications. The Liquid Upper-stage deMonstrator ENgine (LUMEN), is being developed by the Deutsches Zentrum für Luft- und Raumfahrt e.V. (DLR) to showcase capabilities in rocket engine design and innovation. This thesis analyses the proposed LUMEN fuel pump impeller design with a focus on reducing the clearance gap leakage and optimising cavitation performance with the aim of developing both the tools for further optimisation of the engine efficiency and a series of recommendations for changes to the current proposed design. This was completed using a preliminary centrifugal pump design and analysis tool developed by Gülich [1] and two numerical models generated using the commercial modelling software Ansys CFX [2]. The preliminary design tool was optimised and validated against a series of experimental test results and found to predict the mass flowrate through a liquid annular seal to within ±5% for the test data closest to the LUMEN operating envelope and within ±15% for all cases. This was deemed adequate for the intended purpose of preliminary design comparison. A reduced numerical model was then generated for comparison and predicted the mass flowrate to within ±10% of the preliminary design tool estimate and revealed several complex flow features including low pressures at the seal outlet that are likely to result in cavitation. Several alternative seal designs were assessed with this model and a multi z-step seal produced the best performance with an approximately 20% improvement in the estimated pump total leakage which corresponds to a 2.9% increase in pump volumetric efficiency. The manufacturing limitations on seal surface roughness and corner radius were also assess and found to severely limit the potential for further optimisation of the seal design. A complete pump numerical model was then used to assess the flow interactions between the impeller, volute and pump inlet that the reduced model did not simulate. Asymmetric flow features were produced by the volute tongue that extended into the clearance gaps and impacted on the local pressure and leakage flow through the seals. Low pump load cases revealed large recirculation regions at the pump inlet that were heavily influenced by the leakage flow re-entry flowrate and geometry. An alternative pump geometry based on the reduced numerical model results was modelled and estimated a total leakage of 12.6% of the nominal total pump massflow, an increase in pump volumetric efficiency of 1.2% over the baseline seal design. The full pump simulations also revealed the limitation of the steady state model being used as many features appear to be transient in nature such as the fluctuations caused by blade position. Lastly an investigation into the potential for cavitation within the proposed pump impeller design was completed using the preliminary design tool and unsuccessfully attempted with the numerical model. A number of proposed changes to the current impeller design as well as recommendations for future work are presented as a result of these findings.

Contents

List of Figures

List of Tables

Nomenclature

Symbol	Description	Symbol	Description
α	Thermal diffusivity	F_L	Liquid volume fraction
β	Local blade angle	g	Gravitational acceleration
β_f	Brennen correction factor	H	Head
$\dot{m}_{fg}$	Phase change mass flow	H_{sp}	Head drop through seal
$\dot{Q}$	Volumetric flowrate	H_v	Latent heat of vapourisation
$\dot{Q}_{sp}$	Leakage volumetric flowrate	I_{sp}	Specific impulse
$\dot{Q}_E$	Balance hole flowrate	L_{sp}	Seal Length
$\dot{Q}_h$	Auxiliary function flowrate	m_f	final vehicle mass
ϵ	Equivalent sand grain roughness	m_o	initial vehicle mass
η	Efficiency	n	Rotation rate
γ	Surface tension coefficient	n_q	Pump specific speed
λ	Power coefficient	NPSH	Net positive suction head
λ_c	Inlet cavitation coefficient	p	Pressure
λ_d	Hub to tip diameter ratio	P	Power
λ_f	Friction coefficient	p_g	Included gas bubble pressure
λ_w	Blade cavitation coefficient	P_u	Useful power
ν	Kinematic viscosity	p_v	Vapour pressure
Ω	Rotation rate in RPM	Pr	Prandtl number
ϕ	Flow coefficient	R	Bubble radius
ψ	Head coefficient	R_{nuc}	Nucleation site radius
ρ	Density	R_o	Included gas bubble radius
σ	Cavitation number	r_T	Impeller tip radius
Σ	Thermal effect parameter	Re	Reynolds number
ζ_{EA}	Loss coefficient (seals)	Re_u	Circumferential Reynolds number
a	Blade incidence angle	s	Seal width
a_f	Gülich correction factor	t	time
b	Blade width	T	Bulk flow temperature
c	Absolute velocity	T_b	Bubble temperature
c_{ax}	Axial velocity	t_R	Relative blade thickness
C_p	Specific heat at constant pressure	u	Circumferential velocity
d	Diameter	v	Vehicle velocity
d_H	Hydraulic diameter	w	Local flow velocity
d_n	Shaft diameter	X	Experimental cavitation factor
F_{nuc}	Nucleation site volume fraction	z_{st}	Number of pump stages

1

Introduction

The ongoing reduction in cost and size of complex engineering systems is driving a revolution in the demand for reliable, cheap and targeted access to space. From governments to universities and research institutes there are numerous teams developing small satellite projects for purposes such as Earth observation, communications and space exploration. Smaller launch vehicles, termed microlaunchers are being developed to service this demand and require high performance, reliable engines in order to be successful in a competitive market. Liquid propellants are often chosen for their inherently high efficiency, high performance and ability to be throttled and re-ignited. The capability of any rocket is typically described using the Tsiolkovsky rocket equation (shown below as Equation 1.1) which demonstrates that both the engine performance in the form of the specific impulse (I_{sp}) and the launch vehicle initial to final mass ratio (m_0/m_f) have a direct influence on the generation of the rocket output: Δv.

$$\Delta v = I_{sp}\ g\ ln\left(\frac{m_0}{m_f}\right) \tag{1.1}$$

The replacement of heavy, high pressure propellant tanks with a pump assembly that can generate a high propellant pressure prior to injection into the combustion chamber is a common method of increasing the mass ratio and overall rocket performance. Gas generators or regenerative cooling systems are typically employed to provide a high energy fluid for powering a turbine which then drives a shaft or gear linked pump impeller. The complexity and inter-related nature of these propellant pumping systems requires a detailed and iterative approach to design and a robust understanding of all elements that impact on performance from combustion efficiency to impeller leakage losses and cavitation. The Liquid Upper stage deMonstrator ENgine (LUMEN) is a liquid oxygen(LOx)/liquefied natural gas (LNG) rocket engine being developed at the Space Propulsion Institute of the German Aerospace Centre -Lampoldshausen (Deutsches Zentrum für Luft- und Raumfahrt e.V. - DLR) to showcase the capabilities of the institute to the emerging microlauncher market and drive innovation in the design and testing of microlauncher engines. This thesis aims to contribute to the LUMEN project by continuing the development and verification of a preliminary turbopump design tool to ensure an accurate prediction of the major losses in the proposed design and provide guidance for the continued development of the pump through

improvement recommendations based on further detailed numerical modelling of the same pump.

1.1 Thesis Motivation

Successful optimisation of any engineered system requires either a reliable model or a series of testing and design iterations but generally involves both. With the advent of modern computing the use of iterative testing has declined and component and system design are now completed largely with computer models. This allows for the assessment of proposed changes to be made without committing to significant manufacturing and testing costs but increases the consequences of using a low quality model. The complexity of rocket engines and their extreme operating conditions has proven challenging and time-consuming even for the most advanced numerical modelling tools [3]. There exists a vast array of research describing the performance of launch vehicle turbopumps using empirical equations and correlations. Primarily developed during the Apollo and Space Shuttle programs these have almost entirely been replaced with modern numerical models. Although incapable of characterising some of the more complex pump phenomena these tools were used to assess, compare and optimise general pump parameters for some of the most successful rocket programs in history. A tool has been developed based on these empirical equations that allows the rapid characterisation and iteration of preliminary design changes for the DLR LUMEN engine. However, before it can be relied upon this tool must be verified and its performance compared to more sophisticated modelling tools. This not only provides a measure of the tool's accuracy but also a clear representation of any flow features that the empirical tool cannot model.

Leakage losses and cavitation are two of the biggest contributors to the erosion of theoretical peak performance of a centrifugal rocket pump [4]. Leakage refers to the proportion of the pumped fluid that does not exit the impeller through the volute but instead flows through the impeller shroud-to-housing gaps and re-enters the main flow at the pump inlet or is dumped from the system entirely. As this leakage flow passes through the impeller blade channel energy is consumed to increase its total pressure however the leakage flow does no useful work and this energy is lost, directly reducing pump efficiency. This leakage can also impact on the pump inlet flow when exiting the clearance gap, as well as directly influencing the impeller stability by generating asymmetric forces on the impeller shroud and hub. These effects are not well documented in the literature for the extreme operating conditions of a rocket pump with a cryogenic working fluid making this a novel area of research. The dynamic, unstable and potentially damaging nature of cavitation has made it the subject of extensive research for over 100 years. The characterisation of cavitation within a pump is often treated in isolation due to its complexity and computationally demanding nature and so much of the literature on this topic relates to pumping water rather than the more complex cryogenic fluids used in modern rocket engines. Simplified test cases such as a venturi nozzle are also extensively used as simplified substitutes for full pump cryogenic cavitation modelling. Additionally the limited cases of liquid Methane cavitation modelling adds to the novel challenge of the LUMEN application.

A high efficiency, low cost and reliable rocket engine has the potential to open

up new possibilities for improvements in quality of life, assist our care of the planet and provide a better understanding of the universe around us. This thesis is intended to be a small step towards achieving these goals.

1.2 Research Goals and Scope

The core outcome of this thesis is a contribution to the development and understanding of a small scale European launch vehicle by progressing the design of the LUMEN fuel pump impeller through detailed modelling of the major performance losses. The thesis motivation outlined above has lead to a number of research objectives being formulated to provide some guidance and limit the scope of the research project. These are:

1. Incorporate advanced loss models into a preliminary centrifugal pump design tool and optimise it for liquid rocket engine applications through analysis of the existing literature.

2. Verify the accuracy of this preliminary design tool by comparison to a commercially available software package and/or relevant available experimental test data.

3. Utilise the various models to analyse losses and recommend potential improvements to the existing pump design.

4. Investigate the potential for prediction of cavitation performance within both the preliminary and numerical models.

Meeting the main goals of this thesis will give future designers as well as the current LUMEN team the tools to confidently model a key mechanism of performance degradation at the preliminary design stage. The evaluation of potential design improvements will also provide a guideline for anyone seeking to reduce these losses and optimise a rocket turbopump impeller without requiring a costly testing campaign.

To limit the possibilities for continued optimisation, innovation and development of both the preliminary design tool and the pump clearance gaps themselves a number of targets were established. For the purpose of validating the preliminary design tool an error of ±10% in the estimation of the most relevant experimental leakage massflow data was selected as this is adequate for the preliminary nature of the tool. Additionally a difference of ±10% between the seal massflow leakage predicted by the preliminary tool and the numerical models was targeted to give confidence that the two models were capable of reflecting the same design changes. The targeted leakage performance from more complex seal designs was set at a 20% improvement over the nominal baseline design to justify the increased manufacturing costs as well as remain within the possible improvements established by past research ([5], [6]). As the LUMEN pump seal designs had not been investigated in detail it was deemed more appropriate to quantify the potential impact of all avenues of optimisation rather than simply seeking the highest performance design.

1.2.1 Assumptions and Omissions

To limit the scope of the thesis a number of simplifying assumptions and omissions have been made and are briefly outlined here.

1. Operational Transients
   The ignition and cool-down sequence of a rocket engine is a complex and important design consideration, particularly for one that must be restarted without significant maintenance or overhaul such as this. However this project is seeking to optimise performance at the best efficiency point and so these transients are secondary considerations and have been neglected.

2. Fluid Structure Interactions
   The impact of changes to the current design on the rotordynamics and rotational stability of the turbopump will not be considered in detail. This is an extensive area of ongoing research and a future project is planned at the DLR to fully characterise the rotordynamic stability of the LUMEN engine.

3. Other Pump Components
   Pump components such as the collector, volute and inlet pipe will only be considered where they directly influence the flow features within and around the impeller. Any losses or flow features resulting from mechanical linkages, noise and vibration are neglected.

1.3 Thesis Outline

This thesis begins with an overview of the background information relevant to understanding the remainder of the thesis including the design of centrifugal pumps, prediction of their performance and the losses that contribute to the degradation of this performance. A brief overview of the LUMEN engine and its specific challenges is also given in Chapter 2. Following this, the preliminary analytical pump design and performance prediction tool is described in Chapter 3 and then validated against experimental test data in Chapter 4. The development of a reduced numerical model for comparison to the preliminary design tool is described in Chapter 5 and then used to asses a number of potential changes to the proposed baseline annular seal design in Chapter 6 in an attempt to address the key performance loss of clearance gap leakage. The impact of manufacturing limitations is also analysed with this model. A further exploration of other potential design improvements outside the annular seal is given in Chapter 7. A full pump numerical model is also developed to assess the impact of geometric asymmetries and their impact on the leakage flows through the pump. This is also compared to a proposed alternative seal design to provide an indication of the potential for efficiency improvements and is presented in Chapter 8 along the the comparison results. Lastly, an assessment of the likelihood and impact of cavitation within the pump is presented in Chapter 9 beginning with a brief literature study on cavitation, followed by a prediction using empirical equations. An unsuccessful attempt to implement cavitation modelling into the complete pump numerical simulations is also described before the general conclusions and recommendations for changes and future work are drawn in Chapter 10.

2

Centrifugal Pumps

The first machine that could be considered as a prototype centrifugal pump was designed for a mud and water lifting application in 1475 by Francesco di Giogio Martini. This was followed by a straight vaned device closer to true modern centrifugal pumps in the late 17th century and was developed by Denis Papin [7]. Since then pump designs and performance have improved and are now estimated to account for approximately 10% of global electrical energy consumption each year [8] and are the pump of choice for many liquid rocket engines in operation today.

Rocket pumps are typically smaller than industrial equivalents and operate at increased rotation rates to allow for a higher mass flow and greater pressure differential. These higher pump outlet pressures allow for higher combustion pressures which is desirable for maximum thrust generation, making centrifugal pumps the obvious choice for rocketry applications [9]. In a liquid rocket engine the working fluid (propellant) enters the impeller inlet from the storage tanks and is accelerated over the leading edge of the rotating impeller blades. Driving energy, typically supplied by a shaft or gear linked turbine is imparted by the impeller and converted to kinetic energy and pressure within the working fluid. At the blade trailing edge the flow leaves the impeller and is trapped by the collector spiral, converting the high velocity flow into a higher pressure low velocity fluid through free diffusion of kinetic energy. Part of the blade outlet flow leaks through the hub and shroud clearance gaps, returning to the pump inlet or being dumped to a low pressure part of the engine. The fluid within the collector eventually works its way around the spiral to the volute entry where the flow is expanded to further increase the static pressure before reaching the pump outlet [10]. From the outlet, the working fluid is typically passed through the cooling channels of a rocket nozzle or injected into the combustion chamber, or a combination of both [11]. Figure 2.1a below is a cross section of a typical centrifugal pump with the key elements labelled alongside Figure 2.1b which displays the key dimensions that will be referenced throughout this document.

2.1 Performance Evaluation

Rocket turbopumps are interlinked with all other components of the rocket engine that they must be designed simultaneously and this can greatly restrict the available options for pump design along with the general limitations on mass and size.

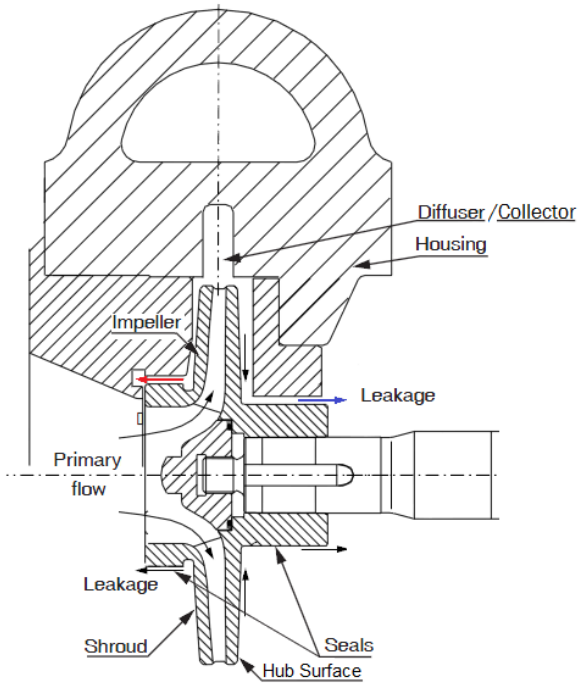

(a) A high speed centrifugal pump with the main components and flow paths labelled. The unlabelled top cavity is the spiral volute and pump outlet. Image adapted from Storteig [12].

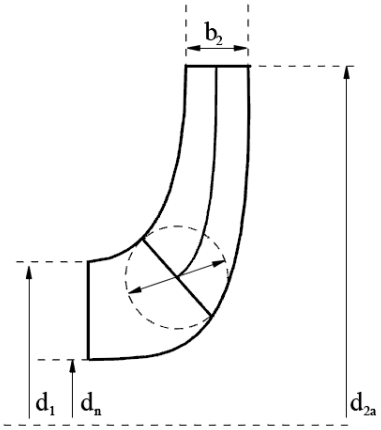

(b) Key meridional dimensions for the definition of an impeller blade channel.

Figure 2.1

However, within these constraints a designer targets certain parameters such as peak output pressure, peak efficiency or minimal chance of cavitation and therefore a method of quantifying these parameters is needed. Equations from the book *Centrfiugal Pumps* by J.F. Gülich are used for this purpose throughout this thesis [1]. Most pumps target high efficiency which can be defined as the ratio of useful power transferred to the working fluid, to the power supplied by the turbine and is shown as Equation 2.1 below. In this equation P_u is the power input to the working fluid via the impeller which is calculated from the difference in total pressure over the impeller multiplied by the volumetric flowrate Q and P is the sum of all energy including the power lost to noise, leakage, friction, recirculation and all other avenues that do not contribute to an increase in pump outlet pressure.

$$\eta = \frac{P_u}{P} = \frac{\dot{Q}(p_{out,tot} - p_{in,tot})}{P} \tag{2.1}$$

Pump engineers also use a variety of performance based coefficients to compare operating points or design options. The most common of these are the flow coefficient (ϕ_x), shown as Equation 2.2, the head coefficient (ψ) as Equation 2.3 and the power coefficient (λ) as Equation 2.4. The flow coefficient is used to describe the influence of the flowrate on other performance parameters and is a simple ratio between the meridional component of absolute velocity (c_m) and the circumferential velocity (u) at the same location. The meridional velocity can also be replaced with a function of volumetric flowrate $\dot{Q}$, location blade diameter (d) and width (b) which makes its relation to the flowrate somewhat more obvious.

$$\phi_x = \frac{c_{x,m}}{u_x} = \frac{\dot{Q}}{\pi d_x b_x u_x} \tag{2.2}$$

The head coefficient is a normalisation of the generated head ($H = \triangle P/\rho g$) with the dynamic pressure at the impeller outlet ($0.5\rho u_2^2$). This coefficient primarily describes the response in generated pump head to changes in the impeller rotation rate and is a key parameter for comparing pump performance.

$$\psi = \frac{2Hg}{u_2^2} \tag{2.3}$$

The power coefficient is a similar normalisation of the power transferred to the working fluid by dividing the calculated power by a function of impeller outlet geometry and velocity. Comparisons of the required power to generate a given head or flowrate utilise this coefficient. In this equation z_{st} is the number of pump stages which is 1 in the LUMEN case.

$$\lambda = \frac{2P}{\rho z_{st} \pi d_2 b_2 u_2^3} \tag{2.4}$$

The pump volumetric efficiency (η_v) which represents the percentage of the working fluid flow through the impeller that is ultimately output from the pump, is of particular interest to this thesis because it captures the influence of leakage in a simple and clear manner. This is calculated using Equation 2.5 where $\dot{Q}$ is the pump outlet flow, $\dot{Q}_{sp}$ is the leakage flow through the annular seals, $\dot{Q}_E$ is the leakage through the balance holes and $\dot{Q}_h$ is the flow rate used for auxiliary purposes. For the LUMEN case only the annular seal leakage must be considered as there are no balance holes and no auxiliary functions utilising leakage flow.

$$\eta_v = \frac{\dot{Q}}{\dot{Q} + \dot{Q}_{sp} + \dot{Q}_E + \dot{Q}_h} \tag{2.5}$$

Although designed for a clearly defined operating envelope rocket engines and their turbopumps are generally less efficient than an industrial equivalent as shown by Campbell in Figure 2.2 below where the peak efficiency of all rocket turbopumps considered is below 80%. Industrial pumps reach a peak efficiency above 90% and do so at greater specific speeds. The specific speed noted here refers to Equation 2.6 where the flowrate $\dot{Q}$ is in m^3/s, the developed pump head H is in m and n is in radians/s when SI units are used however n is typically included in RPM for simplicity. Most microlauncher turbopumps operate in the lower end of the specific speed range and therefore achieve an associated lower efficiency. A comparison of real rocket turbopumps and their integrated assemblies is reproduced from Campbell in Appendix A.

$$n_q = n\frac{\sqrt{\dot{Q}}}{H^{0.75}} \tag{2.6}$$

2.2 Losses

With the given engine requirements and a target for the key performance parameters, it is then up to the responsible engineer to identify, quantify and minimise

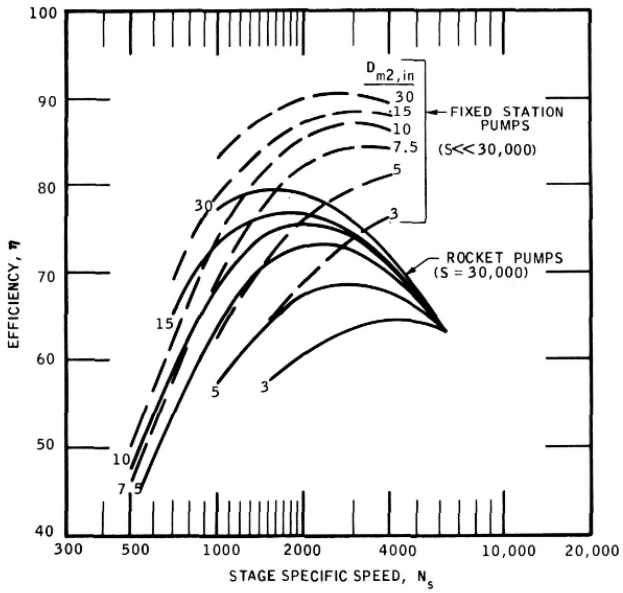

Figure 2.2: Comparison between typical rocket pumps and fixed industrial equivalents. Note specific speed here is calculated with US imperial units of GPM, ft and RPM. Image taken from Campbell [13].

losses to an acceptable threshold. Extensive research has been done on characterising the key losses for all types of centrifugal pumps and Figure 2.3 shows the relative magnitude of the losses as described by Gülich [1]. While authors such as Gülich and Stepanoff [14] attempt to determine the impact of the major losses, Denton [15] has compiled a document detailing the physical origin of the major losses and provides some insights into countering them while Bowerman and Acosta [16] used an experimental test campaign to isolated the key loses. While not an exhaustive list, the expected high losses for a fully shrouded high speed centrifugal pump are presented in further detail below.

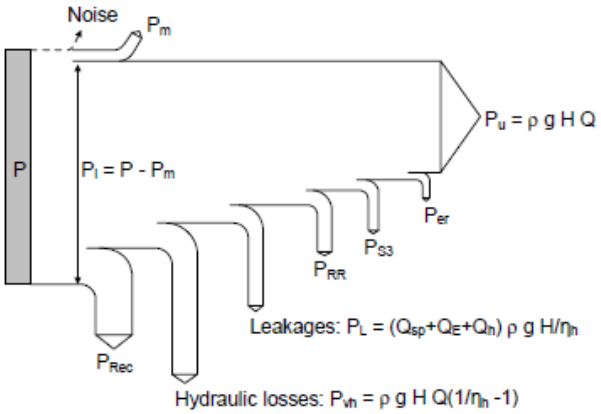

Figure 2.3: A representation of the main contributors to performance losses within a typical centrifugal pump, indicated as additional power required.

2.2.1 Disc Friction Losses

The friction forces on a disk rotating in a viscous medium has been the subject of fluid dynamics research for many years (Gülich [17], Juckelandt et al. [18] and Kurokawa et al. [19] are just three examples of relatively recent work in the field). The interaction of a rotating disk enclosed in a fluid as well as the interaction of the fluid with the stationary casing depends on a number of parameters such as Reynolds number, surface roughness, separation distance, passing flow rate and the development of the associated boundary layers and these can all influence the overall efficiency of the turbopump. As the manufacturing process and materials, size, rotational rate, working fluid and operating temperature of the LUMEN pump are largely fixed the opportunity to reduce friction losses is limited. Fortunately the proposed LUMEN turbine design is expected to be capable of providing much more power than the pump requires and therefore overcoming high disc friction will not be a concern. However the friction generated within the annular seals alters the flow through the seal and can therefore impact on other loss mechanisms, particularly cavitation. Friction losses are noted as P_{RR} in Figure 2.3.

2.2.2 Hydraulic Losses

As the working fluid moves through a centrifugal pump is is subject to expansion, contraction, mixing and other non-uniform forces that all promote an exchange of momentum between flow streamlines that convert the flow energy into turbulence. This turbulence cascades and eventually dissipates into heat, resulting in a net loss of useful pump head and eroding performance. The flow conditions at the pump inlet such as pre-rotation, inlet boundary layers, recirculation, leakage flow re-injection and cavitation can all influence the extent of hydraulic losses [14]. Typically these losses are addressed with splitter blades within the impeller to enforce cohesion in the flow, de-swirlers or inlet guide vanes to prevent excessive pre-swirl at the inlet as well as tailored pump geometries (such as blade leading and trailing edges) designed to prevent or suppress flow separation. In applications such as the LUMEN pump where low manufacturing cost is critical, these complex geometric solutions are avoided and efficiency gains are sought in other areas.

2.2.3 Volumetric Losses

Due to the requirements for separation between stationary and moving components there exists secondary flow paths in every piece of turbomachinery - referred to collectively as clearance gap leakages. The fluid passing though these gaps reduces the total volume of the working fluid available to do useful work in the rest of the rocket engine and as shown in Figure 2.3 they represent one of the largest losses for a typical centrifugal pump. As these flows travel from regions of high pressure to low pressure the work expended in originally increasing their pressure is lost and impacts on pump efficiency according to Equation 2.5.

The two passages that allow the seal leakage Q_{sp} are firstly; between the impeller shroud and casing which typically rejoins the main flow at the impeller inlet (shown in red in Figure 2.1a) and secondly, between the impeller hub surface and the casing (shown in blue in Figure 2.1a) which can re-enter the main flow via balancing holes (holes drilled through the impeller hub shroud), interstage seals

or can be directed back to the impeller inlet via a piping arrangement. As the LUMEN fuel pump impeller will not have balance holes, the axial thrust balance will be achieved with a controlled hub clearance back pressure, set at 3 Bar for the baseline case to mimic the pump inlet pressure experienced by the shroud clearance flow. In general the clearance gaps are designed to limit the flow of working fluid through them and therefore reduce the associated volumetric loss. However all clearance gaps must be wide enough to allow for expansion and contraction of the rotating impeller due to thermal cycling as well as rotordynamic effects and vibration without having the rotor contact the stationary pump components. Achievable machining tolerances, manufacturing cost and the required pump efficiency also influence the size limits of the clearance gaps.

1. Shroud Clearance Gap Leakage
   The clearance gap between the pump impeller shroud and the impeller housing extends from the impeller inlet upstream of the blade leading edge to the blade outlet. Reducing the flow through this clearance has been the subject of much research and can be split into two components: the seal and the remainder of the clearance gap. In 1995 Engeda [7] demonstrated a link between shroud to casing clearance and pump efficiency and found good agreement between experimental data and an equation model in a similar fashion to Gülich [1]. Lei et al. [20] investigated the impact of back-blades on the impeller shroud (external face) and the axial clearance distance and showed that these impacted on the main flow around the impeller outlet. The geometry of the clearance gap itself was considered by Uy et al. [21] who showed that there was little impact from changing from a conical housing to a more typical curved design. Additionally there is a myriad of work demonstrating the impact of seal design on leakage flowrate - Ha et al. [22], Soldatova [23], Stocker [6] and Storteig [12] are four good examples that tie sealing face length, separation distance, labyrinth chamber geometry, surface roughness and fluid friction effects into various models for sealing flow losses and characterisation. Childs [5],[24] assessed some highly complex rotor and stator sealing face geometries and surface finishes including honeycomb patterns and helical pumping grooves as part of the Space Shuttle Main Engine (SSME) program and demonstrated both the potential benefits and difficulty of using advanced seal designs. In addition to the direct loss of energised fluid through the clearance gap, the losses associated with mixing and velocity profile changes caused by the leakage flow re-entering the main flow at the impeller inlet must also be considered. This has implications for other major operational phenomena such as inlet cavitation, recirculation and boundary layer formation/separation.

2. Hub Clearance Gap Leakage
   Again due to the clearance between the impeller rear surface and the impeller housing there will be a free fluid path from the outlet of the impeller blade channel to the area behind the impeller. The flow into this clearance is influenced by the blade outlet geometry and velocity as well as the presence and shape of a diffuser. Following the clearance gap inlet, the leakage flow is influenced by the velocity and roughness of the rotating hub wall and the proximity and design of the stationary housing before entering the

annular annular seal itself. Most available literature agrees that the width of the seal is the key parameter for determining the resistance to leakage however the geometry of the seal inlet and outlet as well as the artificial promotion of flow separation and turbulence within the seal (such as by using labyrinths) can greatly increase its effectiveness as demonstrated by Childs [5], Rapisarda et al. [25] and Stocker [6]. These researchers compared straight seals to complex labyrinth seals resulting in a decrease of up to 25% in the leakage flowrate. The literature suggests little individual consideration is required when determining changes to the hub or shroud seals and they are generally designed together.

2.2.4 Fluid Recirculation

Part load operation is becoming more common in rocket turbopumps as they are throttled and restarted for orbital insertion and manoeuvring. This forces the pump to operate away from its ideal design point, typically with a reduction in total massflow down to 50% of the nominal rate. This results in some fluid recirculating around the impeller inlet area or at the blade trailing edge causing a loss of energy denoted as P_{rec} in Figure 2.3 and described in detail by Tuzon [26]. Recirculation alters the flow conditions within the pump inlet, blade channel, at the blade exit, clearance gaps and further downstream and can lead to asymmetric flow and forces on the impeller. The nominal operating point considered in this thesis is not expected to generate any recirculation and therefore this loss mechanism was not characterised by the empirical design tool. This assumption is validated with the full pump numerical model in Section 8.3.1.

2.2.5 Cavitation

Another key avenue of performance losses in centrifugal pumps is through cavitation which refers to the localised phase change of a working fluid from liquid to gas due to a drop in the static pressure. Cavitation can cause blockages in the main flow paths as well as the clearance gaps, induce separation of boundary layers and disrupt the dynamic stability of the impeller. Cavitation modelling has proven a complex challenge and in recent times is rarely attempted with empirical equations. Gülich [1], Brennen [27], Ovsyannikov [28] and Chebaevsky [29] provide some guidance on calculating the likelihood of cavitation at a given operating point however they suffer from either a too broad focus (Gülich and Brennen) where industrial pumps are the source of verification or too narrow a focus (Ovsyannikov and Chebaevsky) where only rocket pumps with inducers are considered. Conversely, the depth and breadth of numerical cavitation models is almost limitless, with detailed simulations covering the impact on cavitation of everything from working fluid purity [30], inlet fluid properties [31], [32], roughness [33], inlet geometry [1], operating conditions [27], to simulation parameters such as turbulence model [34] and the coefficients of the cavitation model itself [35]. All of these researchers found non-negligible influences on the initiation, form, extent or impact of cavitation from these variable parameters.

In this thesis pure Methane is used as a simple substitute for the Liquefied Natural Gas proposed as the LUMEN fuel. Like any cryogenic operating close to its boiling point additional considerations are required when modelling cavitation in Methane such as thermal effects and low liquid to gas density ratio that produce

foamy cavitation regions rather than larger clear cavities seen in the more common water applications. Research conducted on cryogenics often references the experimental test campaign completed by Hord et al. in 1972 [36] with most others using a venturi nozzle experiment with water as the working fluid to validate their numerical model (such as Senocak et al. [37]).

The compressible nature of a working fluid vapour phase makes cavitation intrinsically linked to the rotordynamic stability of any impeller. Although not included in the scope of this thesis several phenomena that will impact on rotordynamic stability are, therefore the interested reader is encouraged to examine the work by San Andres [38] which gives a basic introduction to rotordynamics and it's analysis, d'Agostino et al. [39] who have extensively detailed the interaction between cavitation and the development of rotor instabilities, San Andres et al. [40] who focused on the impact of the thermal effect of cavitation within annular seals and how that effects the rotor stability and Tsujimoto [41] who has described cavitation instabilities, their causes and attempted to model them with a one-dimensional model.

2.2.6 Other Losses

There are several other loss mechanisms mentioned in the literature that can impact on the overall pump performance but are not considered in detail here as they are either only minor contributors to performance degradation or were left out of the thesis scope due to time constraints. These include:

1. Mechanical Losses
   Mechanical losses refer to the amount of available work that is used to overcome friction within mechanical linkages such as bearings, stuffing boxes, couplings and gears. Mechanical losses account for a relatively small percentage of overall impeller losses with mechanical efficiency of large centrifugal pumps demonstrated above 99% [1] although this is typically not true for smaller pumps. As these interfaces have already been designed they were considered as part of this thesis. This loss is denoted as P_m in Figure 2.3.

2. Secondary Flows
   Secondary flows generally occur in the form of complex 3D vortex flows within the main flow channel as a result of rotational and curvature effects from interaction with the impeller walls. They create non-uniform velocity profiles, promote boundary layer separation and dissipate flow energy through turbulence. Splitter blades or other geometry changes such as rounded corners are used to reduce the impact of secondary flows [1], [42].

3. Noise and Vibration
   As with most machinery it is impossible to perfectly balance all elements of a centrifugal pump for all operating conditions and this results in vibration and noise. As noted by Gülich [1] in Figure 2.3 above, this constitutes only a minor loss and its omission from this thesis is considered acceptable on this basis.

2.3 The LUMEN Engine

The Liquid Upper stage deMonstrator ENgine (LUMEN) is designed as a low cost, high performance example of a small scale liquid rocket engine and will be installed and operated exclusively on a testbench. The pursuit of innovation, low cost and ease of design has resulted in the selection of the relatively non-standard *Expander Bleed Cycle Engine* as shown in the schematic in Figure 2.4. This utilises heat transfer from the combustion chamber walls (MCC in the figure) to boil a portion of the cryogenic fuel - shown in red. The gaseous fuel is passed through the turbine which in turn powers the fuel and oxidiser (shown in green) impellers (with the fuel/oxidiser mixture ratio controlled by the balance valve - OTBV) before being dumped overboard, into the nozzle or expanded in a secondary small nozzle. This is a relatively unusual configuration as most turbines are driven by a gas generator, stored cold gas, or a closed bleed cycle that re-inject the expanded propellant into the combustion chamber after powering the turbine. While the closed bleed cycle can be more fuel efficient, re-injection of the turbine driving fluid back into the combustion chamber limits the turbine outlet pressure and therefore limits the amount of power the turbine can transfer to the pump impeller. The expander bleed engine cycle has been implemented in the Japanese LE series of engines and has shown high performance and reliability from a relatively simple configuration and is being further developed for high thrust first stage applications [43]. In the LUMEN case the propellants will be Liquefied Natural Gas (LNG) which will be modelled as the ideal case of pure Methane at 114 Kelvin and Liquid Oxygen (LOx) at 90 Kelvin. This propellant combination benefits from the similar storage temperatures (requiring less insulation), relatively low handling risks and clean combustion and are planned to be used in a number of modern launch vehicles.

The requirement for low mass drives designers towards smaller pumps which in turn require high rotation rates to maintain the required flowrates. An inducer is then typically employed at the impeller inlet to increase the local static pressure and therefore suppress cavitation that might result from the increased rotation rate. As the LUMEN engine will be operated in a testbench with the ability to increase the supply pressure to >10 Bar an inducer was deemed unnecessary and has been omitted from the design to reduce complexity. Key dimensions are given in Table 2.1 and reference the diagram in Figure 2.1b.

Variable	Value	Units
d_1	31.9	mm
d_n	20	mm
d_{2a}	85	mm
b_2	4.1	mm
β_{1B}	24	°
β_{2B}	28	°

Table 2.1: Key dimensions of the proposed LUMEN impeller as noted in Figure 2.1b. β refers to the local blade angle.

An analysis of the potential operating conditions of the engine has been completed by the LUMEN team [45] and three set points have been selected for the performance comparison in this thesis. These are detailed in Table 2.2. The operating point noted as *BP5* is considered critical because it has the fastest rotation

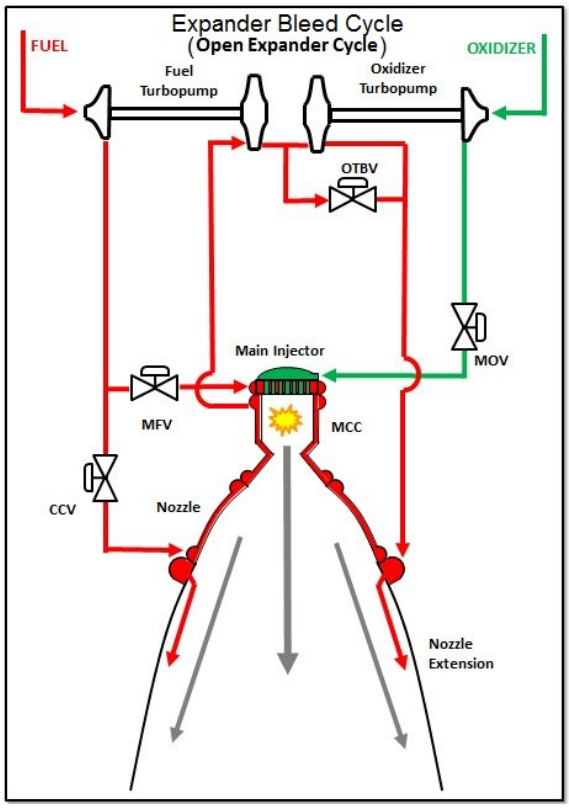

Figure 2.4: A schematic of an expander bleed cycle engine. Image taken from Bill Greene, NASA [44].

rate and highest massflow which is expected to test both the limits of cavitation performance and general output from the pump (such as leakage, developed head and efficiency). Also noted in this table is the expected head generation from the baseline pump. At the critical design point this results in a pump outlet pressure of approximately 125 Bar, which in turn can sustain a combustion chamber pressure of 80 Bar and produce a sea level thrust of approximately 28 kN. A previous analysis conducted by the LUMEN team predicted a pump efficiency of 60% for the critical operating point *BP5*[46].

Operating Point	Nominal Pump Massflow (Kg/s)	Rotation Rate (RPM)	Inlet Pressure (Bar)	Outlet Pressure (Bar)
Critical Case *BP5*	4.00	52000	3	124
Mid-Point Case *BP1*	2.80	43000	3	91
Low Load Case *BP9*	1.43	39000	3	54

Table 2.2: Comparison of three potential operating points and the total seal leakage as a percentage of total impeller flow.

With all of the above elements considered, the baseline LUMEN fuel pump assembly is visualised in Figure 2.5 below. The inlet extends to the left of the figure and the volute extends to the right. The blade surfaces are shown in red and the seals is highlighted in yellow. The baseline seal arrangement are

simple 7mm straight annular faces separated by 50 μm and have been previously estimated to allow up to 30% of the total massflow as leakage [45] [1].

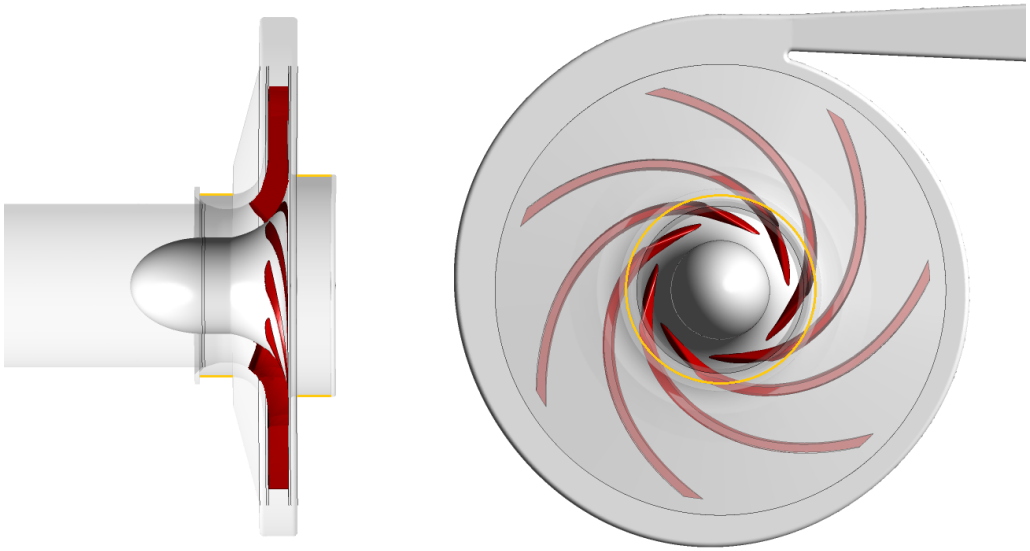

Figure 2.5: Side and top views of the proposed LUMEN fuel pump. The lack of an inducer makes this a relatively simple pump design.

The baseline design of the LUMEN rocket engine described here is a work in progress with many opportunities for change and development still available to the project team. The background information as well as the body of past literature detailed here will aid in the validation and optimisation process to follow and in doing so provide support to the research objectives posed in Chapter 1 while also providing guidance for the future development of the LUMEN fuel pump as well as the work in Methane cavitation and rotordynamics planned at the DLR Lampoldshausen.

[1] Note this previous estimate was made with slightly different geometry, increasing the estimated leakage rate

3

Development of the Preliminary Design Tool

The theory supporting the design and development of the early centrifugal pumps was proposed by Leonhard Euler in 1752 [47] and was based primarily on the conservation of angular momentum using Newton's Second Law of Mechanics. Since then several developments have been made towards a more robust characterisation of centrifugal pump performance and operations culminating in a set of preliminary design tools created by several space agencies and research organisations around the world [1]. Although user and designer experience is still invaluable (as discussed by Xu [51]), the ever increasing availability of powerful computational resources has promoted the use of numerical models in all aspects of turbomachinery design and development. In reality most designers will utilise both preliminary and detailed numerical models to create a robust pump and this is the case for the LUMEN project.

The initial design of the proposed LUMEN centrifugal pump is based on the process described by Gülich in his book - *Centrifugal Pumps* [1]. At the outset of this research project this preliminary design tool, including the estimation of losses was essentially unaltered from the Gülich presentation and little progress had been made to convert the process from its core purpose of industrial centrifugal impeller design to rocket specific applications. Previous comparisons of this tool to numerical models produced an adequate prediction of the impeller performance, however a discrepancy in the modelling of leakage losses revealed some errors [46]. To produce a genuinely optimised impeller the Gülich equation set that forms the basis of the preliminary design tool was updated and these updates are briefly described here. The results of the revised equation set were validated against experimental test data (see Chapter 4) as well as a detailed numerical simulation (see Chapter 6 and 8).

3.1 The Gülich Pump Design Tool

The Gülich method is just one of several tools available for the preliminary design of centrifugal pumps and has been developed over a number of years from de-

[1] PUMPA - NASA/USA [48], CARMEN - CNES/France [49] and HYPROB - CIRA/Italy [50] are examples.

signer experience and an extensive database of test and operational data [1]. Alternative pump design tools presented by Ovsyannikov [28], Storteig [12], Soldatova [23], and Stepanoff [14] were also considered however as the incumbent tool the Gülich method was the easiest to optimise and develop further and accounted for the greatest number of flow phenomena of all considered tools when determining pump geometry and performance. The model relies on assumptions of constant fluid properties and a nominal operating point completely free of recirculation. Equations are included to explicitly define key phenomena and parameters where possible however a number of features and influences (such as the influence of a rotating geometry on surface friction factor) are accounted for with experimentally defined and validated coefficients. Although it takes a broad variety of input parameters and has been used for numerous pump applications the Gülich model is not specifically tailored for the design of rocket turbopumps that sit well outside the typical operating envelope of industrial centrifugal pumps.

With these assumptions, an initial estimate of pump hydraulic efficiency and bounded by the conservation of mass through the pump impeller the geometry can be defined and begins with user inputs for desired mass flow ($\dot{m}$), estimates for inlet and outlet pressures (p_1, p_2) and velocities (c_{in}, c_{out}) and known inlet fluid properties (density - ρ and viscosity - ν). These are used to estimate the required shaft power (P), which then determines the diameter of the shaft (d_n) via the proposed material properties and all other impeller dimensions can be calculated from there. Perhaps the most important of these dimensions is the inlet diameter as described by Equation 3.1 where the shaft diameter, impeller total volumetric flowrate ($\dot{Q}_{tot}$), rotation rate (n) and two selected coefficients λ_c and λ_w which describe the cavitation performance of a given inlet and blade geometry are inputs. A typical value of λ_c is 1.1 for axial inflows and λ_w is between 0.4 and 2.5 depending on the cavitation criterion being considered. The volumetric flow rate, rotation rate and the inlet geometry (including estimated blade inlet angles) can then be used to determine all components of the inlet velocity vectors.

$$d_1 = \sqrt{d_n^2 + 10.6\left(\frac{\dot{Q}_{tot}}{n}\right)^{\frac{2}{3}}\left(\frac{\lambda_c + \lambda_w}{\lambda_w}\right)^{\frac{1}{3}}} \tag{3.1}$$

The impeller outlet geometry is then calculated based on an empirical correlation for the optimal produced head and head coefficient as described by Equations 3.2a, 3.2b and 2.3. Blade width at the impeller outlet is then determined by Equation 3.3. With these equations the components of the outlet velocity can be calculated and the impeller velocity triangles that describe the pump operation are completed.

$$d_{2a} = \frac{60}{\pi n}\sqrt{\frac{gH_{opt}}{\psi_{opt}}} \tag{3.2a}$$

where:

$$H_{opt} = \frac{P_{out} - P_{in}}{\rho g} + \frac{c_{out}^2 - c_{in}^2}{2g} \tag{3.2b}$$

$$b_{out} = d_{2a}\left(0.017 + 0.262\left(\frac{n_q}{n_{q_{ref}}}\right) - 0.08\left(\frac{n_q}{n_{q_{ref}}}\right)^2 + 0.0093\left(\frac{n_q}{n_{q_{ref}}}\right)^3\right) \tag{3.3a}$$

where the pump specific speed is calculated from Equation 2.6:

$$n_q = n\frac{\sqrt{\dot{Q}}}{H_{opt}^{0.75}} \tag{3.3b}$$

and:

$$n_{q_{ref}} = 100 \tag{3.3c}$$

These equations are then iterated along with another equation set to determine the geometry and performance of the spiral collector and straight volute until the calculated efficiency converges upon a stable value. Once the design tool has calculated the impeller geometry the losses can then be estimated. As the topic of interest for this thesis, the leakage losses are descibed in further detail. Equation 3.4 calculates the volumetric leakage flowrate ($\dot{Q}_{sp}$) as a function of sealing face diameter (d_{sp}), seal width (s) and average axial velocity within the seal (c_{ax}).

$$\dot{Q}_{sp} = \pi\ d_{sp}\ s\ c_{ax} \tag{3.4}$$

The value for the axial velocity within the seal has the most variable impact on the total leakage losses and is calculated from Equation 3.5 where $\triangle H_{sp}$ is the head drop through the seal and ζ_{EA} is a user defined parameter that accounts for the effects of seal inlet and outlet geometry. L_{sp} represents the length of the sealing face and is typically specified as a percentage of the seal diameter or in this case has been fixed to a desired value to fit the geometry. The term shown in square brackets is used to determine additional reduction of the axial velocity generated though a cascade of 'i' chambers in a labyrinth seal. ζ_K is an additional loss coefficient used to account for the geometry of the labyrinth chambers. The λ_f terms represent the friction coefficient which accounts for the wall friction within the clearance gap and is calculated using Equation 3.6.

$$c_{ax} = \sqrt{\frac{2g\triangle H_{sp}}{\zeta_{EA} + \lambda_f\frac{L_{sp}}{2s} + \left[\sum_i \left(\frac{d_{sp}}{d_{si}}\right)^2\left(\frac{s}{s_i}\right)^2\left\{\zeta_K + \lambda_{fi}\frac{L_i}{2s_i}\right\}\right]}} \tag{3.5}$$

$$\lambda_f = \frac{0.31}{\left(log\left(0.135\frac{\epsilon}{s} + \frac{6.5}{Re}\right)\right)^2}\left[1 + 0.19\left(\frac{Re_u}{Re}\right)^2\right]^{0.375} \tag{3.6}$$

Here the friction factor depends on the seal axial Reynolds number (Re), the circumferential Reynolds number (Re_u), sealing face equivalent sand roughness (ϵ) and the seal width (s). The Reynolds numbers account for the fluid density and viscosity and in all tested cases suggest a fully turbulent flow within the seals. Further to this the influence of the pre-seal clearance gap is only accounted for when $\triangle H_{sp}$ is calculated from the total impeller head rise and does not take into account the specific local features of the gap. Instead it relies on a function of the blade outlet geometry, flow velocity and Reynolds number, assuming a relatively standard straight or expanding clearance without back blades or other flow arresting geometries.

The various numeric factors and exponents are curve-fit values based on a large database of past experimental data which . However as with many empirical pump equations no information is provided on their applicability to rocket turbopumps. Despite this the Gülich model accounts for more influences that could alter the leakage flow than any other empirical model found in the literature.

3.2 Labyrinth Seal Leakage Model

High performance turbomachinery of all kinds utilise complex labyrinth seals wherever a restriction in fluid flow is required. Labyrinth seals generally comprise of a series of narrow passages that force the fluid to accelerate through them followed by relatively open spaces when the high velocity jet of fluid separates and spreads, generating turbulence. This turbulence generates an increase in local pressure as well as dissipating kinetic energy into heat which help to arrest the flow through the seal, reducing total leakage. The prediction of labyrinth seal performance can be achieved with the complete utilisation of Equation 3.5. Unfortunately there is little to no detailed information in the literature related to estimation of the local chamber loss coefficient - ζ_K other than the suggested range from Gülich of 1.0 to 1.3. This is not surprising given the complexity of labyrinth seals as shown in Figure 3.1. Equation 3.5 can also be expanded to screw-pump type seals as well as seals with honeycomb and hole pattern faces by targeted selection of these key loss coefficients however a numerical model or testing campaign would be necessary to validate the selection.

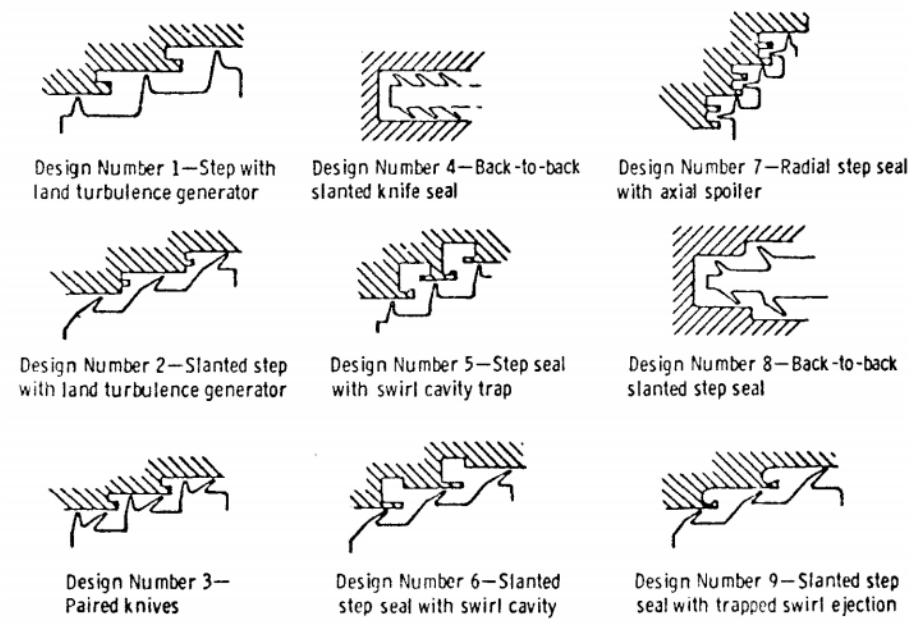

Figure 3.1: Several examples of labyrinth seal designs. The complexity is clear with all cases designed to accelerate the flow through a restricted passage and then dissipate the kinetic energy through turbulence in an open chamber. Image adapted from Stocker [6].

3.3 Improved Leakage Modelling

Optimising the Gülich design model for better prediction of leakage begins with the input of the seal geometry. This is specified at 7 mm long for the baseline LUMEN

case, a width of 50 μm, surface roughness of 0.1 μm and an inlet corner radius of 100 μm. The key area of change in the leakage equations 3.4, 3.5 and 3.6 is the ζ_{EA} term in Equation 3.5. This is included to account for the pressure loss that occurs when a flow transitions from one geometry to another such as at the seal inlet and outlet and has a recommended range of 1 to 1.2. Gradual transitions such as large radius corners prevent separation of the flow at these transitions, reducing the likelihood of turbulence generation and therefore minimising the lost energy. In a seal such as in this application, a high inlet loss reduces the differential pressure across the seal, resulting in a reduced leakage.

The outlet loss coefficient is typically set at 1 as it is assumed that all kinetic energy is recovered and converted into pressure at the seal exit. This is generally based on a pipe outlet being directed into a large tank or reservoir and is not necessarily valid for an annular seal case that retains kinetic energy as it flows out of the seal and back into the pump inlet as well as maintaining a circumferential/swirl velocity through the seal outlet. As an alternative to this, the outlet geometry was modelled as a combination of a 90 degree bend and an expansion from the seal to the outlet region based on equations from Menon [52] resulting in an outlet loss coefficient of 0.73. The inlet loss coefficient can be calculated according to Gülich for inlet corner radii (r) to hydraulic diameter (d_H) ratios of $0 \leq r/d_H \leq 0.2$ however no information is given for larger ratios. Numerical modelling completed by San Andres [53] provides further guidance on the selection of inlet coefficients up to ratios of 5 and suggests a value of 0.24 for geometries such as the baseline LUMEN seal inlet.

With these changes implemented the predicted total leakage falls from approximately 18% of the total pump flow to 14.5% with a similar drop in the predicted seal axial velocity from 145 m/s to 115 m/s. While the changes made to the Gülich equation set implemented in the LUMEN preliminary design tool result in a closer representation of the proposed impeller geometry and operating conditions, the tool itself must be validated against real leakage data before it can be relied upon for analysis of core pump design changes.

4

Validation of the Preliminary Design Tool

All models require comparison to real world data or known good models to ensure they are accurate enough representations of reality to warrant their use in the decision making process. The secretive nature and extreme operating conditions of rocket turbopumps has resulted in relatively little freely available raw test data with enough detail for a reliable comparison to be made to the LUMEN preliminary design tool. Additionally, experimental test data is often presented without complete details of testing conditions, geometry or any approximation of experimental errors and therefore must be treated carefully when it is used for validation. As the LUMEN fuel pump impeller has not yet been experimentally tested for seal leakage the results of an extensive annular seal test campaign conducted by D. Childs as part of the Space Shuttle program has been selected to validate the preliminary design tool [5].

4.1 SSME HPFTP Annular Seal

In the 1980's the NASA Marshall Space Flight Centre undertook an experimental test campaign to examine advanced annular seal designs for use on the Space Shuttle Main Engine - High Pressure Fuel Turbo Pump (SSME-HPFTP). The experimental test apparatus is displayed as Figure 4.1 and shows two test seals between an inner rotating cylinder and fixed housing with square inlet and outlets. The test apparatus includes several pressure and temperature sensors that are used to calculate the change in flow through the seal. Unfortunately no information is provided on the inlet and outlet corner radius so the pressure loss coefficients will be taken unchanged from the NASA data rather than being recalculated with the preliminary design tool. Surface roughness is specified at 0.81 μm for the seal faces. The friction factor (λ_f) that is used to calculate the axial velocity in the Gülich equation set is also derived by the Childs paper as a function of a number of experimentally determined coefficients. However as the Childs method of determining the friction factor is useless without these experimentally determined coefficients (which are unavailable for the LUMEN pump) the Gülich Equation 3.6 for calculating the seal friction factor will be used to more closely replicate the design process detailed in Chapter 3. For completeness the equation from Childs is presented in Appendix B.

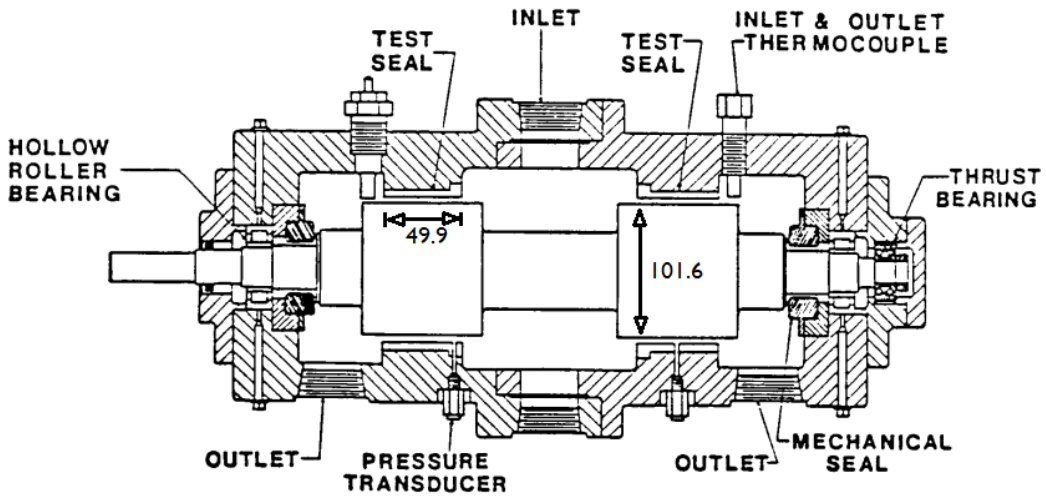

Figure 4.1: NASA high Reynolds number seal test section schematic, the seal face length and diameter are noted in *mm*. Image adapted from Childs et al. [5].

The test data produced for a straight smooth annular seal also includes information on rotation rate, mass flowrate, seal pressure differential as well as the fluid density and viscosity at the given test conditions. The test working fluid was Freon 1381 (chemical name is bromotrifluromethane - $CBrF_3$) and was used as a non-flammable and safe to handle replacement for liquid hydrogen at the time. The relatively similar thermal effect parameter values (8500 $m/s^{\frac{2}{3}}$ for Hydrogen at 20 K, 2000 $m/s^{\frac{2}{3}}$ for Freon 1381 at 298 K and 160000 $m/s^{\frac{2}{3}}$ for Methane at 114 K - as calculated by Equation 9.12) suggests that Freon 1381 will generally reflect the properties of Hydrogen and allows any cavitation results to be converted to the cryogenic Hydrogen case without requiring a cryogenic capable test bench. Freon 1381 has a density of 1550-1570 kg/m^3 and dynamic viscosity of $1.5e^{-4}$ Pa.s at the nominal test conditions (298 K) compared to the 425 kg/m^3 and $1.2e^{-4}$ Pa.s of liquid Methane (at 114 K) resulting in a kinematic viscosity three times larger for Methane than Freon. The result of this is a three times reduction in local Reynolds number for a Methane case operating at the same velocity and characteristic length. This suggests the Methane case would require a higher local velocity and therefore a larger seal pressure differential to achieve turbulent transition of the boundary layers. The effect is greater when compared to water which has a kinematic viscosity approximately one order of magnitude greater than Freon at the nominal test conditions and as the preliminary design tool is based on equations developed for water applications this could lead to inaccurate modelling of the flow regime at low differential pressures as the Reynolds number may be under-predicted. The preliminary design tool does take these fluid properties into account as part of the calculation of the friction factor (λ_f - see Equation 3.6) however the validity of the various fixed values and coefficients used in this calculation is unknown for non-water applications.

The tested geometry is slightly larger than the LUMEN design with a seal di-

ameter of 101.6 mm rotating at a maximum of 7200 RPM compared to the 38 mm of the baseline LUMEN design rotating at 52000 RPM which results in a seal wall velocity of approximately 37 m/s in the fastest NASA test compared to approximately 100 m/s of the baseline LUMEN case. The NASA seal was also much longer, with a standard 49.9 mm length used for all tests compared to the 7 mm LUMEN seal. Three seal widths were tested in the experimental campaign with face separation distances of 0.508 mm, 0.381 mm and 0.254 mm. Additionally the seal width to seal wall diameter ratio that is often used to compare different seals is twice as large for the smallest NASA seal clearance (0.0025) than the baseline LUMEN case (0.0013) which suggests that the LUMEN data will be slightly more influenced by the seal wall velocity and roughness than the NASA test data.

4.2 Comparison and Results

These geometric values, along with the fluid properties and operating parameters were entered into the revised preliminary design tool leakage estimation equations and an estimated mass flowrate was produced and compared to the experimental data. These results are displayed in Figure 4.2 below. The differential pressure as measured by the test apparatus is displayed against the error between the through-seal mass flowrate prediction and the experimentally determined mass flowrate. The three different seal clearance widths are shown, all tested at a range of rotation rates from 900 to 7200 RPM.

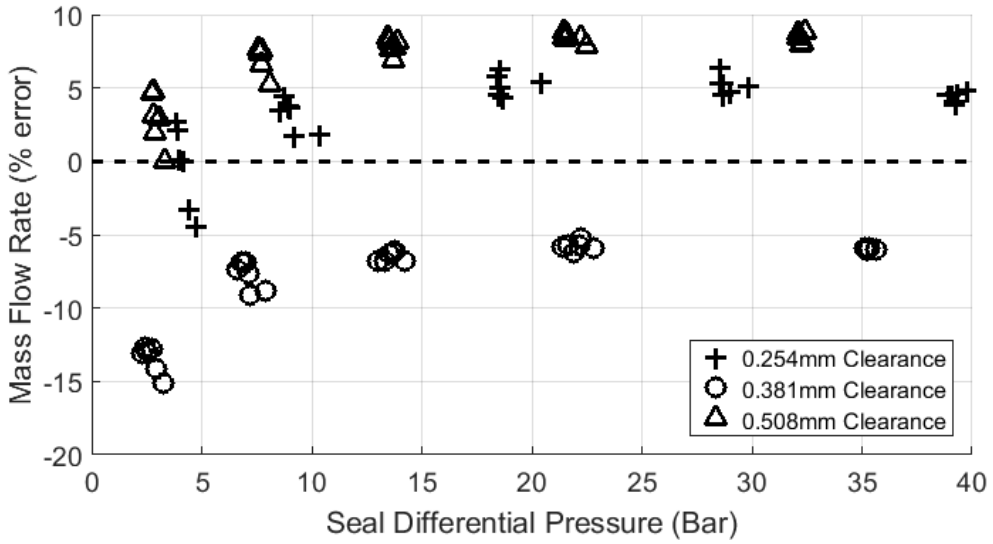

Figure 4.2: The percentage error produced by the prediction of seal leakage using the Gülich model, compared to the experimental data produced by Childs et al. [5] as part of the SSME program.

Two clear trends are evident from the results; firstly that the relative clearance width has an impact on the prediction with a distinction between the error produced by the three datasets and secondly that experiments with low differential pressure appear more difficult to estimate with the greatest spread in error occurring below 10 Bar for all datasets. The spread in prediction accuracy is attributed to the calculation of friction factor that is then used to iterate the seal axial velocity and Reynolds numbers. The friction factor as described by Equation

3.6 accounts for the fluid properties, operating conditions as well as the surface roughness. Through an iteration process this friction factor also takes the total loss coefficient provided by the experimental data as an input and this coefficient also displays the greatest variation at low differential pressures. Given the proposed operating range for the LUMEN project, such low differential seal pressures are extremely unlikely to be encountered therefore the varied predictions of leakage in this area of operation can safely be neglected.

The discrepancy in the mass flowrate predictions between the three clearance gap widths appears more closely related to the given values of total loss coefficient - ζ. The 0.381 mm width seal had a mean ζ value of 1.28 indicating a large pressure drop at the seal inlet compared to the 0.254 mm ($\zeta = 1.19$) and 0.508 mm ($\zeta = 1.21$) seals. These coefficients describe the resistance to the flow generated by the seal inlet and outlet geometries and resulted in the 0.381 mm seal mass flow data being under-predicted by the empirical equation whereas the other two seal leakage flows are over-predicted. Additionally, the magnitude of the mean error increases as the clearance gap width increases (4.7% mean error for the smallest clearance, (-)6.0% for the middle and 8.1% for the largest clearance). As the larger ζ value results in a reduced mass flow prediction from the Gülich equation this suggests that the equations over-represent the influence of the inlet pressure drop when compared to reality. The loss coefficients provided also vary depending on the specific operating conditions of the test such as rotation rate, differential pressure and mass flow which is in contrast to the purely geometric definition given by Gülich. When the experimental loss coefficients are replaced with a fixed value (such as if the coefficient was simply based on geometry) the leakage prediction errors are much larger which indicates that the empirical equations are not accounting for all of the relevant flow features when predicting important losses such as these. Two additional figures are presented in Appendix B to further support these findings.

The most relevant result for the LUMEN project and the validation of the preliminary design tool in Figure 4.2 is the 0.254 mm clearance at the highest differential pressure and this data is predicted to within 5% of the experimental massflow value. Although it shows a generally lower error at low differential pressures (for the smallest clearance) the Gülich equation produces less spread in the results as the differential pressure increases and the total error appears to approach a relatively constant percentage offset. This is beneficial for the proposed LUMEN pump seal which will have a much greater differential pressure than the conditions tested by Childs.

4.3 Discussion

The primary purpose of the Gülich equation set and the preliminary design tool that they contribute to is to provide an estimation of turbopump performance and support the future iteration and optimisation of the LUMEN engine design. Without a prototype or initial test campaign no data was available to directly test the tool so the results from the SSME-HPFTP annular seal test campaign were used instead. Although the empirical equations were not refined for the extreme operating conditions of rocket pumps, the tool performed well enough and demonstrated the continued usefulness of analytical and empirical tools to the

modern rocket engine designer. These results also help to indicate the enormous array of input parameters that can influence the flow through a relatively basic straight annular seal. Analysing more complex seal designs, as well as the rest of the shroud to housing clearance gaps will add to this complexity and may result in greater inaccuracy.

Despite these inaccuracies the empirical equation for predicting annular seal leakage losses presented by Gülich estimated the seal leakage massflow to within $\pm$ 15% of the experimental results produced by Childs for all cases and within ±5% for the test conditions most closely related to the proposed LUMEN operating point. The simplified nature of the equations with their reliance on approximations and empirical correlations appears responsible for most of the inaccuracy, particularly relating to the use of the inlet and outlet loss coefficients and the calculation of the sealing face friction factor at low differential pressures. Inaccuracies such as this are to be expected as the tool was developed primarily from experience with industrial water pumps which operate under vastly different conditions to the Freon filled rocket pump seal being tested and the LUMEN pump being proposed. Lacking any form of flow visualisation and limited by simple pressure and temperature based measurements it is difficult to determine exactly how the equations could be developed, replaced or refined in order to produce a more accurate and robust model for future use however for the intended purposes of this thesis the preliminary design tool is deemed suitably accurate.

5

Development of the Numerical Model

A verified preliminary design tool allows for the rapid iteration and assessment of design changes to be made without the need for extensive human and computational resources. However there is only so much information these tools can provide given the reliance on basic user inputs, empirical correlations and simplifying assumptions. Powerful modern computers and robust modelling algorithms have driven the replacement of these empirical models with numerical ones. These provide estimations of detailed local flow features rather than computing global pump performance which is essential for the further optimisation of a complex piece of machinery such as the LUMEN rocket engine. Additionally the results of the more complex numerical model can be compared to the preliminary design tool as further validation of both models. A reduced model of the proposed LUMEN fuel pump impeller clearance gap was created in the commercial modelling software Ansys CFX 18.2.

The following four chapters of this thesis detail two numerical models that were used to capture the more complex flow phenomena that the empirical model cannot and in doing so provide an additional and more sophisticated tool for analysing alternative impeller geometries. This will contribute to the third research goal presented in Chapter 1 by supporting recommendations for changes to the baseline straight seal geometry and therfore improvements in the expected performance of the LUMEN fuel pump impeller.

5.1 Model Parameters

To reduce the model size, simplify mesh generation and reduce the computation time a 15 degree segment of the impeller outlet, clearance gaps and seals was generated for the comparison of alternative seal designs. As with all previous calculations the baseline numerical model is simulated at the critical design point *BP5* with corner radii of 100 μm, seal face surface equivalent sand roughness of 0.1 μm and a 50 μm wide, 7 mm long straight seal. Liquid Methane was modelled as the working fluid with a temperature of 114 K, density of 425 kg/m^3 and viscosity of $1.2e^{-4}$ Pa.s. Lindemann [46] in his previous work with the LUMEN pump predicted a negligible change in pump performance resulting from changes in temperature and density through the pump and therefore an isothermal and

incompressible liquid model was used here. The inclusion of the restricted sealing face geometry will increase the local heat generation which will in turn effect the local fluid properties such as density and vapour pressure more so than Lindemann predicted. However this will primarily impact on the seal cavitation performance which was not the parameter of interest for the reduced model. Rotationally symmetric boundaries were placed at both sides of the 15 degree segment and a mass flow was specified at the blade outlet plane. Openings with static backpressure were specified at the collector interface as well as the shroud and hub seal outlets as noted in Figure 5.1. These pressures were set to replicate the findings of previous LUMEN full pump simulations completed by Lindemann. The convergence criteria were also taken from the Lindeman model and set to RMS momentum residuals of $< 1e^{-4}$ and global volumetric flow imbalances of $< 0.001\%$ to allow direct comparison to those results.

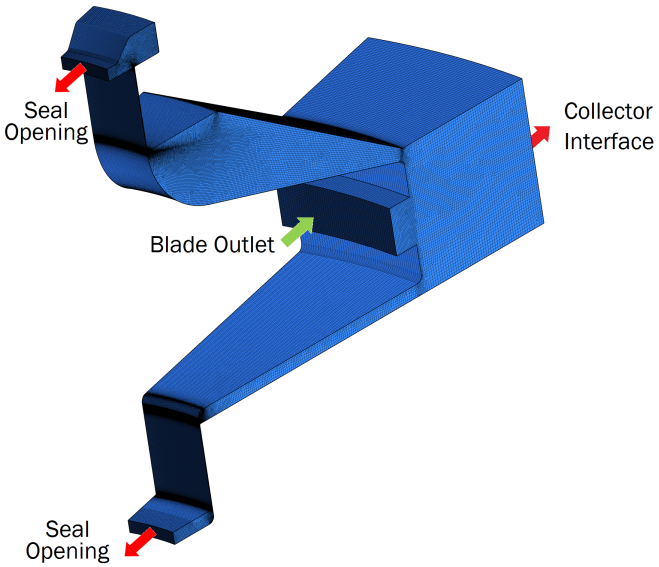

Figure 5.1: The baseline numerical model is shown with the surface mesh lines and indicative mass transfer boundaries. This is the basis for all future numerical simulations detailed in this thesis. High cell density though the seals as well as at the seal inlet and outlet are essential to an accurate model.

The rotating and asymmetric nature of a centrifugal pump results in unsteady flows which can only be truly modelled with a transient simulation. As the reduced numerical model is not intended to capture these features that are expected to have little impact on the massflow through the seals, the steady state assumption was applied for all simulations. The selection of a steady state model is supported by previous work by Berten et al. [54] who found little difference between steady state and transient CFD simulations when compared to experimental centrifugal pump data and Kaewnai et al. [55] who produced an adequate fit between a steady state numerical model and experimental data particularly for flow rates close to the designed best efficiency point flow rate.

5.1.1 Turbulence Model

Past work by the LUMEN team exclusively utilised the k-ϵ turbulence model however this did not converge once the restricted flow path of the seal region and

the associated complex flow features were included in the model. All simulation results displayed in Figure 5.2 and presented in the remainder of this thesis were completed using the Reynolds Averages Navier-Stokes based k-Omega Shear Stress Transport(k-ω SST) two equation eddy viscosity turbulence model developed by Menter [56]. This turbulence model has been assessed along with the current state of the art in centrifugal pump modelling by Shah et al. [3]. The k-ω SST model is generally suited to simulations where flow separation due to adverse pressure gradients is expected or where high shear stress is expected near the walls. The restricted passages of the proposed LUMEN annular seal as well as the seal inlet and outlet corners are such areas and accurate modelling of these regions was found to be key to convergence and repeatability of the simulations. It has been used by many other researchers in successful simulations of centrifugal pumps including high speed rocket applications and multi-phase flows by Mani [57] as well as pump leakage modelling by Liu and Pan [35] and their results add confidence to the selection of this turbulence model for the LUMEN application.

5.2 Mesh Resolution Study

As the main points of interest, the region between the blade outlet and volute inlet as well as the clearance gaps, seals and seal outlet regions were modelled in detail. For the mesh resolution study all walls were set to smooth rather than the nominal surface roughness of 10 μm as this can result in problems with calculating the local y^+ values. The results of the mesh resolution study are displayed as Figure 5.2. The data displayed in the figure is split into two groups, firstly a typical resolution study with progressive global refinement represented with $\triangle$ symbols and secondly a more focused mesh refinement with criteria of $y^+ < 2$ in the seal face and seal inlet/outlet regions represented with $+$ symbols. Both datasets show less variation in the calculated leakage values as the global cell count is increased but the dataset with the seal region y^+ criteria demonstrates a greater response to increased mesh resolution. This is expected due to the leakage flowrate used to compare these meshes being sensitive to the flow at the seal inlet and outlet so resolving these features will lead to a more consistent result. The $+$ symbol dataset clearly demonstrates convergence of the various simulations to a relatively consistent mesh independent leakage flowrate with a minimum cell count of approximately 1 million.

This mesh was then utilised for all future simulations of the baseline geometry. This mesh was generated using ICEM CFD with a specified wall spacing and a swept hexahedral dominant mesh core. As changes were made to the seal design (as described in Chapter 6) the mesh resolution study was not repeated however the criteria for a local $y^+ < 2$ was enforced to ensure continued accuracy of the model and a reliable comparison between seal designs. The mesh parameters of aspect ratio, expansion ratio and orthogonality are another indication of a quality mesh and these were restricted to less than 1% of cells within the unacceptable range as defined by the Ansys CFX defaults.

5.3 Errors and Uncertainty

Errors and uncertainty are unavoidable consequences of applying any model to real world phenomena. In Computational Fluid Dynamics, definitions of uncer-

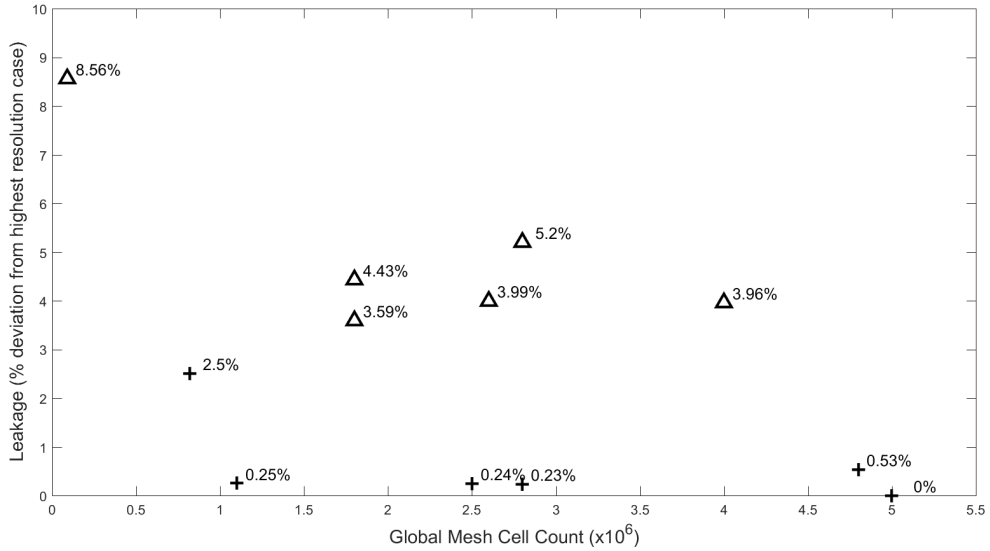

Figure 5.2: Results of the numerical mesh resolution study. Points denoted with triangles refer to simulations with global mesh refinement and those with crosses refer to meshes with a targeted y^+ and high cell count in the seal face, inlet and outlet regions of the mesh.

tainty and error are given by the American Institute for Aeronautics and Astronautics (AIAA [58]) as:

Uncertainty: *"A potential deficiency in any phase or activity of modelling and simulation process that is due to a lack of knowledge"*

Error: *"A recognisable deficiency in any phase or activity of modelling and simulation that is not due to a lack of knowledge"*

Uncertainty can arise in the model due to a lack of knowledge of the exact boundary conditions, initial conditions, geometry and fluid data of the finally produced pump impeller. Although the potential changes in impeller geometry, uncertainty of the simplified fluid properties (pure Methane as opposed to impure Liquefied Natural Gas) may be estimated, the overall model uncertainty cannot be accurately quantified at the preliminary design stage. However the purpose of the simulations detailed here is to assess a relative improvement in performance of the proposed pump impeller and so a well defined baseline case is necessary. This allows the comparison between simulations to be made and the impact of individual changes to the pump geometry or operation to be characterised.

Errors are created when the true partial differential equations (PDEs) are discretised to produce numeric equations suitable for rapid solving by computers. As an exact solution to the PDEs is unknown, this error can only be estimated by quantifying the truncation error of the discretisation scheme being used. Within Ansys CFX, the *High Resolution* scheme available was used in order to reduce this error as much as possible and the highest resolution mesh that the available computer system could reasonably handle was implemented. Even with the best mesh there is still a chance that errors will be introduced by inadequate or misguided model assumptions. This includes features such as steady state operation (non-transient models), heat transfer at the domain walls, specifying inlet and outlet flow temperatures and flow directions. This source of error extends to the selection of boundary conditions which are always an approximation of real flow

features. Some guidance is provided on the selection of appropriate boundary conditions by Baskharone [59], Wu et al. [60], Storteig [12] as well as the Ansys CFX documentation [61] which suggests the most robust configuration is the velocity/mass flow at the inlet and a static pressure at the outlets as implemented here.

A method for estimation of the numerical model discretisation error referred to as Richardson Extrapolation has been described in various forms by Roache [62], Phillips et al. [63] and Xing et al. [64]. This method uses a series of refined computational grids and their corresponding simulation results to estimate an error-free solution and subsequently estimate the difference between the exact solutions to the modelled equations and the exact solution to the partial differential equations used to model them. This calculation for the baseline annular seal simulation produced an estimate discretisation error of ±1% for the prediction of leakage mass flow. This error estimation technique assumes that round-off, iteration and other sources of numerical errors are negligible in comparison to the discretisation error. As the mesh resolution study was conducted using double precision operations and fixed convergence criteria this assumption is considered valid. However the Richardson Extrapolation method also assumes that the solutions follow an asymptotic convergence towards the highest resolution solution which while may be true for simple models is almost impossible to achieve for complex geometries with equally complex and turbulent flows. Therefore this estimate of modelling error is indicative only. Alternative error estimation methods such as a Monte Carlo approach was considered too resource intensive for the potential benefits of a more accurate characterisation of the modelling uncertainty.

Cumulatively these sources of error may have a minor influence on the simulation results however the effort required to quantify them in greater detail as well as the limited availability of alternative modelling options and the comparative nature of the analysis made further efforts to reduce or eliminate these errors unwarranted.

5.4 Discussion

There are numerous detailed research papers and textbooks dedicated to optimising a numerical model for the accurate simulation of turbomachinery fluid flows and this past research, along with past modelling by the LUMEN team has guided the selection of modelling parameters here. The k-ω SST turbulence model, along with robust boundary conditions and a suitable mesh were chosen for simplicity and effectiveness and ensured the convergence of all simulations detailed in Chapters 6 and 7. Although these elements of the numerical model were selected and tested for accuracy (where possible) there remains a level of error and uncertainty within all produced results, especially given the isothermal and non-cavitating models used. As the key purpose of the simulations described herein is comparative in nature and the relative performance between the proposed baseline and potential alternatives is the outcome of interest the absolute accuracy of the numerical model is a secondary concern. As all simulations were completed on a similar mesh with identical inputs and boundary conditions the numerical model is deemed adequate for the intended purpose. The results of the reduced numerical model simulation and a comparison to the empirical equation model implemented

in the preliminary design tool is presented in Chapter 6. A more complete full pump numerical model is then created to explore the proposed pump design in greater detail based on the reduced model developed here.

6

Development of the Annular Seal

The numerical model is first applied to the baseline 7mm straight annular seal and the results are compared to the leakage prediction of the empirical equation set. Two manufacturing limitations are then examined for their impact on general seal performance. Finally, a number of variations on the incumbent 7mm straight seal are presented as well as more complex alternatives commonly found in high performance turbopump applications with varying results. These alternatives were considered after an examination of existing high performance rocket engine turbopumps as well as other rotating machinery applications where a straight annular seal is rarely used. The vast array of complex seal designs was reduced to a select few relatively simple variants that capture the general features of the more complex designs without requiring advanced manufacturing and assembly techniques or alternative numerical meshing techniques. The mass flow measurements are taken at the seal openings as indicated in Figure 5.1 with the other points of interest being the seal inlet and outlet which are magnified in Figure 6.1.

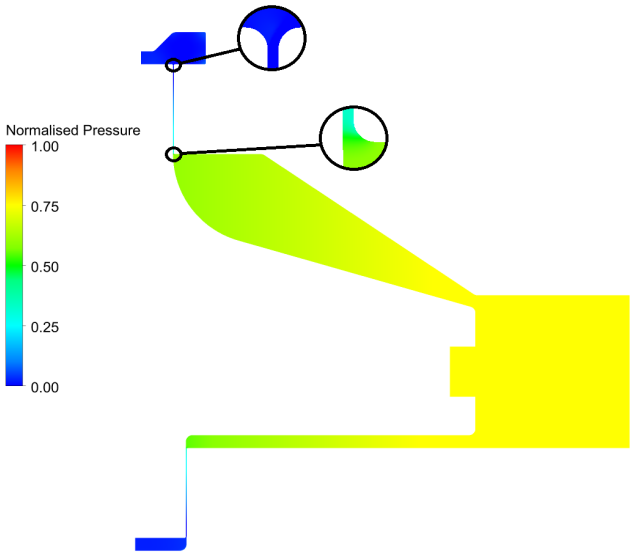

Figure 6.1: A cross section of the baseline reduced numerical model with the normalised pressure shown. The shroud seal inlet and outlet are magnified as these are the regions of the largest changes in flow properties.

6.1 The 7mm Straight Seal

The LUMEN fuel pump impeller baseline design has a 7mm straight annular seal in the hub and shroud clearances. This was based on ease of design and manufacture and the length required to achieve a suitable preliminary leakage rate while remaining within the limits of the available pump geometry. The baseline seal was designed to be 50 μm wide with the two sealing faces manufactured to a surface finish of 0.1 μm equivalent sand roughness with inlet and outlet corners finished to 100 μm radius in line with the initial proposed seal design. The smooth surface finish was a result of the requirement to use a grinding technique to achieve the desired minimal clearance width. Alternatively, the corner radius was chosen as a worst case to allow for a number of cheap and available manufacturers to be chosen without impacting on the expected performance of the pump.

The key area of comparison between all analysed seal designs is the mass flowrate allowed to pass through the given seals as this gives the best indication of volumetric efficiency losses of the complete pump assembly as described by Equation 2.5. A comparison of leakage rates between the various seal designs that were considered is given in Table 6.1 below. The percentage values represent the increase in required pump inlet massflow to overcome the modelled leakage and maintain the nominal pump outlet massflow. Secondary to this is the pressure distribution through the seal as well as the inlet and outlet regions as this can give some indication of the likelihood of cavitation developing. Lastly, the difficulty of manufacture of the seals is considered as an indication of production cost.

Design	Leakage (% of nominal massflow)
Empirical Calculation	14.5
7mm Straight	15.8
5mm Straight	17.5
Single Z Step	14.3
Multi Z Step	12.9
Sawtooth Labyrinth	15.4

Table 6.1: Alternative seal designs and the corresponding leakage rates calculated using a reduced segment numerical model.

The 7mm straight seal produced a leakage rate of 15.8% of the total simulated impeller flow. The pressure distribution through the baseline seal is shown in Figure 6.2 and indicates the rapid pressure drop at the seal inlet (left of image) followed by a gradual pressure drop as the fluid passes through the sealing face from approximately 60% of the pump maximum at the inlet to the back pressure at the clearance outlet which is set to 3 Bar in this case. As shown in the figure, there is a significant region of low pressure before the seal exit. The numerical model predicts this pressure to be well below the 1.2 Bar vapourisation pressure of Methane and therefore will almost certainly cavitate in the real pump. As there is no phase change modelling in this case an artificial negative pressure is generated instead. This region of likely cavitation has the potential to cause rotordynamic instabilities, vibration and damage to the pump and therefore should be designed out of the system if possible.

The influence of the rotating impeller walls on the velocity distribution though

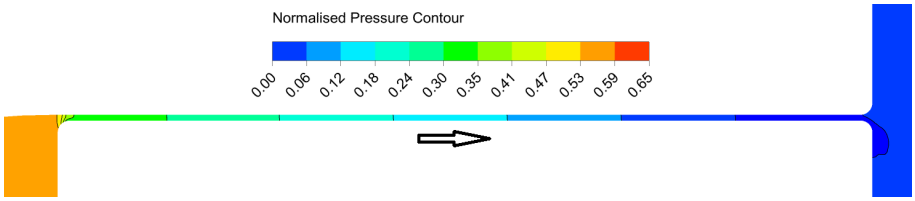

Figure 6.2: A contour plot of the normalised pressure drop as the leakage flows through the shroud seal from the inlet (left) to the outlet (right). Note that a minimum is reached well before the seal outlet.

the clearance gaps as well as the seals is evident from Figure 6.3. The high velocity shown within the seal reflects the empirical equation model prediction however the leakage flow rapidly turns at the seal exit and continues radially outward rather than into the open space above the seal. This suggests the tight clearance and wall friction are imparting a high circumferential velocity on the leakage flow which corresponds to a radially outward acceleration of the flow at the outlet. Although this does not appear to influence the outlet pressure or seal flowrate it may lead to non-uniformities when the leakage flow is re-introduced to the pump inlet and is considered in further detail in Chapter 8.

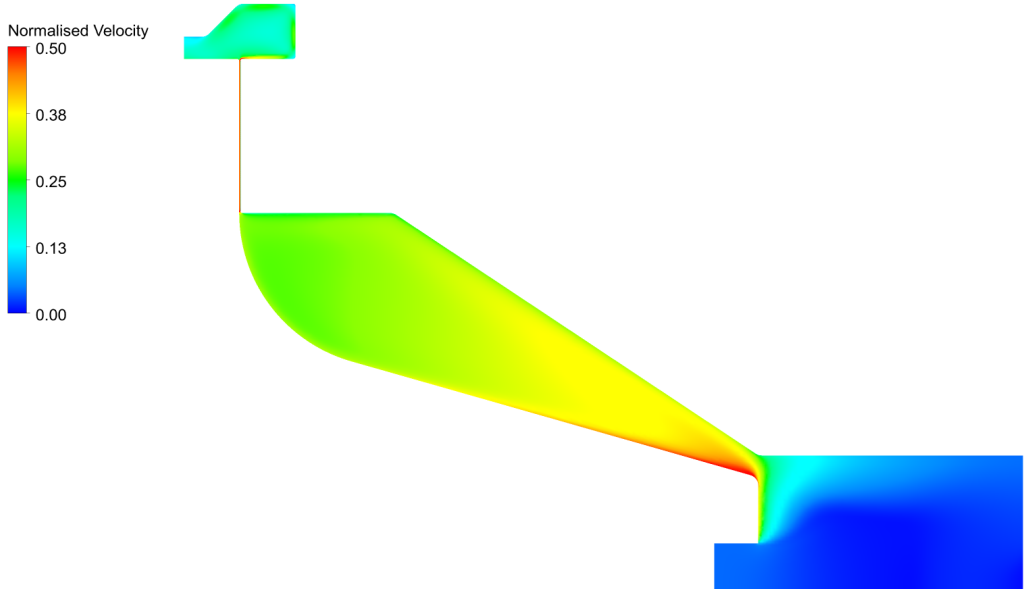

Figure 6.3: The velocity profile at the midplane of the reduced numerical model domain. The influence of the rotating wall is evident in the seal. Note the scale has been exaggerated for clarity.

6.2 Comparison to the Empirical Calculation

As indicated by the results in Table 6.1 above, the numerical model for the baseline 7mm straight seal design predicts the seal total leakage flowrate to within 10% of the preliminary empirical calculation presented and validated in Chapter 4. This was the target accuracy outlined at the start of the thesis, chosen to ensure both models generally reflect the same design performance. Another pertinent result from the baseline numerical simulation is the prediction of axial velocity within the seal as this is a key parameter that the empirical calculation uses to determine

the leakage rate. The numerical model produces an axial velocity of 119 m/s and the empirical tool calculated a value of 115 m/s. This minor discrepancy reflects the uncertain nature of the user defined inlet and outlet loss coefficients that the empirical tool relies so heavily on and suggests that the model used to estimate these coefficients can be further refined. For example the empirical tool uses one value to define the seal inlet losses based on the inlet geometry but assumes this to be the same for both rotating and non-rotating edges of the inlet (which is not the case here) and uses a basic correlation to account for the circumferential flow velocity at the inlet as well as a circumferential Reynolds number to account for the same velocity through the seal itself. Without these simplifications the numerical model is able to effectively predict the loss in pressure at the inlet as shown by Figure 6.2. Further numerical and experimental work would be required to develop these findings into a reliable improvement in the empirical equation set used in the preliminary design tool.

Another potential improvement for the preliminary design tool is the calculation of leakage flowrate which is determined based on a user input pump differential pressure. No iteration or check is performed to evaluate the likelihood of that differential pressure drop, in combination with the seal geometry leading to large sections of the seal predicted to be below the vapour pressure of Methane as shown by the numerical model in Figure 6.2. Other researchers (San Andres [38] is one example) provide alternative methods for predicting the local pressure through annular seals that could be used to check the lower limit of seal pressure, however these again rely upon user defined coefficients.

The comparison of the estimate of the seal inlet pressures of approximately 81.3 Bar for the numerical model compared to the 82.3 Bar for the empirical model demonstrates the potential for accurate predictions from empirical equations. However this baseline case, with straight expanding clearance gap walls is the simplest case and introduction of alternative designs such as those detailed in Section 7.1 will require the use of a loss coefficient or an alternative equation set to capture the more complex degradation of pressure through the pre-seal clearance gap.

The results of the baseline numerical simulation presented here show that the empirical equation set can be used for preliminary pump design with some confidence and the validation of the empirical model against experimental data provides greater confidence in the accuracy of the numerical model. The seal leakage flowrates, as one of the major contributors to pump inefficiency can be predicted to within 10% of a much more detailed and computationally expensive numerical model with a relatively simple empirical model. It was also demonstrated that the accuracy of the preliminary model could be improved by refinement to critical user input parameters such as the seal inlet and outlet pressure loss coefficients. The numerical model revealed additional detail in the flow such as localised pressure drops, potential vortex development and turbulence generation that are impossible for the empirical tool to predict in its current simple form. This added detail allows designers to recommend targeted changes to the baseline model to provide a robust, stable and performance optimised seal design. Some of the potential changes were simulated and the results are presented and discussed in detail in the following sections.

6.3 Manufacturing Considerations

From the initial numerical simulations it became evident that the given manufacturing limits would impact on the potential for a fully optimised impeller and seal design. In particular the 100 μm radius for all rounded corners is detrimental to flow separation at the inlet to the straight seal and therefore likely to impact all labyrinth seal designs as well. The proposed surface finish within the sealing faces of 0.1 μm equivalent sand roughness was a result of manufacturing the minimum separation between the rotating and non-rotating pump surfaces. The smooth surface allows relatively unrestricted passage of high velocity fluid through the seal. The necessity of the sealing face separation distance will be unknown until a rotordynamic analysis or vibration testing can estimate the lateral movement of the impeller. Until then a more rigorous basis for recommending changes to these manufacturing limits can be made from further modelling of these features.

6.3.1 Seal Face Roughness

The surface roughness of these simulations is determined from the equivalent sand roughness parameter which is a user input to the numerical model. The nominally smoothest surface finish of 0.1 μm was compared to a series of sealing faces with increased roughness and the total leakage was calculated at the critical operating point - *BP5*. Figure 6.4 displays the simulated total leakage for a series of different seal roughness values, and demonstrates the enormous effect this parameter can have on seal leakage. The corresponding axial velocity profiles for all simulated cases is shown as Figure 6.5 and displays an apparent step change in the seal flow when surface roughness is increased from 0.2 μm to 0.5 μm which supports the graphical results. Additional simulations at 1 and 5 μm were conducted to ensure no further improvement in leakage performance was possible above this step change.

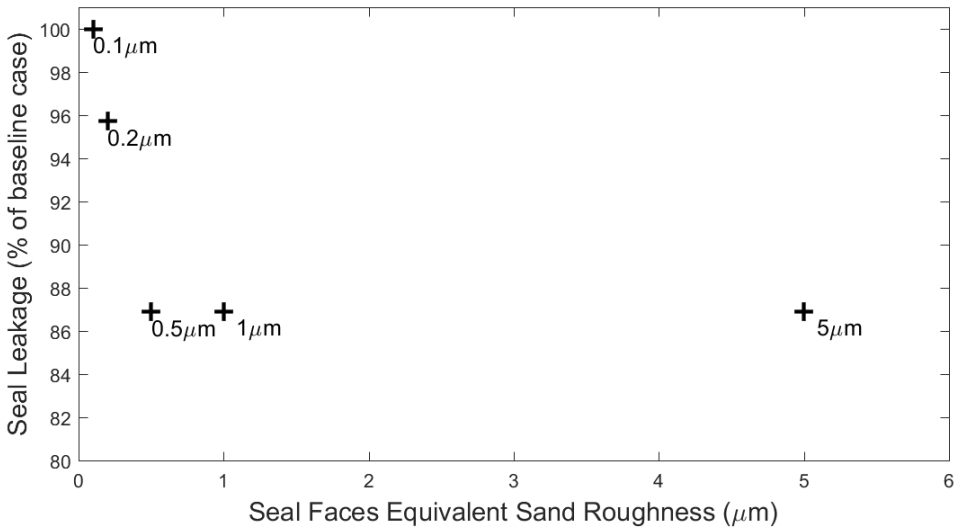

Figure 6.4: Comparison of seal leakage rates for various seal surface roughness'.

The reduced leakage and axial velocity is attributed to the disruption of the boundary layer within the seal, effectively increasing the size of the low velocity near-wall region and impacting on the bulk flow velocity. This is typically described

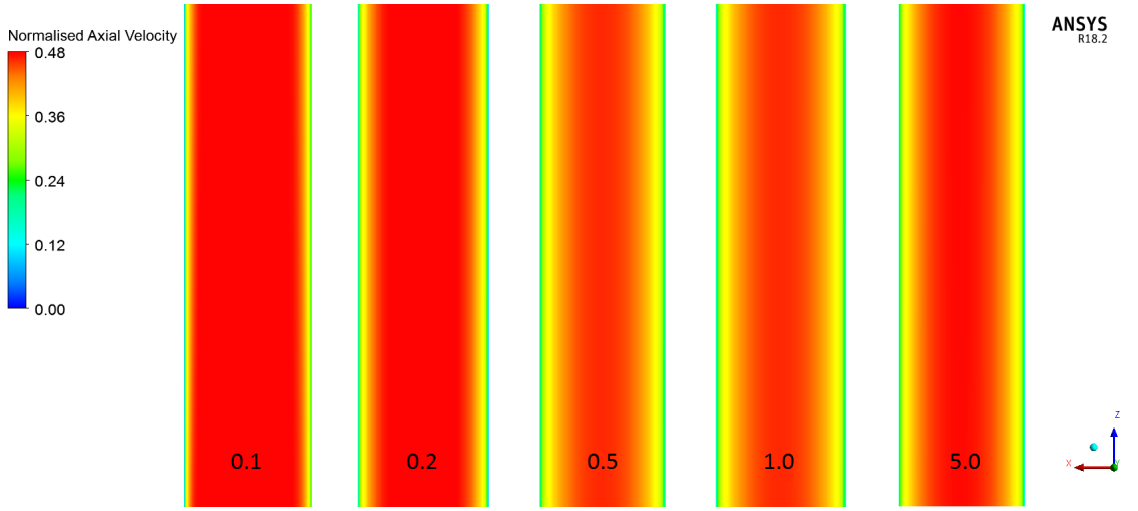

Figure 6.5: Comparison of the mid-seal axial velocity profiles within the sealing face for various surface roughness simulations. The numbers indicate equivalent sand roughness in μm.

as a transition from a hydraulically smooth surface, where the peaks in the surface roughness are contained within the viscous sublayer of the near wall boundary, to a hydraulically rough surface where the roughness peaks extend through the viscous sublayer which then generates local vortices leading to mixing between the near wall and free stream flows. Once these fluid layers begin mixing, viscous and turbulence effects reduce the velocity further away from the wall and therefore the bulk massflow through the seal.

Gülich [1] provides a simple estimation for this transition point using the equations in Table 6.2 which takes kinematic viscosity (ν) and local flow velocity (w) as inputs to determine the critical values of equivalent sand roughness (ϵ). As noted in the table, the calculated values for the LUMEN baseline seal design suggest the transition from hydraulically smooth to hydraulically rough will occur between an equivalent sand roughness of 0.2 and 2 μm which supports the results in both the graph and velocity profiles presented here. The relatively small increase in surface roughness required to enter this transition region makes it an attractive option for improving the performance of the seals and therefore reducing total impeller leakage without greatly reducing the allowance for lateral motion and vibration of the impeller within the pump housing.

Flow Regime	Hydraulically Smooth	Transition Region	Hydraulically Rough
Equation	$\epsilon < \frac{100\nu}{w}$	$\frac{100\nu}{w} < \epsilon < \frac{1000\nu}{w}$	$\epsilon > \frac{1000\nu}{w}$
Baseline LUMEN Seal	$\epsilon < 2.1e^{-7}$	$2.1e^{-7} < \epsilon < 2.1e^{-6}$	$\epsilon > 2.1e^{-6}$

Table 6.2: An analytical approximation of the transition from hydraulically smooth to hydraulically rough flow, and the predicted values for the LUMEN case.

This result was produced only considering the straight baseline seal where the development of the near wall features such as the boundary layer is steady and unobstructed. A more complex seal design, such as a labyrinth seal will generate more disruption to the near wall flow and therefore promote interaction

between the flow and rough surface features regardless of whether it is considered hydraulically smooth or not. It must also be noted that increasing the surface roughness can lead to degradation of other key pump performance criteria such as cavitation inception as the flow is accelerated over the rough wall features, reducing the local pressure and acting as nucleation sites for cavitation bubbles. Without a detailed model of the rotordynamics and cavitation phenomenon within the seals it is difficult to determine if these effects will outweigh the potential benefits of increasing the sealing face surface roughness. However an increase in seal face roughness to beyond the theoretical hydraulically smooth condition should be considered. Additionally, the determination of the transition from hydraulically smooth to rough is not included in the preliminary design tool and may provide a valuable check for rapid iteration of the pump design.

6.3.2 Corner Fillet Radius

The 50 μm seal clearance width of the proposed design magnifies the impact of the 100 μm radius manufacturing limitation placed on rounded corners as the transition from the open clearance gap into the seal if forced to be a gradual one. The influence this has on the leakage through the baseline straight seal is graphed in Figure 6.6 and the corresponding velocity profiles are shown as Figure 6.7.

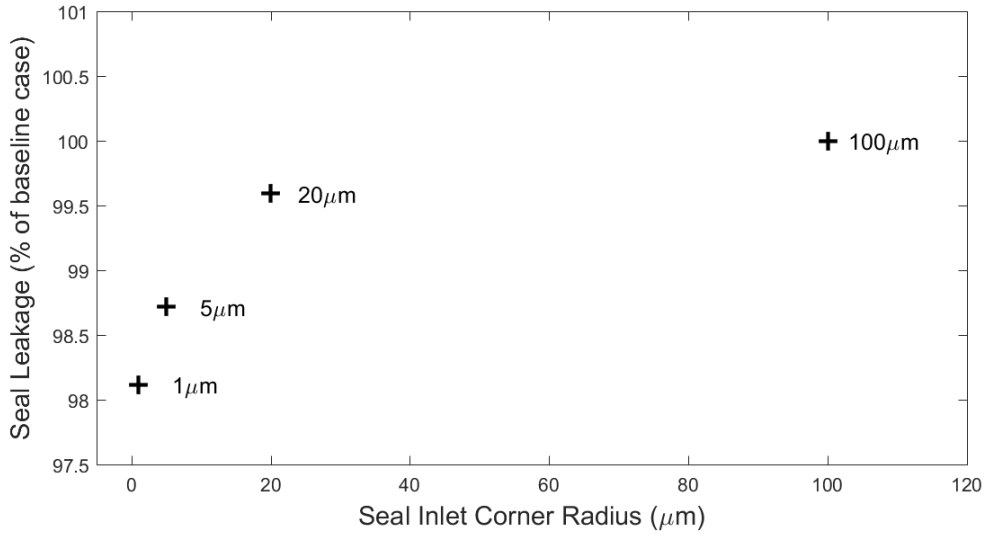

Figure 6.6: Comparison of seal leakage rates for various seal inlet corner radii.

The key mechanism that produces the improved performance with smaller inlet corner radius is flow separation at the seal inlet producing a *vena contracta* effect. In this case the leakage flow is forced around the inlet corner and in the baseline 100 μm model there is no separation. As the corner radius is reduced, the adverse pressure gradient produced at the inlet becomes too great and the flow separates. The separation results in a large region of low velocity as indicated by the blue near-wall areas in Figures 6.7a and 6.7b. This low velocity region reduces the effective sealing clearance width - in the 1 μm case only two-thirds of the physical clearance width contains free flowing fluid -which restricts the leakage flow. It is also apparent from Figure 6.7a that the reduction in effective clearance width produced by the flow separation is accompanied by an increase in local velocity in

the remainder of the seal width near the seal inlet which will partially compensate for the reduction in effective clearance width.

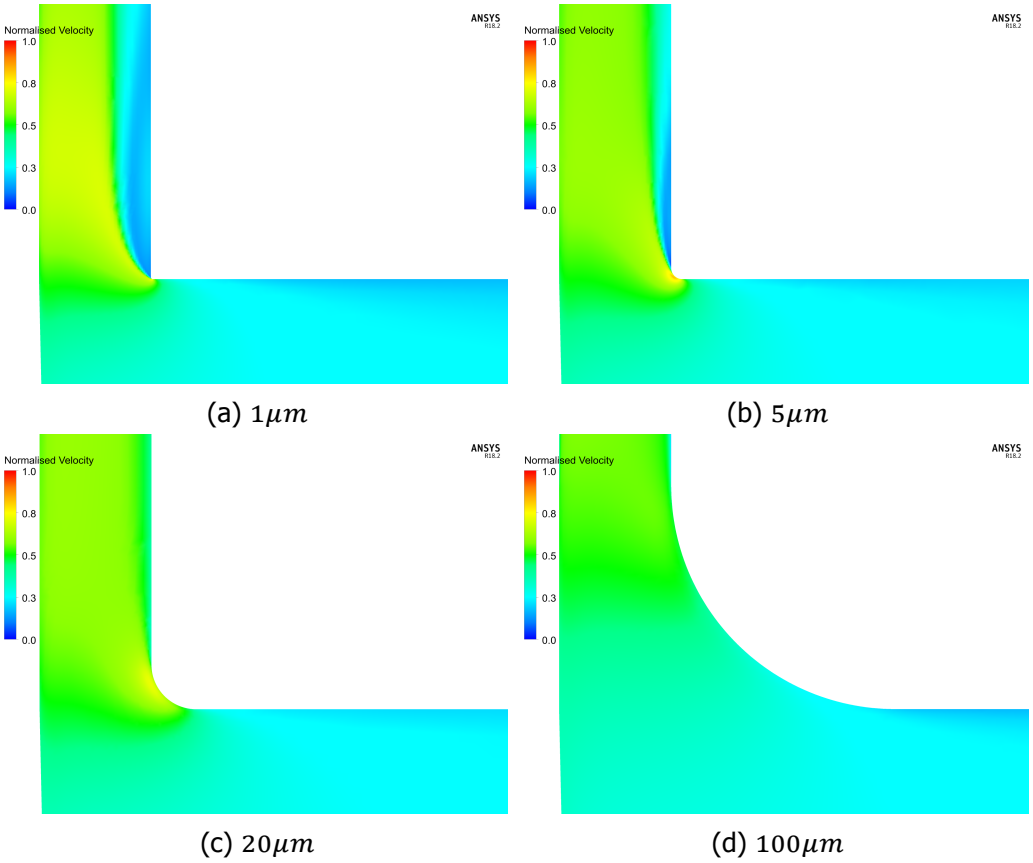

(a) $1\mu m$ (b) $5\mu m$

(c) $20\mu m$ (d) $100\mu m$

Figure 6.7: Normalised velocity profiles for various seal inlet corner radii.

While the approximately 2% reduction in leakage produced by the smallest inlet seal corner radius may seem relatively minor and too small to justify the potential increase in manufacturing cost, a detailed labyrinth seal could have many such areas of flow restriction that will all benefit from the induced separation and *vena contracta* effect. To demonstrate the idealised potential of sharp cornered labyrinth seals a test case simulation was completed without rounded edges (zero radius corners). This resulted in a 50% drop in the leakage flowrate through the seal compared to the equivalent 100 μm design, representing a potential albeit unobtainable 7% increase in pump volumetric efficiency. Therefore this manufacturing limitation should be re-considered for the final LUMEN pump design. The remaining numerical simulations were conducted assuming these manufacturing improvements were not feasible and the original limitations are implemented for all cases.

6.4 Short Straight Seal

Given the relatively large region of low pressure near the exit of the the 7mm baseline seal and the goal of reducing the likelihood of cavitation within the sealing face the first alteration to the baseline design was to reduce the length of the sealing face in an attempt to eliminate this low pressure region. Reduced length seals of 5 mm to 3mm total length were simulated and all resulted in an increase

in total seal leakage flowrate without eliminating the negative pressure region at the seal exit. The increase in leakage was expected as a shorter seal has less impact on the leakage flow however this was also expected to result in a reduced pressure drop through the seal therefore increasing the seal outlet pressure above the vapourisation pressure of Methane. However the results indicate that the seal opening pressure, set at 3 Bar, and rapid expansion of the geometry causes the seal leakage flow to accelerate out of the seal regardless of its length, resulting in the local low pressure. Therefore cavitation remains likely to occur for all straight seal lengths that were tested (from 7mm to 3mm). Changes to this seal outlet region and the impact this has on the seal outlet pressure and therefore the liklihood of cavitation are explored in further detail in Section 7.3. The 5 mm seal is included for comparison in Table 6.1 as the best performing of all reduced length seals.

6.5 Stepped Z Seals

Several researchers have demonstrated the effectiveness of using geometry to promote turbulence and improve the performance of a given axial seal (Stocker [6] and Baskharone [65] are two examples). Stepped seals are a very common axial seal design used in all forms of turbomachinery where straight seals are deemed inadequate. The steps promote flow separation as the geometry forces the leakage to change direction and generate turbulence over the steps. This turbulent kinetic energy cascades, produces local eddies and dissipates into heat - which is modelled by the energy dissipation term (ω) in the chosen turbulence model. The flow then passes into another restricted passage where it accelerates, reducing the local pressure. As the flow exits this second restricted passage it separates or turns again, generating turbulence and the cascade is repeated. The step chambers also arrest the high velocity flow, returning some of the kinetic energy to pressure which also helps to oppose further leakage through the seal. Over several steps this results in a drop in the kinetic energy within the leakage flow which reduces the total leakage. Two step seal designs are considered here; firstly a single step with a large cavity space (figures from this case are shown in Appendix C) as well as a seal with four smaller stepped cavities. The steps were designed with a Z rather than a simple square step to promote core flow separation and increase the generation of turbulence in light of the manufacturing limitations. The velocity profile displayed as Figure 6.8b demonstrates the variability of the flow through each successive step chamber. The first (counting from the seal inlet at bottom of figure) shows separation, high turbulence and no cohesive flowpath which then results in a relatively low velocity being generated through the restricted transition from the first to second chambers. In contrast, higher velocities are produced between later chambers as the lack of separation and mixing within the step causes a clear flow path between passages and therefore a greater retention of kinetic energy through the seal. The changes in local velocity through these transitions is mirrored in the pressure profile shown in Figure 6.8a This indicates that although the multi-step z seal achieves the goal of reduced leakage, further optimisation of performance is possible.

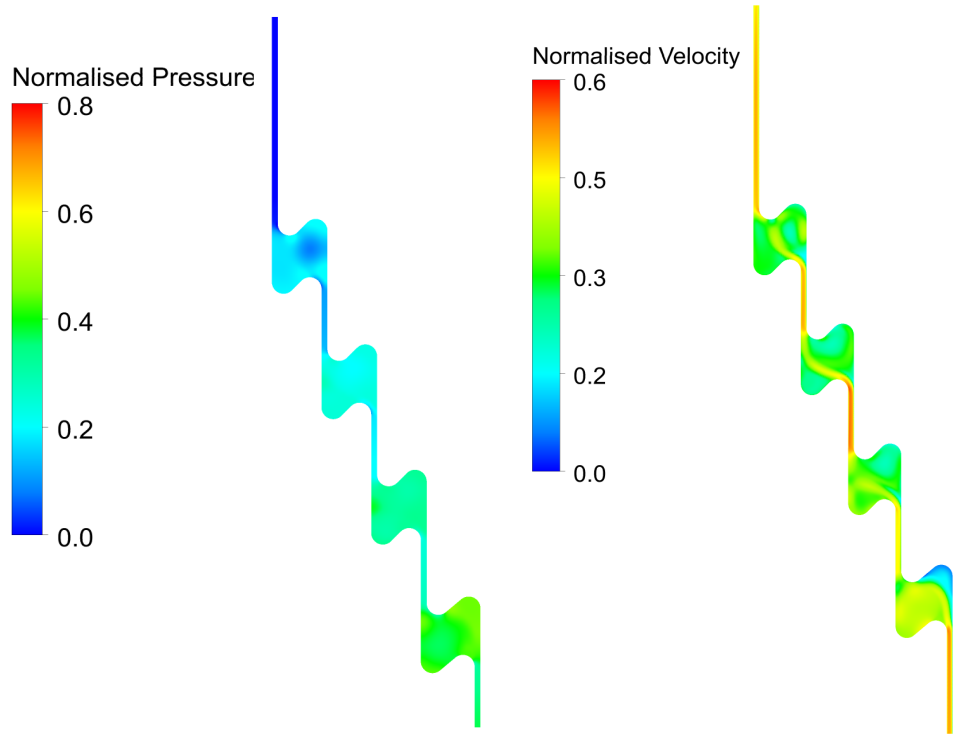

(a) Pressure profile through a multi z-step seal.

(b) Velocity profile through a multi z-step seal.

Figure 6.8: The pressure and velocity profiles for a basic z-step seal. The stepped left hand face is rotating and the right hand face is fixed, leakage flows from the bottom of the figure to the outlet at the top of the figure. Note these scales have been adjusted for clarity.

Both the single z-step and multi z-step seals outperformed the baseline straight seal and demonstrate the potential of relatively simple changes in geometry to restrict a high energy, rapidly rotating clearance leakage flow. The 1.5-2.9% drop in nominal pump flow lost to leakage shown in Table 6.1 which corresponds to a direct increase in potential pump volumetric efficiency is a decisive indicator that the straight annular seal of the baseline LUMEN design should be replaced.

6.6 Labyrinth Seal

A simple evolution of the stepped seal design is the sawtooth labyrinth seal. These are similar to a stepped seal however usually replace one stepped sealing face with a series of protruding teeth or knives to restrict and disrupt the leakage flow and have been implemented in all kinds of high performance turbomachinery. The sharp points of the teeth result in a reduced sealing face contact area, less friction and therefore a lower input torque requirement. Labyrinth seals have been tested in a variety of configurations and some designs are reproduced in Figure 3.1. The research conducted by Stocker used water flow visualisation techniques to demonstrate the effectiveness of this type of seal with a potential reduction in total leakage of 10 - 25% compared to the stepped seal design he used as a baseline [6].

For the sake of reducing manufacturing costs as well as keeping the simulation as simple as possible a very basic sawtooth stepped labyrinth design was chosen

for assessment against the other potential LUMEN seal designs. The shape can be seen in Figure 6.9a with the pressure profile displayed and the general geometry has been selected in accordance with the findings of Chaudhary [66]. Alternative configurations place the labyrinth teeth on the rotating surface, or utilise radially inward steps or both. While these changes impact on the seal performance the configuration shown here was deemed adequate for comparative assessment. The gradual reduction in pressure as the flow passes through each labyrinth chamber can be seen with localised pressure drops around the pointed teeth as the flow is accelerated through the narrow clearance. The velocity profile displayed as Figure 6.9b shows this feature as well but also demonstrates the preference for the bulk of the flow to pass from one chamber to the next without separating from the rotating sealing face (except for the first chamber).

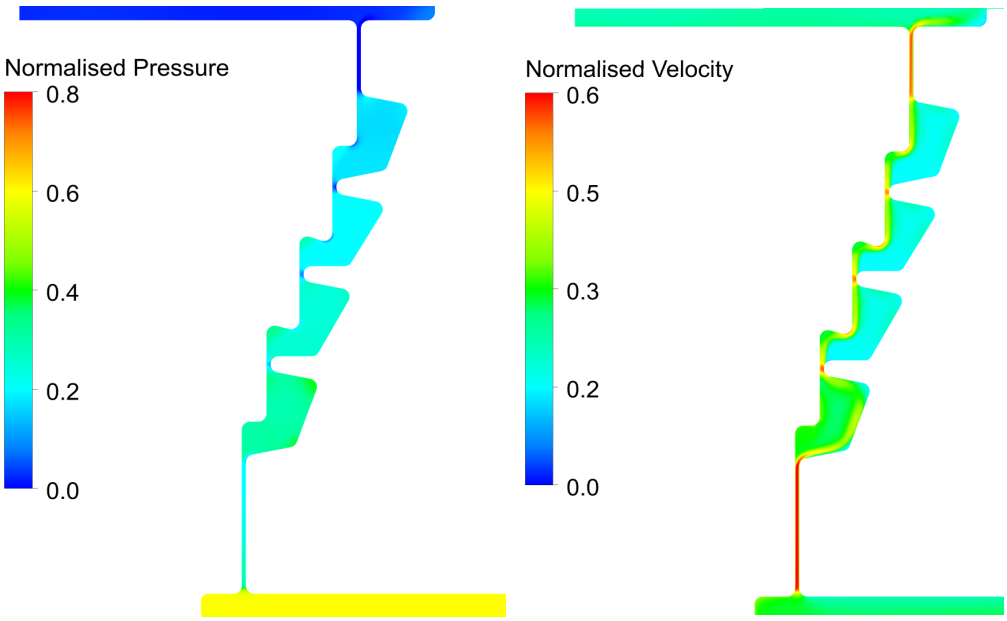

(a) Pressure profile through a basic sawtooth labyrinth seal.

(b) Velocity profile through a basic sawtooth labyrinth seal.

Figure 6.9: The pressure and velocity profiles for a basic sawtooth labyrinth seal. The stepped left hand face is rotating and the right hand face is fixed.

This is attributed partly to the manufacturing limitations on the seal rounded edges discussed in Section 6.3 which allow the flow to remain attached to the rotating walls at sharp corners designed to promote separation and generate turbulence in the labyrinth chambers. Figure 6.10 displays the results of this process, where the first chamber (bottom of image) shows the flow separating from the rotating wall and an anti-clockwise rotation and all subsequent chambers show a clockwise rotation and the flow attached to the rotating wall. The clockwise rotation appears to further suppress flow separation at the chamber entrance and over the step. It is unclear if this is simply a feature of the geometry promoting an undesirable bulk flowpath or if the rapid turning of the bulk flow at the entrance to the first labyrinth chamber and at the seal exit is caused by the longer seal passages before these locations imparting a greater circumferential velocity and therefore radial acceleration on the flow in these areas. The result of the increased internal chamber mixing is a greater pressure drop through the

first labyrinth chamber than through the subsequent chambers and therefore a greater contribution to reduced leakage.

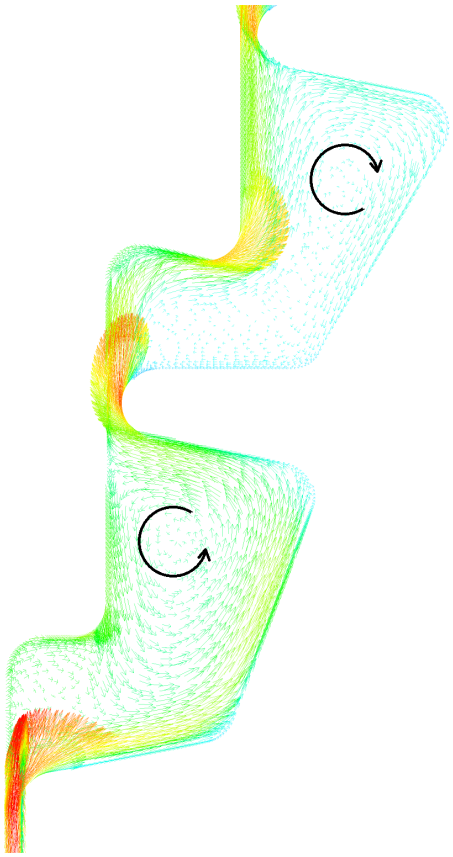

Figure 6.10: Velocity vector plot in the first two chambers of the sawtooth labyrinth seal. Length and colour of the arrows reflect the magnitude of the velocity. Standing rotation direction within the chambers is superimposed in black for clarity.

Labyrinth seals rely on the same fluid dynamics principles as stepped seals to restrict leakage flows; narrow flow paths to accelerate the flow and reduce local pressure; and turbulence generation to dissipate the kinetic energy and recover the static pressure. Flow separation around sharp corners benefits both of these via the *vena contracta* effect in the narrow clearances as well as separation induced turbulence downstream of the narrow clearances. An effective seal employs these features in a complex cascade from seal inlet to outlet as shown by the examples in Figure 3.1 above. Rounded corners, such as those included in the LUMEN design prevent separation in many locations and significantly impair the core function of labyrinth seals. As a result the labyrinth seal implemented here provides a minimal benefit of 0.4% reduction in nominal pump flow lost to leakage compared to the baseline straight seal. Additionally the lack of full separation and mixing within the labyrinth chambers makes it difficult to separate the effects of rounded corners from the specific chamber geometry (step width, chamber length and knife angles) which would be required to use the numerical results to generate empirical loss coefficients (such as ζ_K in Equation 3.5) that could be used in the preliminary design tool.

6.7 Other Designs

Due to time constraints and limited computational resources the depth and breadth of investigation into alternative seal designs was limited to the above options however there are others that warrant mentioning for the sake of completeness. In particular there are several examples of seals designed in a way that effectively pumps the working fluid against the inherent pressure differential within the seal itself. This is achieved using a helical spiral cavity on the rotating surface resulting in a rudimentary screw pump. This increases the effective back pressure in the seal and therefore reduces the leakage rate. Modelling these seals requires a detailed transient simulation that was beyond the capacity of the available computational resources. Extensive experimental testing of helical grooved pumping seals by Childs [24] demonstrated that leakage was comparable to a straight annular seal with rough rotor and rough stator but that helical grooved seals perform better than smooth annular seals while consuming approximately twice the input power. Childs also noted that at high rotation rates the helical seals demonstrate a substantially better rotordynamic stability that the other seals considered.

Hole pattern and honeycomb stator sealing faces are also popular as they work as both a rudimentary swirl brake as well as providing a damping effect for unstable rotordynamic excitations [67],[68]. These seals replace the flat or stepped sealing face of a toothed labyrinth seal with an open sided hole pattern or hexagonal honeycomb design. As the leakage flow moves over this surface it is disrupted by the uneven topology which generates local turbulence as well as providing a column of fluid that can act as a dampener for lateral movement of the impeller within the housing. For this reason they are often referred to as damper seals but have also been shown to reduce the total leakage flowrate by as much as 30% compared to a smooth annular seal [5]. Once a complete rotordynamic analysis or testing campaign of the proposed LUMEN fuel pump is complete the potential benefits and manufacturing costs of these advanced seal designs should be assessed in more detail.

6.8 Discussion

A number of alternative annular seal designs have been assessed with a reduced segment numerical model and compared to the baseline 7mm straight seal in an attempt to improve the leakage performance of the proposed LUMEN fuel pump impeller. All modified geometries resulted in improved leakage performance with the multi-z step seal performing the best with a total seal leakage of 12.9% of the nominal pump flowrate and provides a clear recommendation for change from the current baseline. The leakage performance appears to be greatly influenced by the manufacturing limitations on surface roughness and corner radius and has a particular impact on the performance of the more complex sawtooth labyrinth seal. It is therefore recommended from these results that further effort is utilised on reducing the nominal minimum corner radius or all seal corners to as low as possible as well as increasing the sealing face roughness to above the hydraulically smooth limit to approximately 0.5 μm. Helical pumping seals and hole pattern/honeycomb sealing faces were not modelled but have been demonstrated to aid pump rotordynamic performance and should be considered if rotordynamic stability is proved to be an issue for the LUMEN pump. Lastly, all simulations

predicted a seal outlet pressure below the vapour pressure of Methane, indicating that cavitation in the seal is likely regardless of the seal design.

7

Optimisation Outside the Annular Seal

Outside the annular sealing faces the pump leakage flow must pass from the blade channel exit, into the housing clearance gap and seal inlet area and once past the sealing faces must then re-enter the main flow through a post seal region and re-entry gap. The design of all of these features can impact on the flow within the seal itself as well as contributing to reducing leakage on their own. This is generally achieved by reducing the pressure from the blade exit before it reaches the seal inlet or increasing the pressure at the seal outlet. The desired pressure distribution within this region must also account for the resulting axial force placed on the impeller shroud and hub external surfaces as any imbalances are likely to result in unwanted vibration. In these areas of the pump the surface roughness is somewhat less important than in the seal because the relative size of the boundary layer compared to the bulk flow. In the discussions presented below the shroud clearance is used as an example however the key outcomes are applicable to both shroud and hub clearance gaps. Very few examples were found in the literature where geometries were intentionally used to restrict flow or generate turbulence before the seal inlet or after the seal outlet however a couple of examples were produced to analyse the impact on clearance leakage and pump efficiency that changes in this area might have. The comparative leakage flowrates of the analysed cases are presented in Table 7.1 and the details of each case discussed.

7.1 Pre-Seal Inlet Region

The default geometry of the pre-seal inlet is based on relatively common impeller designs which achieves a modest drop in pressure prior to the seal inlet. Figures 7.1a shows one example of a common design and 7.1b represents the baseline geometry considered for the LUMEN case, with the normalised local static pressure displayed.

Two types of flow manipulation were targeted for numerical simulation - firstly a simple restricted flow path and secondly a geometry intended to promote mixing of the leakage flow to produce turbulence and reduce the pressure before the seal. Figure 7.2 shows the pressure distribution and velocity vector plot for the first case. It can be seen that while there is a drop in pressure as the leakage flow

Design	Leakage (% of total)	Seal Inlet Pressure (Bar)	Mid-seal axial velocity m/s	Mid-seal circ. velocity m/s
Baseline	15.8	81.3	118.7	57.1
Pre-inlet Reduced Flowpath	14.3	77.3	110.9	57.3
Pre-inlet Turbulence Generator	14.4	79.9	113.4	54.2
Swirl Brakes*	17.4	86.8	137.9	18.2
Modified Post Seal	14.2	90.8	115.7	40

Table 7.1: Performance parameters for various alternative seal inlet and outlet designs using the reduced numerical model. * denotes a simulation run on a modified unstructured mesh.

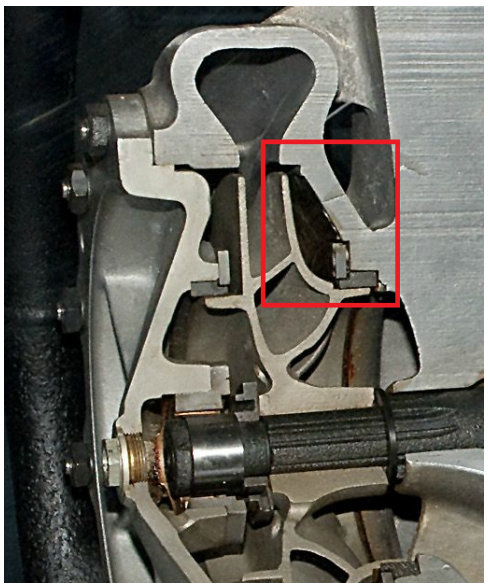

(a) Cut-away section of the V2 rocket engine pump. In red is the clearance gap leading into the seal. Image taken from [69].

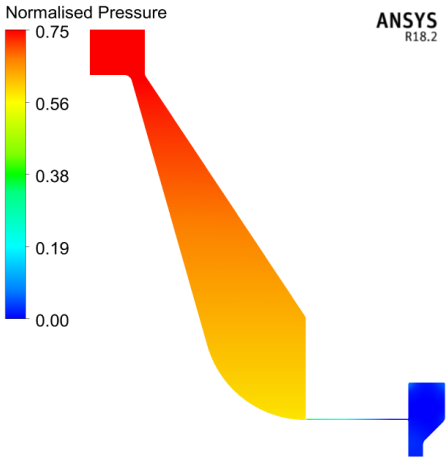

(b) The baseline model for the LUMEN fuel pump has a similar geometry. The pressure profile is displayed as a percentage of the pump global maximum.

Figure 7.1

moves away from the blade exit, this is not noticeably greater than the baseline geometry. This case was simulated with a reduced clearance of 0.5 mm which was calculated to be wide enough to prevent interaction between the shroud and housing boundary layers which should further reduce the clearance gap by the width of the boundary layers. As shown in the results table, the restricted pre-seal flow path produced a seal inlet pressure of 77 Bar compared to the 81 Bar of the baseline case, resulting in a reduction in leakage of approximately 1.5% of the total pump flowrate. The step change in passage width occurs with the same 100 μm limitation on rounded corners and although there is a large change in the bulk flow direction at this location as shown in Figure 7.2b there appears to be very little flow separation. Reducing the radius of these corners is expected increase the drop in pressure through this restricted clearance gap resulting in a lower seal inlet pressure and therefore a reduced leakage through the straight seal.

The second change to the pre-seal clearance geometry is displayed in Figure

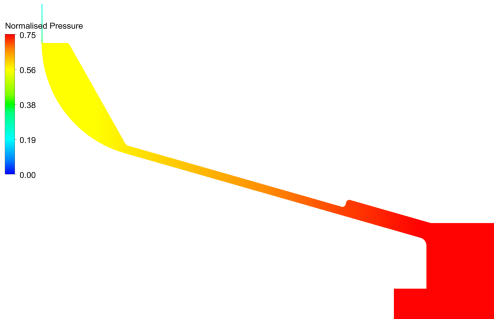

(a) Global normalised local pressure distribution. Note this view is rotated from that shown in Figure 7.1b above.

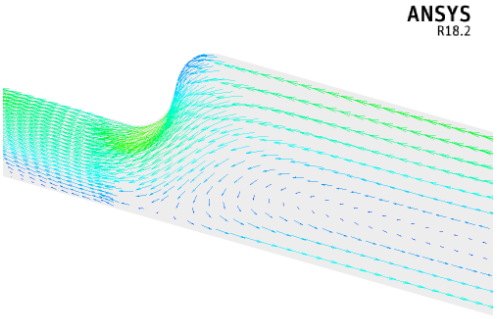

(b) Normalised velocity vector plot at the width reduction point of the altered clearance.

Figure 7.2

7.3 where the pressure profile in the clearance gap as well as on the shroud face is shown. The design was intended to encourage the leakage flow to follow the impeller housing wall around the curved wave-like geometry and then return to mix with the flow close to the impeller shroud wall, promoting back flow towards the blade outlet region increasing turbulence and reducing the pressure before the seal inlet. The results displayed in Table 7.1 indicate that this design change was somewhat successful with approximately 1% reduction in total pump leakage over the baseline case, however the seal inlet pressure results show a minimal change. Figure 7.3b also shows a slight step-change in the impeller shroud wall pressure near the narrow passages. This is relevant for axial thrust balancing of the impeller and discontinuities such as this can lead to instabilities if the leakage flow is not circumferentially uniform.

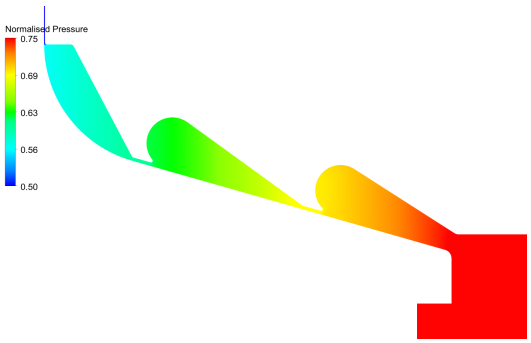

(a)

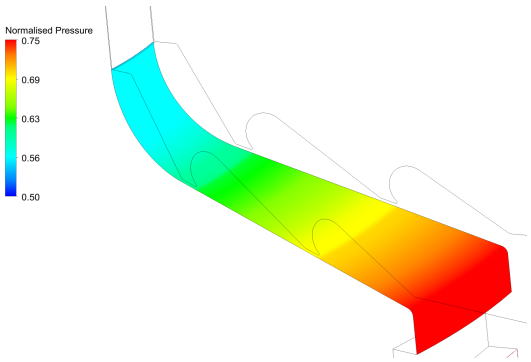

(b)

Figure 7.3: Two images showing the normalised pressure in the wave shaped turbulence generator modified housing clearance design. The reduction in pressure is reflected on the surface of the shroud with clear fluctuations near the narrow sections. Note the reduced scale.

Despite the two positive outcomes described above it must also be noted that this area of an impeller assembly is often used for fixing the sealing faces, floating wear ring or other pump components in place as can be seen in Figure 7.1a. Additionally, San Andres [53] in his notes on rotordynamic stability in annular pressure seals demonstrated that the pre-seal inlet region can be manipulated to greatly influence the impeller cross-coupled stiffness and therefore it is beneficial at this stage in the design of the LUMEN turbopump (without a completely characterised

rotordynamic analysis) to leave this area open for future changes.

7.2 Swirl Brakes

Another relatively common tool for manipulating flow through a pump clearance gap is referred to as swirl brakes. Swirl brakes are intended to disrupt the circumferential flow within a clearance, reducing the total kinetic energy of the leakage before it enters the seal and therefore reducing the total leakage. Acosta et al.[70] also demonstrated the effectiveness of swirl brakes at improving the rotordynamic performance of pump impellers with swirling flows at the clearance seal inlet (such as the LUMEN case) by assisting the damping of impeller lateral motion.

The circumferential non-uniformity of the swirl brake design introduced additional challenges for mesh generation which ultimately resulted in a new mesh being generated. An unstructured mesh with inflation layers on all walls was created and appeared adequate for comparative purposes however no mesh resolution/sensitivity study was conducted. Past research by Baldassarre et al. [71] presents an array of possible swirl brake sizes, shapes and circumferential distributions however it was found that all swirl brakes were effective in reducing seal inlet swirl and were insensitive to optimisation of geometry. Therefore for simplicity, one protrusion per 15 degree segment was chosen (see Figure 7.4), with a thickness of 2°, axial height of 1.5mm and radial depth of 1.5mm and was modelled on the baseline straight seal geometry in addition to a small step-out on the impeller side of the seal inlet to force the flow to interact with the swirl brakes.

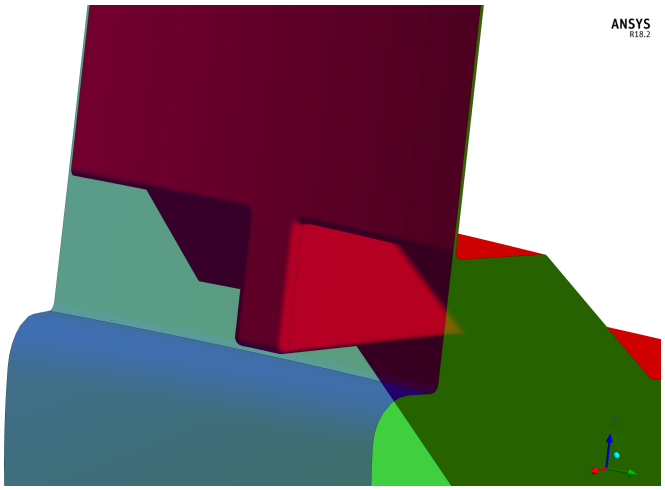

Figure 7.4: A close-up view of the swirl brake geometry. The stationary components, including the swirl brake vane, are in red and the rotating shroud and sealing face is in blue. This geometry represents 15° of the full pump assembly with the green faces defining the periodic symmetry of the domain.

The first result from the simulation of swirl brakes was an increase in leakage flowrate through the seal of 1-2% of the pump total flow as shown in Table 7.1. This was attributed to an effective shortening of the total sealing face length to make room for the swirl brakes. Secondly a comparison of the velocity vectors in the seal shows an approximately 60% reduction in the circumferential velocity from the baseline case when swirl brakes are implemented. An increase in the seal

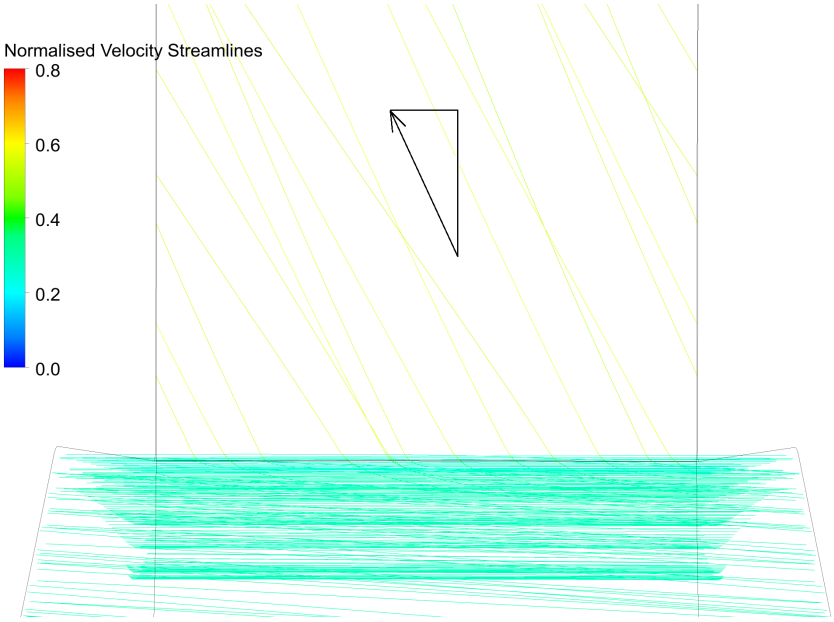

(a)

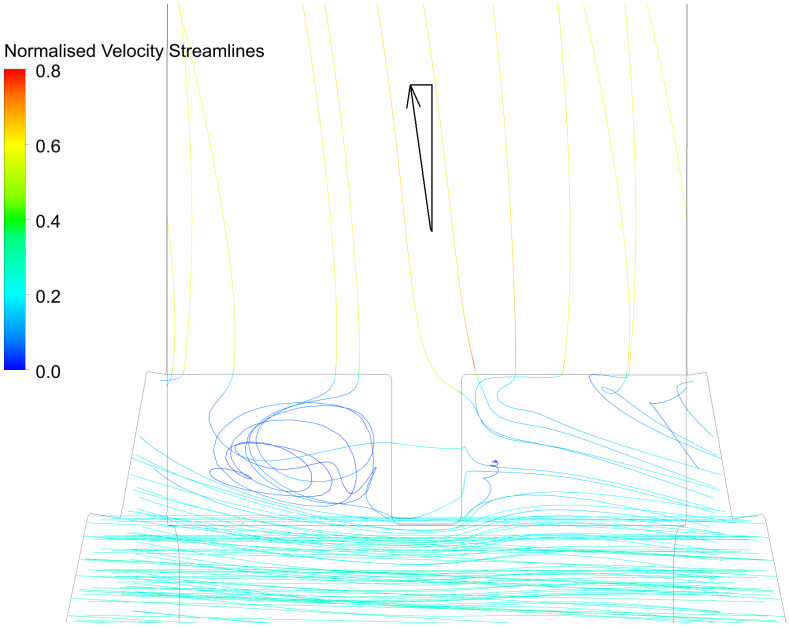

(b)

Figure 7.5: A comparison of the normalised velocity streamlines in the seal and seal inlet region for (a) without swirl brakes and (b) with swirl brakes. The leakage flows from the bottom of figure to the outlet at the top.

axial velocity also results from the use of swirl breaks which reflects the effective reduction in seal length required to accommodate the swirl brakes. Figure 7.5 is a velocity streamline plot which depicts the highly circumferential flow through the shroud to housing gap prior to the seal inlet as horizontal tightly packed green lines at the bottom of figure. Following the typical leakage path in Figure 7.5a, the flow continues from bottom to top entering the seal. The restricted geometry increases the velocity of the flow (streamlines move from green to yellow) however in the baseline case it retains some of the pre-seal circumferential velocity resulting in a diagonal flowpath through the seal as shown by the superimposed black vector.

While the simulation with swirl brakes shown in Figure 7.5b displays the same pre-seal horizontal (circumferential) flow, the velocity vectors are disrupted by the swirl brakes at the seal inlet resulting in a much straighter(more axial) flowpath through the seal itself which is again shown by a superimposed black vector. The difference in horizontal component of this vector reflects the 60% reduction in the circumferential velocity mentioned above. Figure 7.5b provides some insight into the mechanism of how the swirl brakes interact with the flow. In the stationary frame of reference, the flow enters the domain from the right, impacting on the swirl brake surface and then generating a low pressure recirculation region on the left hand side of the swirl brake vane. This mixing and turbulence generation dissipates the circumferential energy in the flow allowing it to enter the seal with a relatively axial velocity.

The results displayed here show that the interaction between these features and the bulk flow can be well represented by a relatively simple numerical model. Despite the increase in manufacturing complexity and additional space required to accommodate them, swirl brakes are a valuable element in the design of a high performance pump impeller. Especially in cases where large rotordynamic instabilities are expected or difficult to counteract by other means. Additionally, geometry and distribution of the swirl brakes investigated here were chosen for model simplicity and further increases in performance may be possible with a more detailed analysis of these factors.

7.3 Post Seal Outlet Region

As discussed in Chapter 6 the initial baseline simulations indicated low pressures near the seal exit which would potentially result in cavitation and all the negative consequences associated with it. One potential method of suppressing this cavitation is to increase the backpressure on the seal by increasing the pump inlet pressure or by manipulating the geometry at the seal exit to increase the seal backpressure independently of the pump inlet pressure. The expansion of the leakage flow from the restricted seal into the open exit region will always result in a drop in pressure, however it was hypothesised that if the flow could be forced to recirculate within the exit region before eventually re-entering the pump inlet flow this might reduce the size of any cavity forming on the seal faces and instead move the low pressure region away from the rotor where it the impact of pressure fluctuations would be less severe. The rounded outlet region corners were intended to promote circulation and potentially sustain a vortex which could alter the pressure and velocity at the seal outlet. The altered outlet path (from straight and wide to narrow and turned) was intended to generally increase the back-pressure on the seal outlet. However the pressure at the re-entry point to the pump inlet (left hand side of Figure 7.6) needed to be far enough above the vapourisation pressure of Methane to ensure no entrained bubbles remained when the flow enters the impeller as this will negatively effect the pump inlet cavitation performance. This lead to the restricted flow path leading

Figure 7.6 displays the alternative geometry (a) that was devised to encourage the recirculation in the seal exit region along with a comparison to the baseline design (b). The increase in pressure in the outlet region has been achieved and greater recirculation of the flow around the outlet region and back towards the

seal outlet is also evident. The impact on the pressure in the seal itself is limited and yet these changes resulted in a reduction in the leakage flowrate of 1.6% of the total pump flow. Unfortunately the model still predicts a region of negative pressure at the seal outlet which remains likely to result in cavitation and therefore may lead to rotordynamic instabilities.

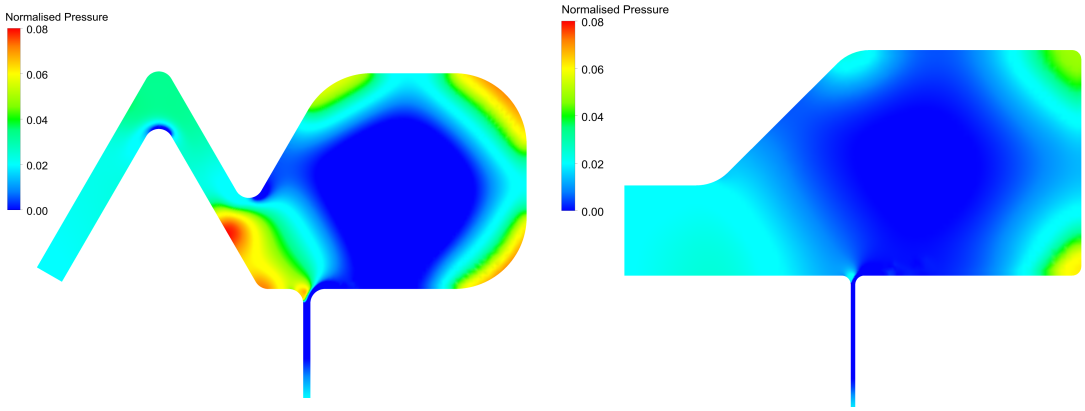

Figure 7.6: Both alternative (a) and baseline (b) designs have a similar velocity and pressure profile at the seal outlet however a tighter vortex is formed in the alternative design. High pressure regions and flow separation in the alternative design result in a restricted passage out of the top clearance region. Note the normalised pressure scale has been reduced for clarity.

7.4 Other Alternatives

There are of course numerous alternative changes that could be used to reduce the leakage flowrate through the seal and improve pump performance that were not investigated here. Some of these warrant a brief explanation:

- Pump Inlet Pressure
  Simply increasing the pump inlet pressure would create a larger back pressure at the seal outlet, reducing the seal differential pressure and therefore the axial velocity and total flowrate through the seal. The 3 Bar inlet pressure was chosen as an ideal case for cryogenic fluid tank storage pressure and as the LUMEN pump will not have an inducer the pump will be exposed directly to this tank pressure. The proposed LUMEN test bench will have the capability of increasing the tank pressure to >10 Bar if required.

- Pump Out Vanes
  Pump out vanes are small blades machined onto the clearance facing side of the impeller shroud that impart a pumping action on the clearance flow when the impeller rotates in the same way that the impeller blade impacts the main flow. These have been successfully employed in several centrifugal pumps [72] and effectively reduce the pressure at the seal inlet, resulting in a lower leakage flowrate. Modelling this would require a transient full pump simulation and an additional blade design and manufacturing process that was deemed unnecessary at this point in the LUMEN pump design.

- Blade Exit Region
  At the blade exit the bulk flow is split in three; the hub and shroud leakage flows which flow around the shroud and into the clearance gaps, and the outlet flow that is collected in the spiral volute casing and discharged from the pump. The geometry immediately at the blade exit can influence the flow split at the blade outlet by restricting the flow path or forcing rapid changes in direction. However it is common to leave a relatively large separation between components in this area to avoid excessive turbulence and the associated pressure fluctuations as well as allowing the impeller enough room to flex under load if required. Therefore this was not considered for further changes in this thesis however a couple of potential alternatives have been superimposed on the baseline design in Figure 7.7. While this may improve the flow of leakage into and through the clearance gaps it will require a complete re-design of the pump volute which is not feasible at this stage of the LUMEN project.

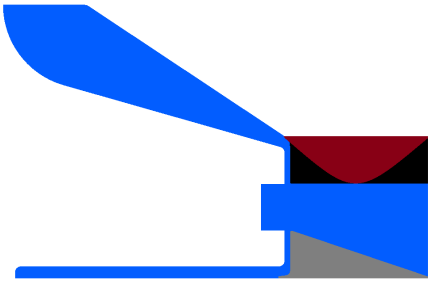

Figure 7.7: Three alternative blade outlet regions are superimposed (black, grey and maroon) on the baseline design (in blue). These will alter the flow into the seals but will require a complete re-design of the pump volute which is not feasible at this stage of the LUMEN project.

7.5 Discussion

Several potential design changes to the pump clearance gap geometry have been assessed with the reduced segment numerical model. Most changes showed a potential to benefit the overall pump leakage performance with the pre- and post-seal geometry changes resulting in reduced leakage flowrate of approximately 1.5% compared to the baseline geometry. The ability of basic swirl brakes to alter the circumferential flow at the seal inlet and therefore benefit the rotordynamic stability of the impeller is also clear however this came at the cost of increased leakage. Although these outcomes suggest the increased manufacturing effort required to implement these changes is warranted, these clearance gap regions and the shroud seal inlet area in particular is often used for pump assembly which can restrict its geometry. Although not a decisive recommendation the modelling results presented here provide an additional option for future pump impeller designers to tackle potential problems such as seal cavitation, rotordynamic instabilities, axial force imbalances or excessive leakage without having to rely solely on changes to the annular seals.

8

Full Pump Numerical Model

The design of the typical centrifugal pump makes them an inherently asymmetric machine and this asymmetry cannot be simulated with the reduced segment model described in Chapter 6. In particular the interaction of the impeller blade outlet with the volute tongue has been shown to produce pressure fluctuations around the impeller outlet [46] as well as influence the leakage flow into the clearance gaps [73]. The impact of the clearance gap leakage on the bulk flow through the impeller as well as on the overall pump performance is difficult to estimate without a complete pump model although a recent numerical study by Veggi et al [74] indicated that increased leakage leads to a direct reduction in pump efficiency as well as head coefficient. These findings were attributed to the development of a recirculation zone at the leakage re-entry point (near the impeller inlet) altering the blade leading edge flow. The authors also noted that the simplified nature of their simulation could introduce non-physical phenomena at the blade outlet as no collector or volute was modelled. Wu et al [60] also noted large interactions between the impeller outlet flow, volute tongue and the pressure distribution within the clearance gaps with particularly large asymmetric forces predicted at lower than design flowrates. All of these phenomena have implications for the LUMEN Methane turbopump design, operation and service life and although a numerical model of the complete pump has previously been completed, leakage flows and the seal design was not considered in detail.

The impeller inlet, blade passage and collector/volute mesh from previous full pump numerical simulations by the LUMEN team have been utilised here without change. Details of this mesh, including a mesh resolution study are outlines by Lindemann [46]. A mesh similar to that described in Chapter 5 was implemented for the shroud and hub clearance gap geometries, with the front clearance re-entering the impeller inlet flow 0.5 inlet diameters upstream of the blade leading edge. The full pump numerical model is shown as Figure 2.5 and a cross section of the baseline model as Figure 8.1. Note in the cross-section image, the impeller shroud is thinner than the reduced numerical model and this is a result of a dimensional error in the previous full pump simulations. This was expected to have a minimal impact on the results of interest and so was not rectified. The final model contains a transition from an unstructured mesh at the pump inlet, to a structured impeller blade channel mesh, to a semi-structured clearance gap mesh and an unstructured collector and volute mesh. Step changes in mesh qual-

ity, grid size and type were avoided using structured inflation layers at the mesh interfaces. Minor mesh size differences remained at the mesh interfaces however the generated pressure and velocity profiles revealed no evidence of mesh influence in these locations.

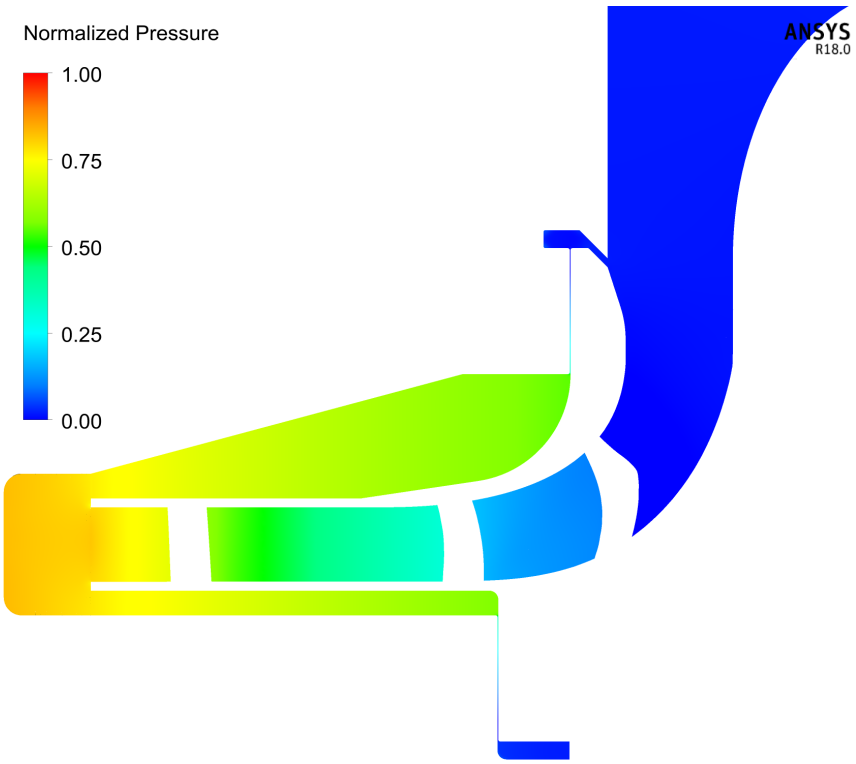

Figure 8.1: A cross-section of one half of the baseline full pump numerical model with the normalised pressure profile displayed. The hub and shroud clearance gaps are shown along with the straight annular seals.

Total pressure at the pump inlet and total massflow at the pump outlet boundary conditions have been used to allow direct comparison to the previous work with an additional static backpressure opening implemented for the hub clearance gap outflow to mirror the reduced numerical model described in Chapter 5. As with the previous numerical model a steady state simulation was implemented due to both computational resource constraints as well as a desire to produce comparable results to the previous work completed by the LUMEN team. As a result, the frozen rotor model has been used to define the interface between the rotating impeller and stationary frame to conserve the velocity and pressure distribution at the impeller outlet as well as allow for the stationary collector and volute geometry to influence the local impeller flow. The alternative mixing plane method that averages flow properties at the interface was considered less desirable as it filters the asymmetric features that are of interest [2]. The previous modelling completed by the LUMEN team utilised the $k-\epsilon$ turbulence model however a recommendation for changing to $k-\omega\ SST$ was one of the key findings and this was implemented here [46].

With these parameters set a number of simulations were completed including a model of the baseline 7mm straight seal design to allow comparison with the empirical and reduced numerical models, the impeller was then rotated to

determine the significance of the blade position on the pump and leakage flow, two alternative operating points were simulated in an attempt to characterise the extent of inlet recirculation at low flow rates and lastly an alternative seal design was then tested for performance comparison to the baseline seal and reduced numerical models.

8.1 Baseline Case

The baseline straight seal full pump simulation is compared to the Gülich based empirical model as well as the reduced segment numerical simulation results in Table 8.1 below. The full pump simulation predicts the lowest total leakage of the models compared and is within 5% of the experimentally validated empirical model. As the most complex model, with the least number of simplifying assumptions and a high resolution mesh the full pump result gives confidence to the findings from the reduced and empirical models. It shows that although outdated and targeted at industrial rather than rocket pumps, the Gülich model does an adequate job of estimating centrifugal pump performance and leakage when provided with suitable inputs and remains a useful tool for rapid and low cost pump design iteration and optimisation. This result also helps to support the validity of the reduced numerical model results which estimated 15.8 % of total pump flow lost to leakage compared to the 13.8% estimated with the full pump model. The discrepancy is partly attributed to the presence of the collector and volute in the full pump model that allows the high energy blade outlet flow to travel around the collector rather than being immediately forced against a high pressure outlet in the reduced model. This results in relatively less flow passing into the clearance gaps.

Simulation Method	Leakage (% of total inflow)	Axial Velocity (m/s)	Seal Inlet Pressure (Bar)
Empirical (Gülich)	14.5	115	85
Numerical - Reduced	15.8	119	81
Numerical - Full Pump	13.8	122	77
Numerical - Full Pump (Alternative)	12.6	110	76

Table 8.1: Comparison of total seal leakage between the basic empirical model and the numerical models at the critical operating point *BP5*.

In addition to the performance predictions presented in Table 8.1, the full pump simulations provide a detailed view of the flow within the clearance gaps and through the seals. Figure 8.1 presented previously displays the increase in pressure as the flow enters the pump impeller (top right of the image) and passes over the first blade (the white gap in the main flow path profile) and eventually exits the blade channel with a much higher pressure. The shroud and hub clearance gaps show a decreasing pressure as the flow moves away from the blade channel exit, eventually returning to the pump inlet pressure after the tight annular seals. Other than the general flow and performance results, the impact that the blade passages, volute tongue and outlet have on the flow within the clearance gaps is of particular interest as large asymmetries can lead to non-uniform forces on the impeller which may result in damaging vibration.

Figure 8.2 is a typical pressure contour produced at the mid-span of the blade channel and continued through the volute. As expected the pressure increases steadily from the pump inlet, through the blade channel and into the collector and volute. The pressure rise begins relatively slowly at the blade channel throat and rises more rapidly as the flow continues through the blade channel as shown by the progressively closer pressure contours. The flow through each blade appears relatively uniform with all blades displaying a low pressure region at the blade leading edge which suggests cavitation is likely to occur here, as well as a localised high pressure region in the volute ahead of each blade trailing edge. The flow around the volute tongue is an obvious source of asymmetry in the impeller but in this figure the impact appears limited to a single blade passage and some fluctuations over the blade leading edges.

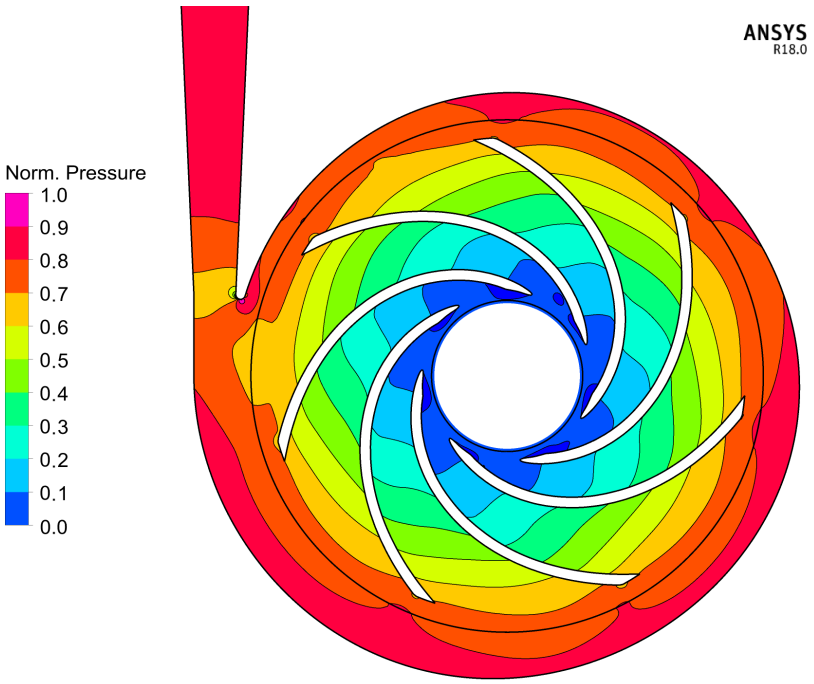

Figure 8.2: Normalised pressure contour plot at the impeller blade mid-span. Note the gradual increase in pressure - shown by the size of the red contour - in the spiral collector moving clockwise from a minimum at the volute entrance to a maximum just before the volute. This asymmetry can not be simulated with less detailed models.

Figures 8.3a and 8.3b are normalised pressure contours from radial cross-sections of the shroud and hub clearance gaps and suggest that the impact of the volute tongue extends all the way to the seal inlet (near the inner-most ring of the images). For example, the variation in pressure at the centre of the images, where the lowest pressure at the seal inlet(shown by the darkest blue contour) coincides with the volute tongue for the hub and is slightly offset for the shroud clearance. There is also a notable variation in pressure around the circumference of the seal inlet which in the worst case produced a pressure differential of approximately 3-4 Bar. Although a less significant contributor to rotordynamic (in)stability than non-uniform blade outlet flow, asymmetry in the clearance gaps does influence the rotordynamics [75]. The asymmetric result is somewhat less severe than reported by Wu et al. [60] which showed a much greater propagation of the volute tongue pressure into the clearance gap, this is partly attributed to the vastly different

pump dimensions and operating conditions being considered here but shows that this phenomena is genuine and not a result of modelling errors.

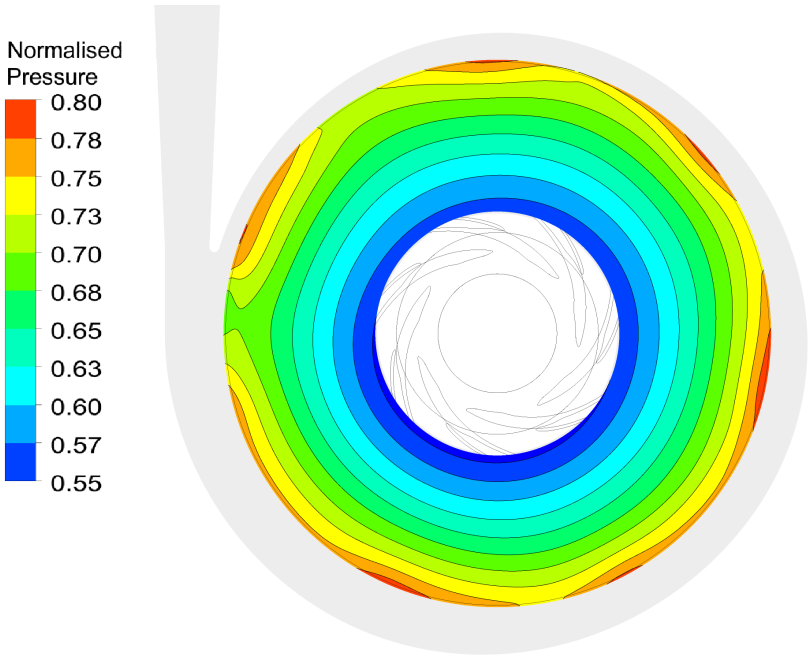

(a) Shroud clearance gap pressure contour.

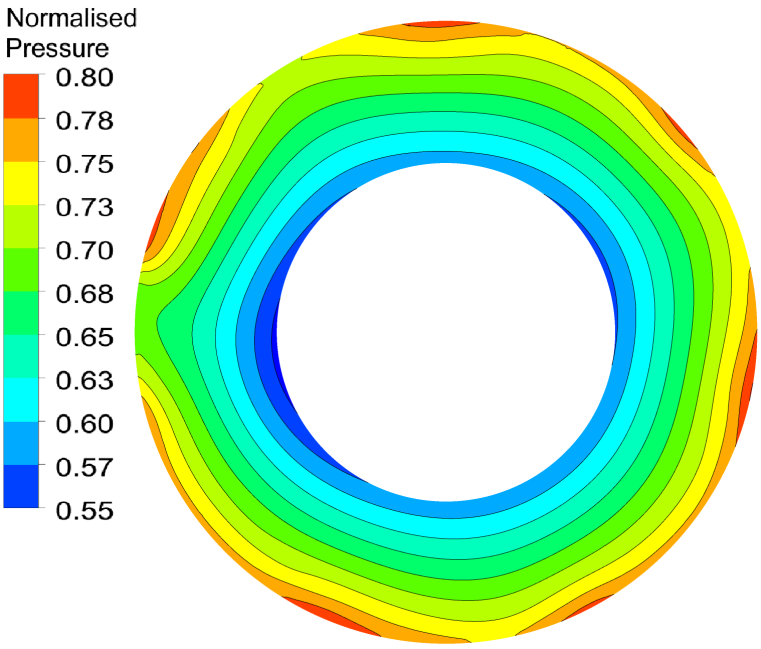

(b) Hub clearance gap pressure contour.

Figure 8.3: Normalised pressure contours for the shroud and hub clearance gaps. Note the reduced scale compared to the mid-span plot in Figure 8.2.

To examine the flow at the seal outlet and how it flows back into the pump inlet, Figure 8.4 was produced and clearly demonstrates non-uniform flow around the circumference of the shroud seal outlet as well as the re-entry gap to the pump inlet. The wavy streamlines indicate a strong vortex structure in the seal outlet clearance that is maintained around most of the top of the image. The

vortex forms in the seal outlet region with the lowest local velocity (shown by the green velocity profile of the inner ring in the image) and eventually breaks down at the region with the highest local velocity. The top side of this image corresponds the higher pressure area of the clearance gap shown in Figure 8.3a, however it accounts for approximately 5% less of the shroud seal leakage than the bottom half. This suggests the higher seal inlet pressure results in greater momentum at the seal outlet which sustains the vortex and prevents the fluid exiting the post-seal clearance, back into the pump inlet. This vortex is unlikely to be stationary within the seal outlet region, however any travelling vortex phenomena requires a transient simulation to model. As the flow re-enters the pump inlet and mixes with the bulk pump inflow, the pressure and velocity becomes relatively uniform which supports the theory that the fluctuations in the seal are due to the clearance gap and ultimately the blade outlet flow rather than disruptions at the pump inlet such as recirculation. In contrast to the shroud seal, the hub seal outlet does not display any vortex structure and the small circumferential variation in mass outflow corresponds directly to the higher pressure areas of the seal inlet displayed in Figure 8.3b.

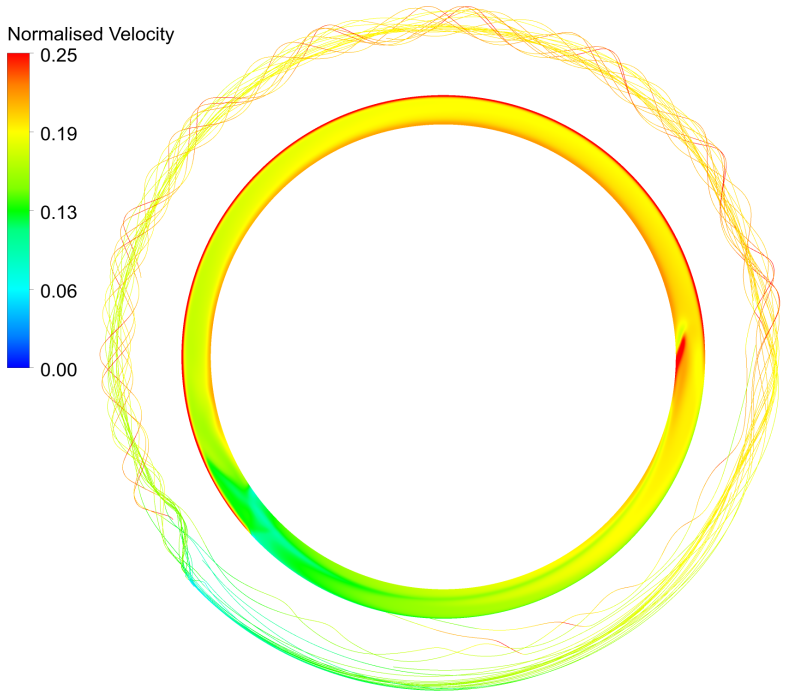

Figure 8.4: A combination plot of normalised velocity streamlines as well as the normalised velocity profile for the shroud seal outlet region. The profile (inner) plot has been scaled down so the data can be shown together. Volute tongue is located on the LHS of the image.

The observations resulting from the baseline full pump simulation demonstrate the strengths of a complete numerical model as well as the limitations of empirical and reduced numerical alternatives. The generation of asymmetric flow features, particularly as a result of interactions with the volute inlet and tongue were not apparent until the complete pump geometry, including clearance gaps was simulated and provide valuable insights into the potential for pressure variations and non-uniform flow that could lead to instability and vibration if not addressed. These results only represent one steady-state simulation at the critical operation

point, and the results will change as the blades rotate and at lower pump mass flowrates where seal leakage re-entry can have an appreciable impact on the inlet recirculation. To examine these effects, further simulations were completed.

8.2 Blade Position

The steady state nature of the full pump simulations mean that the effects of a rotating impeller and blade position in particular are not captured. To provide some insight into these interactions a secondary simulation was completed with a 16° rotation of the impeller relative to the volute tongue. Each of the seven impeller blade channels is approximately 51° wide so the 16° offset represents approximately one third of the transition between identical blade positions. This analysis revealed a negligible change in total pump leakage however was also used to characterise the asymmetry caused by the finite number of blades and determine the need for additional transient simulations. The pressure contour plot presented for the baseline model above is replicated here as Figure 8.5.

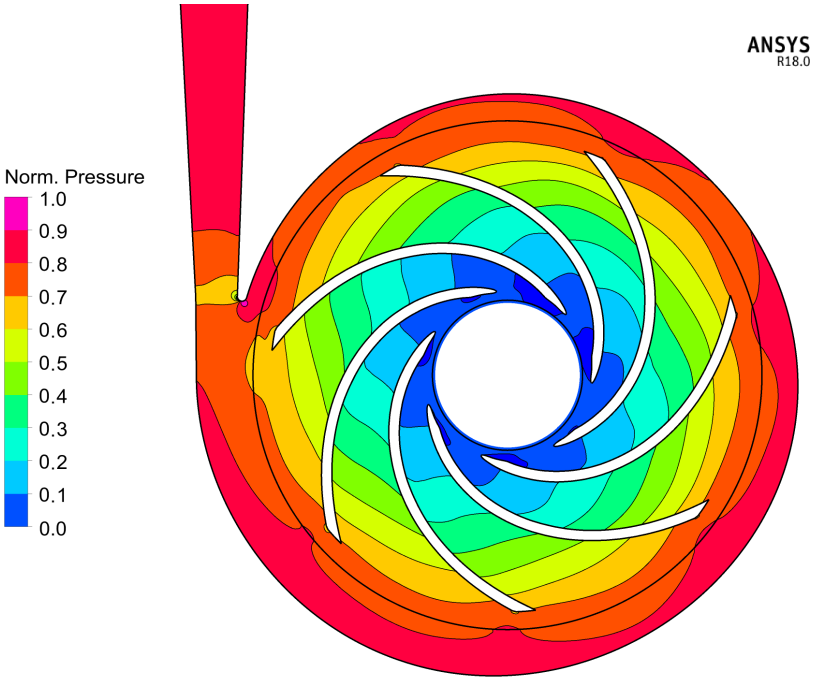

Figure 8.5: Normalised pressure contour plot with the impeller rotated 16° from the baseline case shown in Figure 8.2. The movement of the blade has little impact on the pressure contour resulting in a very similar figure to the baseline case.

Again it shows uniform pressure generation through the blade channel and into the collector and a very similar overall pressure distribution (and calculated performance) to the baseline case. The most evident difference is the size of the low pressure region at the inlet of the blade channel with its outlet approaching the volute. This is expected as the lower blade channel outlet pressure produced by the volute opening propagates through the blade channel and lowers the pressure at the channel throat. Every blade will experience this fluctuation each rotation resulting in oscillating low pressure region or if the inlet pressure is low enough, oscillating cavity generation. Again this result demonstrates the power of a detailed full pump numerical model in simulating asymmetries. The generation of a

high pressure region on the volute tongue surface is also more pronounced in the offset blade case as the blade is now closer to the tongue, restricting the flowpath and increasing the flow interaction with the stationary wall as well as influencing the pressure at the volute inlet. Eventually this results in an increase in pump volute outlet pressure of approximately 0.5% over the baseline case.

Figure 8.6 shows the normalised radial velocity profiles at the impeller to volute interface for the baseline and offset cases, unwrapped onto a 2D plane with both the blade exit channels as well as the shroud and hub clearance inlets displayed. The leading edge positions of the seven blades are indicated as well as the location of the volute tongue for reference. Positive velocity (red) indicates flow moving radially outwards. The first observation from this figure is the non-uniform nature of the velocity at both the blade channel outlets as well as the seal inlets. In particular is it clear that the rough surface on the rotating walls of both clearances are producing a *friction pump* effect that is pushing flow out of the clearance gaps and back into the collector. This result is similar to what would be expected if the pump out vanes described in Section 7.4 were implement and suggests that they would be effective in this application. The second key observation is the impact that the volute tongue has on the local impeller outlet region, with the maximum positive radial velocity produced just before the volute tongue, including large positive radial velocities out of the clearance gaps which is expected given the relatively unrestricted flow path offered by the volute entrance. Just after the volute tongue, as the blade exit flow is restricted by the minimal collector volume, the flow is turned resulting in the maximum negative radial velocity. The transient nature of this asymmetry is evident and has the potential to further degrade the rotordynamic stability of the LUMEN pump. One common solution to this is the implementation of a second or double volute to reduce the circumferential variation in collector pressure and to balance the forces generated by the volute tongue.

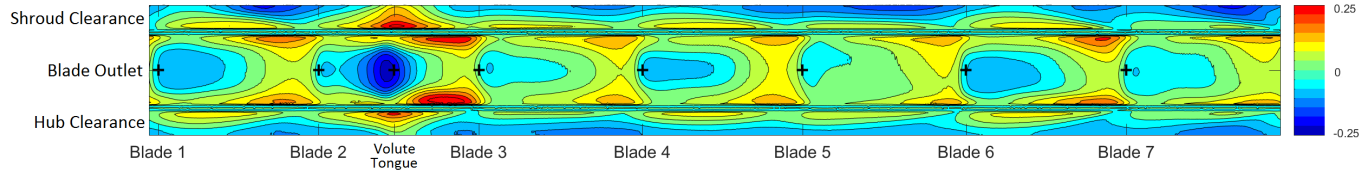

(a) Baseline case, 7mm straight seal at the nominal operating point.

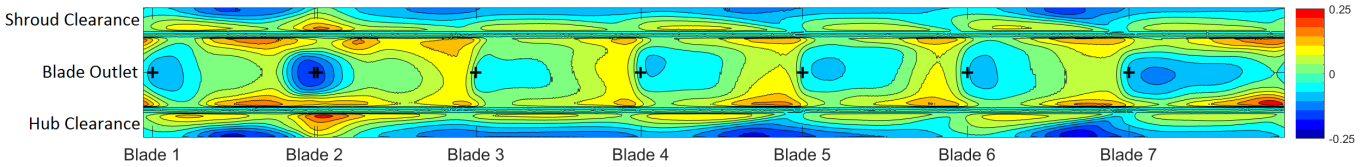

(b) The same operating conditions with the impeller rotated 16°. The blades have been imaged so that the volute tongue is now aligned with *Blade 2*.

Figure 8.6: Normalised radial velocity contours at the interface between the impeller and volute. The blades are *rotating* from right to left. Note this image was produced with MATLAB 2017.

8.3 Low Load Cases

The operating envelope of most centrifugal pumps cover a variety of possible inlet pressures, outlet pressures and target flowrates. In a rocket pump the ability to adjust the pump massflow allows for added capabilities such as throttling and restarting of the engine but introduces new risks and performance loss mechanisms such as flow recirculation. As the LUMEN Methane pump has not previously been modelled with the leakage flow re-directed to the pump inlet a true characterisation of this phenomena was impossible until now. The input parameters for these operating points, as well as the calculated output pressure and total leakage rate is presented in Table 8.2.

Operating Point	Modelled Pump Massflow (Kg/s)	Rotation Rate (RPM)	Pump Inlet Pressure (Bar)	Pump Outlet Pressure (Bar)	Leakage Rate (%)
Critical Case *BP5*	4.00	52000	3	133.3	13.8
Mid-Point Case *BP1*	2.80	43000	3	99.2	14.5
Low Load Case *BP9*	1.43	39000	3	86.4	23.5

Table 8.2: Comparison of three potential operating points and the total seal leakage as a percentage of total impeller flow.

The scaling of developed pressure with rotation rate shown in the above results is in line with expectations as more energy is input into the pump and ultimately converted to static pressure through the impeller and volute. The low leakage rate result for the highest flowrate case is also expected as the higher massflow produces increased velocity within the clearance gaps and sealing faces which promotes mixing, turbulence and greater retardation of the leakage flowpath. Until a critical value of clearance gap massflow is reached the leakage is relatively unobstructed hence the high percentage of leakage seen in the low load case.

8.3.1 Leakage Re-entry and Inlet Re-circulation

The low load leakage results are generally independent of the extent of recirculation at the pump inlet which occurs when the impeller draws fluid into the blade channel but the large pressure differential caused by low inlet massflow results in reverse flow from the blade channel towards the inlet. This is also often seen at the clearance gap re-entry point as shroud leakage flow causes separation of the inlet flow near the shroud wall which extends the region of recirculating flow from the blade leading edge further into the pump inlet. This degrades pump efficiency as energy is expended in drawing flow into the impeller and wasted as the flow recirculates. Recirculation is not accounted for in either the empirical or reduced numerical models presented earlier as neither of these model the pump inlet in detail.

Figure 8.7 displays the development of a recirculation region at the impeller inlet by comparison of the critical load case *BP5* in Figure 8.7a to the low load case shown in Figure 8.7b where the superimposed black arrow tracks the path of recirculation. Both load cases feature high velocity through the seals as indicated

by the large red arrows as well as relatively uniform free stream flow at the pump inlet as shown by the large field of small blue arrows. The sharp corner at the clearance gap re-entry point contributes to the recirculation region by promoting separation of the flow. Also note the general reduction in the bulk flow velocity in the low load case. Given this level of recirculation is only present in the lowest potential load condition, where peak performance is not required this result is not troubling. However, the interaction of this recirculation with the non-uniform seal leakage flow described in Section 8.1 and subsequently on the impeller inlet flow will have implications for the force balance and stability of the impeller. In turn this can impact the expected service life of the impeller as well as the operational efficiency at the low load point [1]. As a well known and well documented phenomena within centrifugal pumps there are several technologies available to help suppress inlet recirculation including restricting inlet orifices, rotating inner shroud rings, inlet diffusers and additional inlet clearance gaps known as recirculation brakes. As the LUMEN engine is not anticipated to operate under such low load conditions for long these design changes appear unnecessary at this stage in the impeller design process.

8.4 Alternative Design Case

To assess the potential performance improvements of an alternative clearance gap and seal design the outcomes of the reduced numerical simulations were reviewed and a single alternative design was produced. This is presented as a pressure profile cross section in Figure 8.8. The multi-z step seal design which produced the best leakage performance in the reduced numerical model has been enlarged to allow more turbulence generation and mixing in each chamber at the cost of reducing the total number of chambers from four to three. The shroud seal inlet region has been left open to allow future modifications if required to address rotordynamic instabilities and the shroud to housing clearance passage width has been reduced to restrict the flow path in line with the results of the reduced model simulations. Two flow obstructions have been included in the hub clearance pre-seal gap to disrupt the flow before it enters the same stepped seal as the shroud clearance. Both seal outlet regions were left open and unrestricted, the hub seal outlet is unchanged and the top seal re-entry to the pump inlet was modified to reduce potential separation of the re-entry flow from the wall and therefore prevent excessive flow recirculation at the impeller inlet under low load conditions. While additional modifications were possible, this design remains relatively easy to manufacture and does not eliminate the potential for further changes if required and is intended to provide . As shown in Table 8.1 above, the alternative seal design provided a 1.2% decrease in total pump flow lost to leakage compared to the baseline straight seal.

The geometry changes result in a lower seal inlet pressure and a greater step change in pressure as the leakage flow passes through each successive seal chamber. The length of the straight section of the seal before the first chamber has also been increased which generates a higher axial velocity into the first chamber promoting turbulence and mixing. Figure 8.9 shows that this high velocity is recovered in the subsequent inter-chamber restrictions so the increased mixing is repeated for all chambers unlike the simplified multi z-step seal that created a

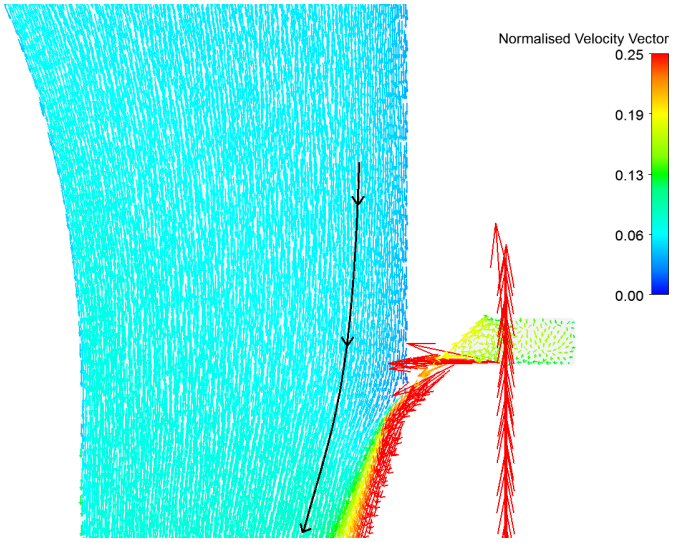

(a) Velocity vectors at the impeller inlet at the nominal operating point *BP5*, 52000 RPM and 4 kg/s.

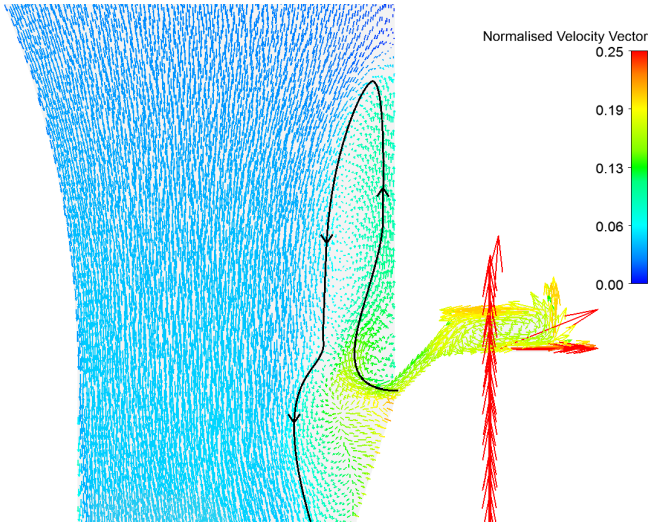

(b) Velocity vectors at the impeller inlet at the low load operating point *BP9*, 39000 RPM and 1.43 kg/s.

Figure 8.7: Normalised velocity vector plots from the impeller inlet where the shroud clearance leakage flow (from right hand side) re-enters the main impeller inlet (out of frame bottom of figure). Black arrows are superimposed for clarity and indicate the general local flow direction.

through-flow in the later chambers and showed minimal mixing. Also note the seal outlet flow remains attached to the rotating shroud wall until it is completely mixed with the bulk pump inlet flow.

The attached flow at the leakage flow re-entry point displayed in Figure 8.9 is reflected in the low load operating point case simulated on the alternative geometry in Figure 8.10a. The reduction in bulk velocity is similar to the baseline geometry case however the large area of recirculating flow is missing and this is partly attributed to the much smoother transition between the clearance gap outlet and pump inlet. This is not the case for the entire alternative clearance gap outlet as Figure 8.10b displays the velocity vectors in a plane at the pump impeller inlet revealing the presence of recirculation in one part of the inlet but a uniform flow in the remainder. Although not displayed here, a similar plot for the

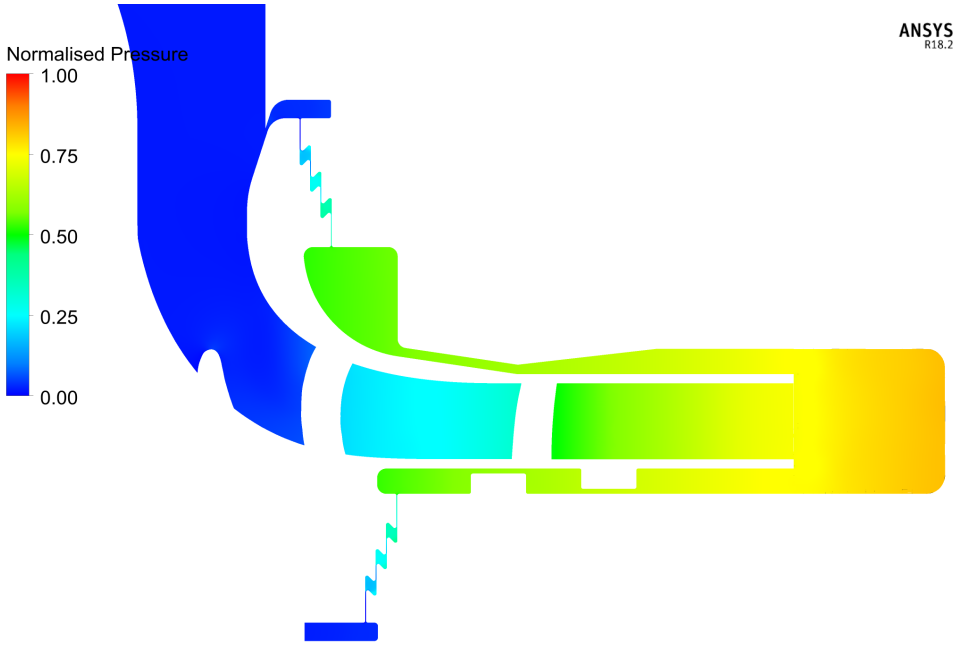

Figure 8.8: Normalised pressure profile of the impeller. Note the changes to the seals as well as the impeller to housing gaps and the pump inlet re-entry point.

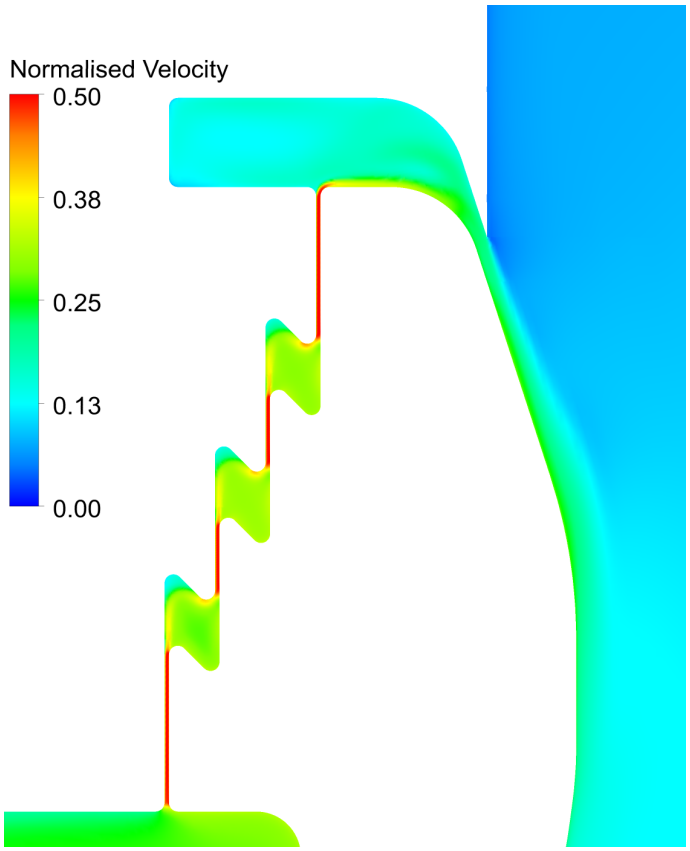

Figure 8.9: Normalised velocity profile of the alternative stepped seal design.

baseline geometry revealed circumferentially uniform recirculation rather than the asymmetric result produced by the alternative design.

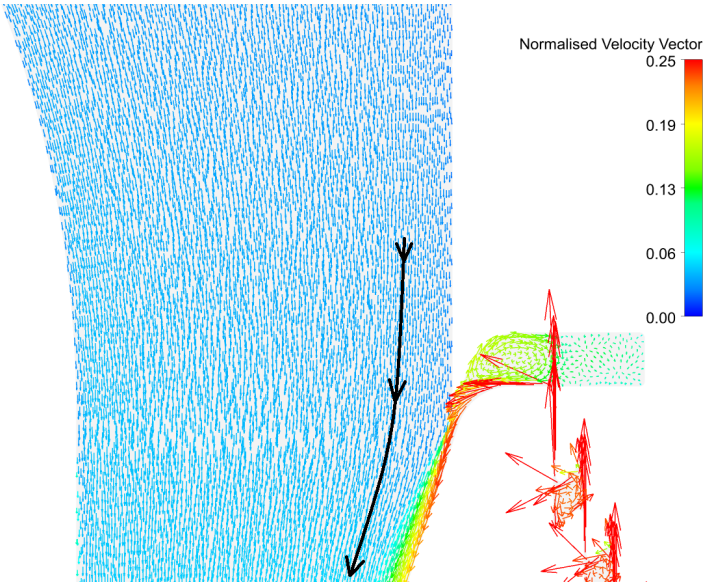

(a) Normalised velocity vector cross section near the impeller inlet for the alternative seal and re-entry design at the low load operating point *BP9*.

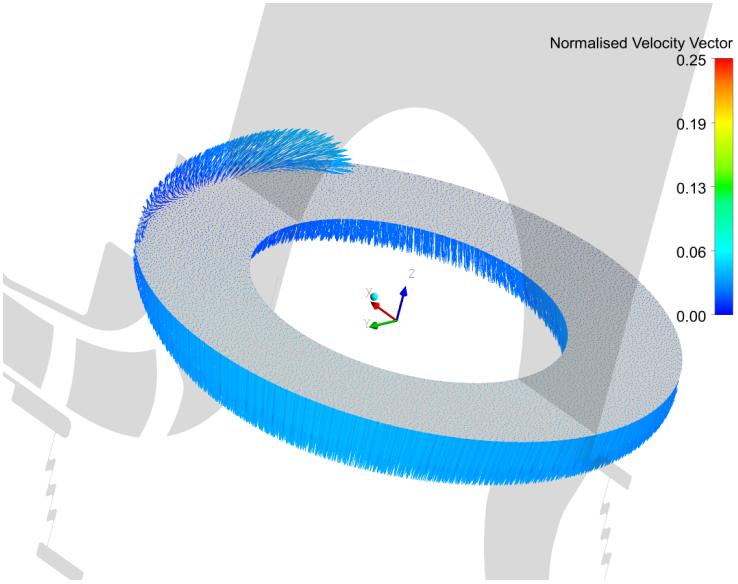

(b) Velocity vector plane near the impeller inlet for the alternative seal and re-entry design at the low load operating point *BP9*.

Figure 8.10: Normalised velocity vector plots. Note the asymmetry of the recirculation shown in image (b) but absent from (a). The volute tongue is located in the positive ***y*** direction in this image - indicated with the green axis arrow.

8.5 Performance Comparison

The development and optimisation of the LUMEN Methane pump impeller design is a key outcome of this thesis and some of the potential changes to the baseline geometry and their expected impact on pump performance have been simulated with the full pump numerical model presented here. Although the alternative seal geometry has shown a reduction in total leakage and this relates directly to an improvement in volumetric efficiency according to Equation 2.5, this is not the only measure of pump performance. An estimation of the power coefficient using

Equation 2.4 provides an insight into the relative power that must be supplied to the pump to achieve the desired output pressure and flowrate for a given operating point and geometry. This comparison is graphed in Figure 8.11 for the three operating points BP5 (critical/high load case), BP1 (mid-point case) and BP9 (low load case) as indicated by the changes in flow coefficient and a comparison is made between the three full pump simulation results of the baseline seal design, the alternative seal design and a comparative case where no clearance gaps or leakage were included in the model at all. As expected the no-leakage model has the lowest power coefficient as no input power is required to drive and circulate the increased massflow created by leakages. Also expected based on the leakage rates presented in Table 8.1 is the slightly higher power coefficient for the baseline seal compared to the alternative design although this is not true for the low load case. This may be due to the difference in wall friction between the baseline and alternative seal designs becoming more significant than leakage at the low load operating point. The no leakage baseline simulation at the low load case did not converge and so has been omitted.

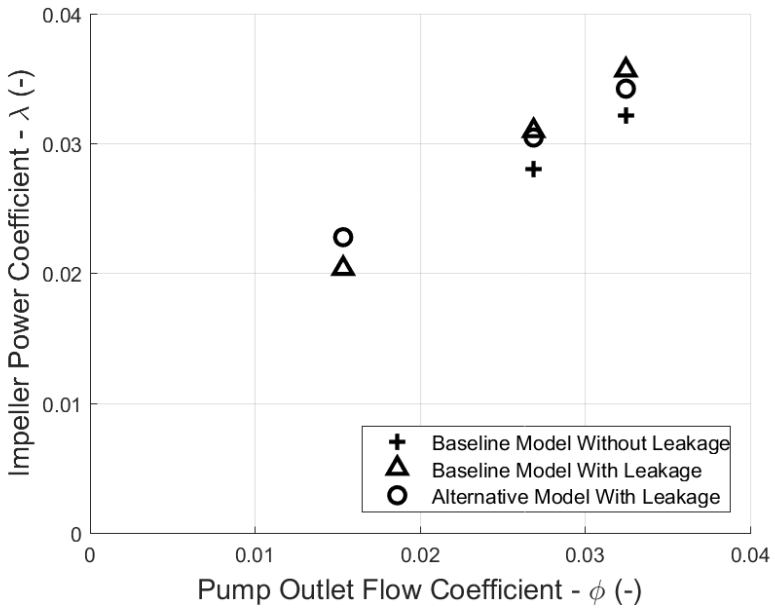

Figure 8.11: The required power coefficient plotted against the pump outlet flow coefficient shows the increase in input power required when leakage is modelled despite the pump providing the same output.

The numerical modelling results also provide an estimation of the total pump efficiency and this is displayed as Figure 8.12. This efficiency plot mirrors both the leakage results and the power coefficient figure and describes a requirement for the pump to work harder to produce the same outputs when leakage is modelled. Also evident here is the slight decrease in efficiency generated by the change to the alternative seal design. This is attributed to the method of estimating the shaft power (P in Equation 2.1) which relies on an area averaged dot product of the absolute velocities and applied forces on the rotating pump surfaces to estimate the shaft power. The increased clearance gap and seal surface area of the alternative design increases the disc friction and therefore reduces efficiency when this method is used. As noted previously the proposed turbine design for

the LUMEN engine has an excess of available power that makes the volumetric efficiency - reflected by the total leakage losses in Table 8.1 perhaps more relevant. Also included in this figure is an estimation of pump efficiency based on the empirical equations from Gülich [1] which models the straight annular baseline seal and estimates a lower efficiency than the numerical models. The discrepancy can partly be explained by the omission of some loss mechanisms from the numerical model such as mechanical losses.

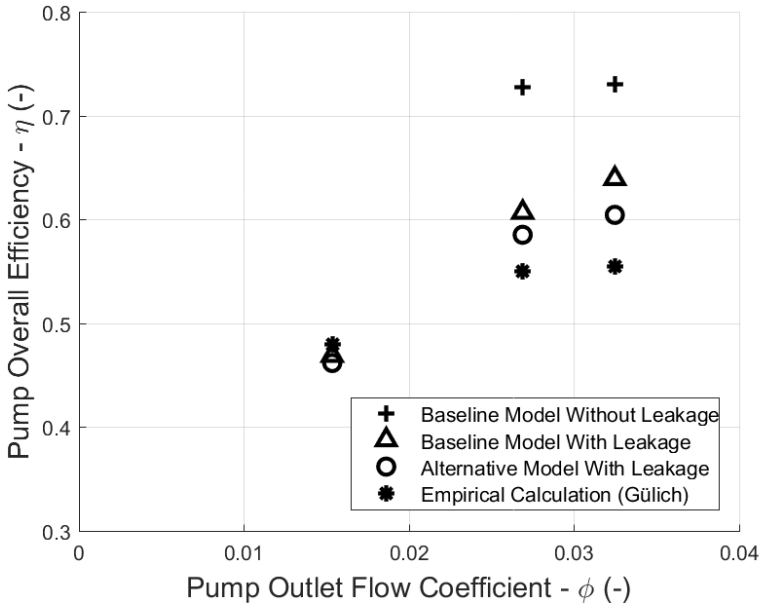

Figure 8.12: Pump overall efficiency as a function of pump outlet flow coefficient. The critical operating point *BP5* is shown on the right. The alternative design shows a slightly lower efficiency than the baseline case which is attributed to the emphasis placed on wall friction in the chosen method of calculating overall efficiency.

8.6 Discussion

The full pump numerical model and the simulation results presented here support the results of the reduced segment numerical model as well as the empirical equation based preliminary design tool. Particularly the comparison of the parameter of interest - leakage flowrate - all models are in close agreement for the critical operating conditions tested. The full pump model demonstrated further value with the capability to model a number of complex flow features and interactions within the pump that the other models simply cannot define such as inlet recirculation, volute tongue interactions, leakage flow re-entry and blade position effects. Some of these findings raise concerns for the design of the LUMEN pump however no issue appeared catastrophically detrimental to the proposed pump operation. An alternative seal and clearance gap design was also presented and demonstrated improvements in most performance parameters over the baseline design, including the main thesis goal of leakage flowrate. The empirical equation model predicts approximately 5-10% worse pump efficiency than the numerical models however this is much closer than previous cases when leakage was omitted entirely [46].

The steady state nature of the model and the lack of a cavitation model prevented a detailed analysis of transient flow phenomena. Additionally the isothermal assumption, although shown by others to provide adequate results [46] does introduce inaccuracies. Several other potential improvements were identified for future attempts to model the LUMEN pump impeller; firstly the use of both structured and unstructured meshes within one simulation should be rectified, secondly the impeller inlet piping should be extended further upstream to ensure a fully developed and uniform inlet velocity profile and thirdly the implementation of a more realistic hub seal outlet boundary condition should be considered. These recommendations will ensure a more successful and accurate model in the future however a numerical model can only provide so much insight and a comparison to relevant physical test data is also recommended to verify the assumptions upon which these models rely to heavily.

9

Cavitation

Cavitation, the term used to describe vapour formation driven by a local pressure drop is an ongoing area of research for many different pumps and industries. Rocket pumps are a particularly challenging application because the requirement for low mass penalises the use of heavy charge pumps and inducers or thick walled high pressure propellant storage tanks and promotes the use of smaller, high speed pumps instead. Therefore an understanding of the development and influence of cavitation is vital to fully optimise a rocket engine impeller and this was attempted with both an empirical and numerical model for the LUMEN Methane pump. Due to limited time, computational resources and an inadequate model the numerical approach proved unsuccessful. However, as a future project is scheduled to begin in this area at the DLR Lampoldshausen, the results of the empirical cavitation model as well as details of the failure of the numerical model are presented to provide some guidance for this future work.

Cavitation is typified by the localised phase change of a fluid from liquid to vapour, due primarily to a drop in local static pressure below the vaporisation pressure of the fluid corresponding to a transition across the purple line from top to bottom in Figure 9.1. This phase change is initiated at nucleation sites - small inclusions in the bulk flow such as trapped gas or particles or small protrusions on the pump surface. Once initiated, a cavity will grow according to the physical properties of the fluid and the surrounding flow, typically in an approximately spherical bubble shape which can combine to form long attached cavities known as sheets, or alternatively remain suspended individually to produce a foamy cloud-like region. These cavities impair pump performance by obstructing flow passages, increasing turbulence and generating secondary flows leading to inefficiencies. The process of bubble collapse produces a high velocity fluid jet, localised heat and a shockwave that has the potential to impact and over time erode surfaces such as a pump impeller blades as well as introduce vibration and instabilities that can damage the impeller and other sensitive pump components. The expansion of the liquid into a gas also produces a local drop in temperature as well as a drop in bulk fluid density resulting from the now two-phase flow and modelling all of these dynamic changes presents several challenges.

There are many different types of cavitation that can occur in a centrifugal pump and these have been extensively documented by Brennen [27]. As the LUMEN pump is shrouded and the full pump numerical simulations showed limited

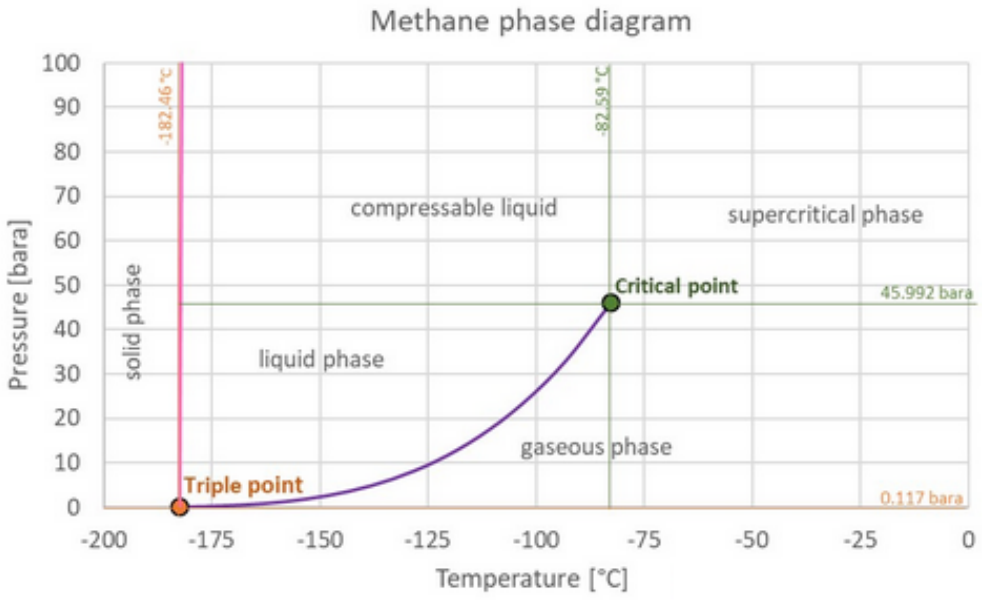

Figure 9.1: The phase diagram for Methane. Note the vapour pressure at the nominal inlet temperature of 114K (-159 °C) is approximately 1.2 Bar. Image taken from Engineering Toolbox [76].

or no recirculation at the pump inlet at the critical operating point, backflow cavitation and tip clearance vortex cavitation are not expected to be significant. Blade leading edge (sheet) cavitation was considered most likely to occur and was modelled in this thesis as well as cavitation between the sealing faces. As the LUMEN Methane pump has been designed without an inducer as described in Chapter 1, the liquid Methane will enter the pump inlet at tank pressure (nominally 3 Bar) before being accelerated over the leading edge of the pump blades. With the highest absolute velocity occurring at the blade tip, an attached cavitation bubble is expected to be established there and grow along the leading edge towards the hub. The rapid increase in pressure through the blade channel will be beneficial in limiting the length of any formed cavities.

The pressure drop through the tight sealing faces is also likely to result in cavitation as noted by all previous numerical models. The transition to full cavitation within the seals is expected to be almost immediate given the modelled pressure profiles and re-pressurisation or cavity collapse will not occur until after the seal outlet is reached. Cavitation within the seals should improve the leakage performance of the seals by limiting the differential pressure across the seal however the unstable and non-uniform nature of cavitation can produce fluctuating forces on the seal faces which may result in excessive vibration and dynamic instabilities in the pump.

Liquid rocket turbopumps must also contend with the added challenge of cryogenic working fluids that have vastly different cavitation properties and performance to common pumped fluids such as water or oil. In general, cryogenic fluids such as liquid nitrogen or liquid hydrogen form 'mushy' or 'foamy' two-phase cavitation regions comprised of numerous small bubbles rather than the intense and cohesive complete vapour cavities seen in water applications. This

is partly due to the much smaller phase density ratio that results in a relatively smaller volume expansion upon evaporation of the working liquid (ρ_l/ρ_v is 1600 for water but 200 for Methane) as well as the much lower thermal conductivity which effectively localises the effect of evaporative cooling upon phase change, impacting on bubble growth.

Given the extremely short service life of a rocket turbopump the gradual erosion of an impeller surface is not critical. In contrast, the degradation of pump performance (namely a reduction in the developed head) is the important measure of the impact of cavitation and the generation of cavitation induced pump instabilities the other major concern. Therefore a tool is needed to estimate both the inception of cavitation within the pump as well as the point at which it begins to undermine overall pump performance.

9.1 Modelling Cavitation

The introduction of a second compressible fluid phase to the already complex flow through a pump invalidates many simplifying assumptions used in the previous numerical models. The mass and energy transfer between the two phases, as well as the changing shape and size of the phase interface and pressure and density fluctuations through both phases must all be accounted for in a complete model of cavitation. In some cases the added complexity of modelling these phenomena is unwarranted and a simplified model is sufficient. Examples of these models are presented and discussed below, however all refer to two parameters to describe the likelihood of cavitation occurring; the cavitation number (σ) and the pressure head required to suppress cavitation - Net Positive Suction Head - Required ($NPSH_r$).

The cavitation number is a non-dimensional parameter calculated with Equation 9.1 as the difference between the machine or flow inlet pressure (p_{1_x}) and the fluid vaporisation pressure at the given temperature (p_v) divided by the fluid dynamic pressure ($\frac{1}{2}\rho u^2$) where the inlet blade tip velocity is taken as the reference velocity (u) in this case. From this equation it is clear that a higher inlet pressure (p_{1_x}) or a lower blade tip velocity (from a reduced rotation rate - u) will result in a higher cavitation number and therefore a lower likelihood of cavitation occurring in a given flow. As the cavitation number is reduced it reaches a point where cavitation begins and this is known as the inception cavitation number σ_i. As the cavitation number is further decreased, the percentage of the flow experiencing cavitation increases until a noticeable drop in performance is reached. This point is referred to as the critical cavitation number σ_c and is usually set at a 3% drop in the total pump developed head. Further reducing the cavitation number continues to degrade the pump performance until complete breakdown of the internal flow structure occurs and this is referred to as σ_{BC}, or the breakdown cavitation number.

$$\sigma_x = \frac{p_{1_x} - p_v}{\frac{1}{2}\rho u^2} \tag{9.1}$$

$$NPSH_x = \frac{p_x - p_v}{\rho g} \tag{9.2}$$

If the cavitation number is known, the inlet pressure required to avoid that

level of cavitation (p_{1_x}) can be directly calculated with Equation 9.1 and then simply converted to the corresponding $NPSH_r$ using Equation 9.2. Most empirical tools focus on producing an estimate of the various σ values that define a pumps cavitation performance. All calculations here consider a pure Methane liquid at 114 K with an instantaneous phase change when the local pressure drops below 1.2 Bar. Gaseous fluid properties are determined (where required) using a real gas property (RGP) table generated from REFPROP [77]. Using pure Methane instead of the more realistic mixed hydrocarbon known as Liquefied Natural Gas (LNG) is considered a neutral assumption as the non-Methane hydrocarbons will have a higher vapour pressure that pure Methane however these impurities can serve as cavitation nucleation sites, effectively lowering the cavitation initiation point for the pump.

9.2 Empirical Modelling of Cavitation

As with pump performance prediction before the advent of powerful computational resources the prediction of cavitation performance was done using empirical equations based on experience, experimental result and a number of user defined coefficients. Several of these models are presented and compared here however as no experimental data is available for validation the accuracy of the models remains in question.

9.2.1 Gülich Model

Although not utilising the definition of cavitation number given above, a empirical approach to determining cavitation performance is included in the Gülich pump design method and is based on Equation 3.1 where the cavitation performance parameters λ_c and λ_w are used to define the impeller inlet geometry. This is intended to produce an inlet diameter that will allow the nominal mass flowrate while remaining cavitation free. The coefficient λ_c accounts for the pressure losses as the flow accelerates at the impeller inlet and is fixed at 1.1 for an axial inflow and the coefficient λ_w accounts for the drop in pressure as the flow is accelerated over the suction surface of the impeller blades. These are combined with the inlet velocity (c_{1m}) and the local relative velocity (w_1) to provide an estimate of the $NPSH3\%$ according to Equation 9.3. The λ_w coefficient is based on the experimental results provided by Gülich and reproduced here as Equations 9.4 and 9.5 where $\beta_{1B,a}$ is the blade inlet angle at the outer streamline and β_{1a} is the flow angle at the outer streamline. These equations demonstrate the emphasis that Gülich places on the blade interaction with the incoming flow when determining the likelihood of cavitation. Table 9.1 displays the results of the various empirical cavitation models including the Gülich equations that predict a pump inlet pressure of 5.7 Bar is required to prevent cavitation from significantly impacting on pump performance.

$$NPSH_r = \lambda_c \frac{c_{1m}^2}{2g} + \lambda_w \frac{w_1^2}{2g} \tag{9.3}$$

$$\lambda_{w_i} = 3(tan(\beta_{1B,a})^{0.9} \tag{9.4}$$

$$\lambda_{w_3} = 0.3(tan(\beta_{1a})^{0.57} \tag{9.5}$$

An equation for predicting the likelihood of cavitation occurring in the pump seals is also provided by Gülich, and is presented as Equation 9.6 where u_{seal} is the axial velocity in the seal and c_{seal} is the corresponding circumferential velocity which estimates a seal inlet pressure of 17 Bar will be enough to suppress cavitation inception. The literature notes that this equation is based on a limited number of test campaigns and its applicability to cryogenic methane cavitation is questionable given the lack of any consideration of thermohydrodynamics which is of particular importance for rough long narrow seals as outlined by San Andres [40].

$$\sigma_{seal} = \frac{p_s - p_v}{\frac{1}{2}\rho c_{seal}^2} = 1.2\left(\frac{u_{seal}}{c_{seal}}\right)^{0.8} \tag{9.6}$$

The numerical simulations described in Chapters 6 and 8 indicate this estimate is too low given that all modelled cases resulted in a seal outlet pressure well below the vapour pressure of Methane - regardless of seal design or massflow.

9.2.2 Ovsyannikov and Chebaevsky Model

Two Russian authors; Ovsyannikov[28] and Chebaevsky[29] have also developed an empirical method to estimate the pressure required to avoid cavitation in a centrifugal pump. The two textbooks use a similar approach to estimate the inlet pressure associated with four cavitation regimes as noted in Figure 9.2 below. These points refer to; 0 - cavitation inception, I - 3% head reduction, II - cavitation breakdown and III - supercavitating conditions. The lengthy set of inputs and equations used to predict these points are reproduced in Appendix D. This method is based on the design of rocket turbopumps and therefore should be better suited to cavitation in high speed applications than the more general Gülich method. However a number of additional geometric values are required as inputs as well as more coefficients with little explanation on how to calculate them. Given that this method is also used to calculate the cavitation performance of inducers the uncertainty surrounding the selection of these coefficients makes the output from the equations somewhat unreliable as inducer fed pumps accept a higher amount of inlet cavitation than non-inducer pumps such as the LUMEN case. Consequently, this model predicts a pump inlet pressure of 3.5 Bar will be enough to prevent major impacts to the pump performance.

9.2.3 Brennen Model

In his 1994 book *Hydrodynamics of Pumps* [27], Brennen described in great detail the various types of cavitation and their potential impact on pump performance, particularly relating to the point where cavitation chokes the flow through the pump - the breakdown cavitation point. Similarly to the Ovsyannikov method, Brennen compares the empirical model to rocket pumps with inducers and notes that some parameters become increasingly inaccurate as the blade incidence angle increases beyond the typical 5-10° found on an inducer. The remainder of the inputs to Equations 9.7 and 9.8 are similar to the Gülich model with a clear focus on the impeller inlet and blade leading edge geometries. Here the required

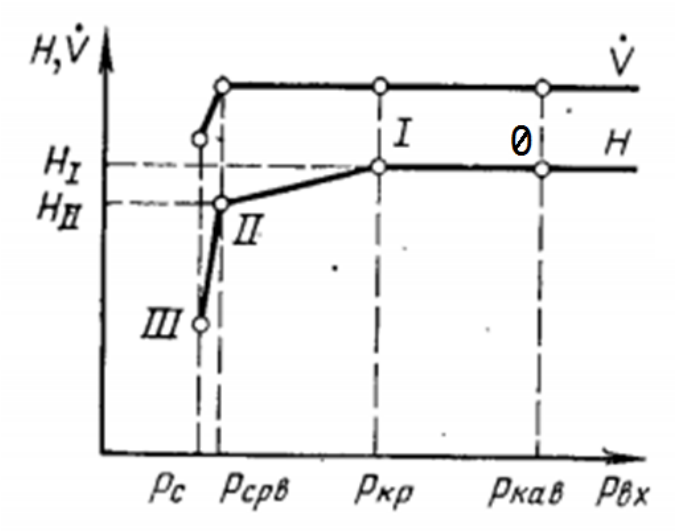

Figure 9.2: A graphical representation of the various cavitation states and their corresponding impact on developed head (H). The empirical equations that describe these points are presented by Ovsyannikov and Chebaevsky and reproduced in Appendix D. Image adapted from [28]

suction head is a function of the breakdown cavitation number (σ_{BC}), the fluid velocity in the stationary frame (v_{m1}), the rotation rate in RPM (Ω), the impeller tip radius (r_T) and gravity (g). The calculation for the breakdown cavitation number includes inputs for the blade angle of incidence (α), the inlet blade angle (β_b) and the relative blade thickness (t_R). Unfortunately no equivalent equation is provided for calculating the 3% or inception cavitation numbers however a value of $\sigma = 0.3$ is suggested for cavitation inception which results in a predicted 6 Bar inlet pressure required to suppress all cavitation which appears optimistic given the relatively large regions of low pressure predicted over the blade leading edges predicted by the full pump numerical model.

$$NPSH_r = ((1 + \sigma_{BC})v_{m1}^2 + \sigma_{BC}\Omega^2 r_{T1}^2)/2g \tag{9.7}$$

$$\sigma_{BC} = \left[1 + 2sin\frac{\alpha}{2}sec\frac{\beta_b}{2}sin\frac{(\beta_b - \alpha)}{2} + 2t_R sin^2\frac{\beta_b}{2}\right] - 1 \tag{9.8}$$

The results of the three empirical cavitation prediction tools are compared in Table 9.1, with the $NPSH_r$ values converted to inlet pressures for ease of comparison. The variation in these results is clear and reflects the different focuses of the chosen equations. For example, the rotation rate of the LUMEN pump is extremely high for an industrial style pump and so the Gülich model predicts cavitation at relatively high inlet pressures. Alternatively the Brennen and Ovsyannikov models were developed for rocket pump impellers and inducers and although the equations account for the blade leading edge geometries and the incidence angle, the characteristic blade sweep that separates inducers from impellers is not included which may lead to inaccuracies such as the relatively low inlet pressures required to suppress breakdown cavitation. The lack of relevant experimental test data of any kind makes it impossible to verify these models for the LUMEN case and they should remain as indicative estimates only. However, taking a conservative approach it appears that the current nominal baseline pump inlet pressure of 3 Bar

will be inadequate in suppressing cavitation with all models predicting cavitation inception well above this value. Additionally, the models that predicted a 3% cavitation number suggest an inlet pressure in the range of 4-6 Bar will be required to ensure that cavitation has a minimal impact on overall pump performance. For the LUMEN project this will necessitate the increase of the testbench supply tank pressure or alternatively a redesign of the impeller geometry or the inclusion of an inducer if a performance degradation greater than 3% is deemed unacceptable.

Inlet Pressure (in Bar) required to avoid:	Gülich Model	Ovsyannikov Model	Brennen Model
Cavitation Inception	32	17	6
3% drop in developed head	5.7	3.5	N/A
Breakdown Cavitation	4.5	1.7	1.7
Supercavitation	N/A	1.4	N/A

Table 9.1: Results of the empirical cavitation models.

9.2.4 Thermodynamic Effect of Cavitation

The expansion of a small fluid parcel into a vapour bubble requires energy that can only be provided by the immediate surrounding fluid. The result of this is a cooling of the surrounding flow at the point of cavitation initiation as well as a localised heating of the fluid at the point of bubble collapse. This is referred to as the thermodynamic effect of cavitation and is particularly relevant for cavitation in cryogenic fluids that operate close to their boiling points. The localised cooling effect helps to suppress further cavitation by moving the fluid left in the phase diagram (Figure 9.1) - away from the phase change line and this has been demonstrated with extensive numerical models ([78],[79] and[80]) and some experimental testing campaigns ([36] and [81]).

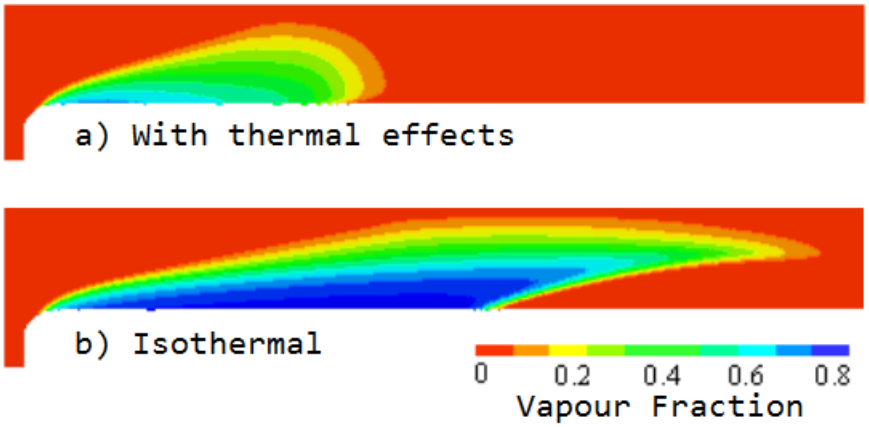

Figure 9.3: The typical representation of the impact of thermal effects on a cavitating flow is with volume fraction comparison as shown here from an ogive simulation of liquid nitrogen. Image adapted from Shi and Wang [79].

Although typically displayed as a contour of vapour volume fraction as in Figure 9.3, the effect can be estimated empirically by calculating an offset to the

cavitation number at a chosen operating point and several researchers have developed equations for this purpose including Utturkar, Brennen and Gülich which are compared here. In these equations the subscript l refers to the liquid phase and subscript v refers to the vapour phase. R is the universal gas constant, r_T refers to the blade tip radius, T is the nominal bulk flow temperature, H_v is the latent heat of vapourisation, α is the thermal diffusivity, C_{pl} is the specific heat at constant pressure of the liquid, n is the rotation rate in rad/s, β_f is a correction factor set to 5e-6, a is an experimentally defined correction factor, H_{ref} is the reference height set to 1m and Pr is the Prandtl number.

Utturkar:

$$\Delta\sigma = \frac{dp_v}{dT}\frac{\Delta T}{0.5\rho_l u_\infty^2} \tag{9.9}$$

Where ΔT is calculated using the Clausius-Clapeyron equation:

$$\Delta T = T_\infty - \frac{1}{\left\{ln\left(\frac{p_{in}}{p_v}\right)/\left(\frac{H_v}{R}\right) + \frac{1}{T_\infty}\right\}} \tag{9.10}$$

Brennen:

$$\Delta\sigma = \sigma_0 \frac{2\beta_f \Sigma^2}{r_T^2 n^3\, \phi_{(\sigma_0)}} \tag{9.11}$$

Where Σ is defined as the thermal effect parameter by the equation:

$$\Sigma = \frac{\rho_v^2 H_v^2}{\rho_L^2 C_{PL} T_\infty \alpha_L^{0.5}} \tag{9.12}$$

Gülich:

$$\Delta NPSH_r = a_f\left(\frac{\Delta P}{\rho_l g H_{ref}}\right)^{0.58} \tag{9.13}$$

Where the temperature and pressure are again related by the Clausius-Clapeyron equation as:

$$\Delta P = \frac{\rho_l \rho_v}{\rho_l - \rho_v}.\frac{H_v \Delta T}{T_\infty} \tag{9.14}$$

and,

$$\Delta T = 2Pr^{0.67}\frac{H_v \rho_v}{C_{PL}\rho_l} \tag{9.15}$$

The Gülich equation results in a reduction in required inlet pressure of only 0.1 Bar which appears inadequate when compared to the literature results from Goncalves [78] and San Andres [40]. In contrast, the Brennen and Uttukar models suggest a reduction of required inlet pressure to suppress cavitation between 0.8 and 1 Bar. Although Gülich and Uttukar rely on an energy balance defined with the Clausius-Clapyeron equation, and predict a very similar local temperature change the calculation for the change in inlet pressure by Gülich is focused on changes within an individual bubble and depends greatly on the experimentally derived factor a_f, which although is defined for water and common hydrocarbons is not given for cryogenic applications such as this.

9.2.5 Discussion

Empirical modelling of cryogenic fluid cavitation through centrifugal pumps is a limited field of study largely due to the advancement of computers and difficulty of capturing the inherent complexity of the problem with simplified equations and coefficients. The available models detailed here produced varied results for the proposed design however all predict cavitation to have some impact on performance at the nominal baseline inlet pressure of 3 Bar which is an expected result due to the high rotation rate at the critical operating point (52000 RPM) and the lack of an inducer. As the LUMEN engine will be operating in a testbench with the ability to increase the propellant tanks storage pressure to >10 Bar the findings do not warrant drastic changes to the impeller design at this stage and a moderate increase in inlet pressure to approximately 6 Bar is anticipated to suppress the majority of negative impeller inlet cavitation effects based solely on the findings of the empirical equations. The likelihood of cavitation within the annular seals appears more difficult to suppress and significant changes to the seal geometry may be required however a complete cavitation and rotordynamic model should be completed to accurately characterise the impact of cavitation in the seals first.

9.3 Numerical Modelling of Cavitation

In the early 20th century, Lord Rayleigh expanded the Navier-Stokes equations to include a model for empty spaces within a fluid and how they are influenced by the pressure field in the bulk flow. This became known as a bubble-dynamics approach to cavitation modelling and was later expanded by Plesset to include the effects of viscosity, surface tension and a non-uniform pressure field ([82], [83] and [84]). The resulting Rayleigh-Plesset equation is widely used in CFD packages today as Equation 9.16 where the change in cavity bubble radius (R) with respect to time (t) is dependant on the vapour pressure (p_v), liquid/vapour interface surface tension coefficient (γ), liquid density (ρ_L), liquid volume fraction (F_L) and the local pressure (p).

$$R\frac{d^2R}{dt^2} + \frac{3}{2}\left(\frac{dR}{dt}\right)^2 + \frac{4F_L}{R}\frac{dR}{dt} + \frac{2\gamma}{\rho_L R} = \frac{p_v - p}{\rho_L} \tag{9.16}$$

Within the chosen numerical modelling tool this equation is simplified by neglecting the second order term and the surface tension term (refer to [85] for details of the simplification) to isolate a function describing the mass flow between fluid phases as noted in Equation 9.17. This equation replaces the bubble radius with the initial radius of the modelled nucleation sites (R_{nuc}) which is initially set to 1 μm, and introduces some other user defined values for the nucleation site volume fraction (F_{nuc}) set to $5e^{-4}$ and the empirical factor X which is used to specify the rates of condensation and vaporisation which are set to 0.001 and 200 respectively based on the numerical study completed by Liu [86].

$$\dot{m}_{fg} = X\frac{3F_{nuc}(1 - r_g)\rho_g}{R_{nuc}}\sqrt{\frac{2}{3}\frac{|p_v - p|}{\rho_L}}sgn(p_v - p) \tag{9.17}$$

The cavitation model was initially implemented using the full pump mesh and non-cavitating simulation results as initial conditions and a K-ω SST turbulence

model. Unfortunately the full pump mesh proved to be inadequate primarily due to the change from unstructured to a structured grid at the inlet causing localised fluctuations in calculated fluid properties that lead to divergence of the simulation. A simplified domain was then produced in the form of a converging-diverging venturi nozzle and cavitation was implemented using fixed fluid properties and specified pressure boundaries at the inlet and outlet. Although the simulation became more stable, the results produced were unrealistic with excessive velocities and large sections of the domain dominated by vapour flow.

Analysis of these results files provides some information on potential causes and therefore avenues for future improvements. The Rayleigh-Plesset equations and the specified coefficients are generally designed and validated for water, which shows long cohesive cavities compared to the foamy nature of cryogenic fluids. When the fluid properties of Methane are implemented, these parameters appear to underestimate the reverse transition of vapour back to fluid, resulting in a large percentage of the flow domain containing mostly vapour. The computation then predicts an exceptionally high pressure and speed of sound in order to meet the domain outlet conditions, eventually over-ranging the fluid property tables. The simulation continues by clipping the fluid properties to the largest value in the table but fails to return to a realistic value and never converges upon a solution.

Given the extremely large limits of the RGP table, use of robust boundary conditions and the lack of any localised mesh generated instabilities (on the simplified venturi domain) it appears the computational issues were related to an oversimplification or misdirected use of the cavitation modelling equations. This conclusion is supported by the successful simulation of a cavitating water flow using the same mesh and boundary conditions (results are presented in Appendix E). Liuzzi [87] attributes similarly unstable results to the nature of the RP equation that assumes each bubble is isolated within a continuous cryogenic fluid domain. As the bubbles grow and begin to interact and eventually dominate the local fluid region this assumption is no longer valid. Liuzzi artificially limits the bubble size below a critical value to ensure a valid model however this option was not available in the chosen modelling software. Mani [88] also presents a detailed investigation of the influence of RANS based turbulence models on cryogenic cavitation simulation and produced successful simulations based on a R-P equation which includes the omitted surface tension and second order terms from Equation 9.16 as well as additional terms to describe the influence of non-condensable gases and thermal effects which as noted previously are much more important for cryogenic fluids than they are for water. These additional terms are shown in square brackets as the second and third terms respectively on the RHS of Equation 9.18 below. In the additional terms p_g refers the non-condensable gas pressure, T_b the bubble temperature, R_o the gas bubble radius and Σ is equivalent to the thermal effects factor described as Equation 9.12.

$$R\frac{d^2R}{dt^2}+\frac{3}{2}\left(\frac{dR}{dt}\right)^2+\frac{4F_L}{R}\frac{dR}{dt}+\frac{2\gamma}{\rho_L R}=\frac{p_v-p}{\rho_L}+\left[\frac{p_g}{\rho_l}\left(\frac{T_b}{T_\infty}\right)\left(\frac{R_o}{R}\right)^3\right]+\left[\Sigma\frac{dR}{dt}\sqrt{t}\right] \quad (9.18)$$

The necessity for a specific cryogenic targeted equation set is further supported by researchers such as Utturkar [32], Tseng et al. [89] and Senocak and Shyy [37] who developed successful cavitation models that included the simpli-

fication of neglecting surface tension and viscosity effects but specifically target features seen in cryogenic cavitation experiments. This is usually done with a revised definition of the vapourisation and condensation process through customised source and sink equations similar to Equation 9.17, however the limited timeframe of this thesis precluded the implementation and comparison of these within the LUMEN application. Although the models still rely upon a number of user defined values they demonstrate the possibilities of numerical cavitation models when they are formulated for a particular purpose.

Despite the failure of the cavitation models within the full pump simulations, some indication of the likelihood of cavitation occurring within the pump is still possible. The Eulerian theory of cavitation suggests cavities will form at the instant the local static pressure drops below the fluid vapourisation pressure and this can be visualised on the full pump numerical model as shown with the black coloured regions in Figure 9.4. As expected, the low pressure regions are concentrated at the blade leading edges however they do not appear to entirely block the blade passage, suggesting that impeller stall - where cavitation prevents all flow - is not likely at this operating point. While the use of negative pressures to model these results makes them inherently non-physical they are still useful for pump designers seeking to improve cavitation performance.

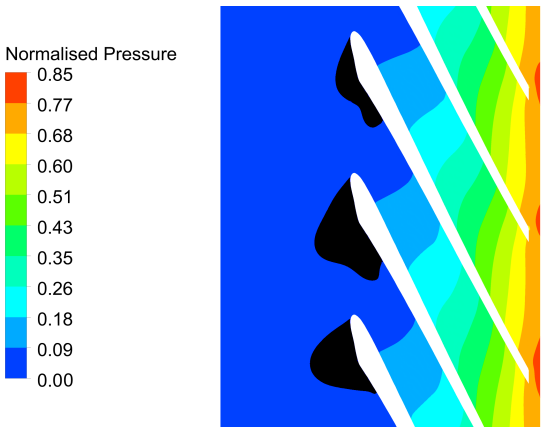

Figure 9.4: Blade to blade plane view at 50% span of three blades. A normalised pressure contour is shown with the regions below the vapour pressure of liquid Methane in black. Note there is no cavitation model implemented in this simulation.

9.4 Improving Cavitation Performance of the LUMEN Pump

Despite the difficulties in modelling cavitation described above and the unclear estimation of the exact impact of cavitation on the proposed pump design, cavitation is still expected to occur. The ability of the proposed LUMEN test bench to increase the pump inlet pressure to >10 Bar provides a large margin of error should the predicted cavitation performance be accurate. However, this will not be verified with a testing campaign in the near future so potential changes to the baseline design to achieve an improved cavitation performance are proposed.

Firstly the blade geometry itself can be altered according the research by Pearsall [90] which stipulates a cavitation optimised impeller design based on

a revised inlet diameter. This inlet diameter is calculated according to Equation 9.19 in place of the one proposed by Gülich (Equation 3.1). In this equation σ_b refers to the cavitation number calculated with Equation 9.1 at the nominal inlet conditions ($p_{1x} = 3Bar$), λ_d is the hub to tip diameter ratio, $\dot{Q}$ is the nominal volumetric flow rate and n is the rotation rate in RPM.

$$d_{1_{cav}} = 1.72\Big((2\frac{(1+\sigma_b)}{\sigma_b}^{0.5}\frac{\dot{Q}}{2\pi n/60}\frac{1}{((1-\lambda_d^2)}\Big)^{\frac{1}{3}} \tag{9.19}$$

Revising this equation and leaving the rest of the preliminary pump design tool unchanged resulted in the blade profile displayed in Figure 9.5b which is comparable to the baseline case in Figure 9.5a. Each figure contains a 3D profile of the pressure and suction surface profiles at five equally spaced blade spans starting from the shroud in red and ending with the hub surface profile in black. The leading and trailing edges are not defined in detail with the preliminary tool and therefore are omitted from the figures. Each of these profiles is then projected onto the x-y plane to emphasise the change in curvature of the blades. The origin of the x-y plane corresponds to the axis of rotation of the impeller and all dimensions are scaled with the impeller outlet radius - ***r***.

Three results are evident: firstly that the blades are longer and have a higher curvature(most obvious in the x-y plane images), secondly - the blade entry angle is reduced to $16°$ from $28°$ in the baseline case and thirdly that the impeller inlet diameter increases. The reduced inlet angle should produce a much less aggressive acceleration of the flow at the leading edge and therefore the local drop in pressure that initiates cavitation will be reduced as well. The longer sweeping blades support this as well with a more gradual increase in pressure through the blade channel. Increasing the impeller inlet diameter gives more room for cavitation to start at the blade tip and grow towards the hub before it blocks the inlet and has a noticeable impact on the overall performance of the pump. The revised design resulted in an approximately 1.5 Bar drop in the predicted inlet pressure required to suppress cavitation to below 3% of the nominal head rise and no change in the calculated overall pump efficiency.

Although not accounted for in the preliminary design tool the interaction between leakage flow re-entry at the inlet and the blade leading edge is evident from the full pump simulation results displayed in Section 8.3.1. This is particularly important for cavitation performance as the shroud leakage is re-injected at the blade tip, increasing the local mass flow and swirl velocity. This can effectively reduce the differential velocity generated over the blade leading edge and therefore the local drop in pressure that leads to cavitation [27] and is not accounted for in any of the empirical models.

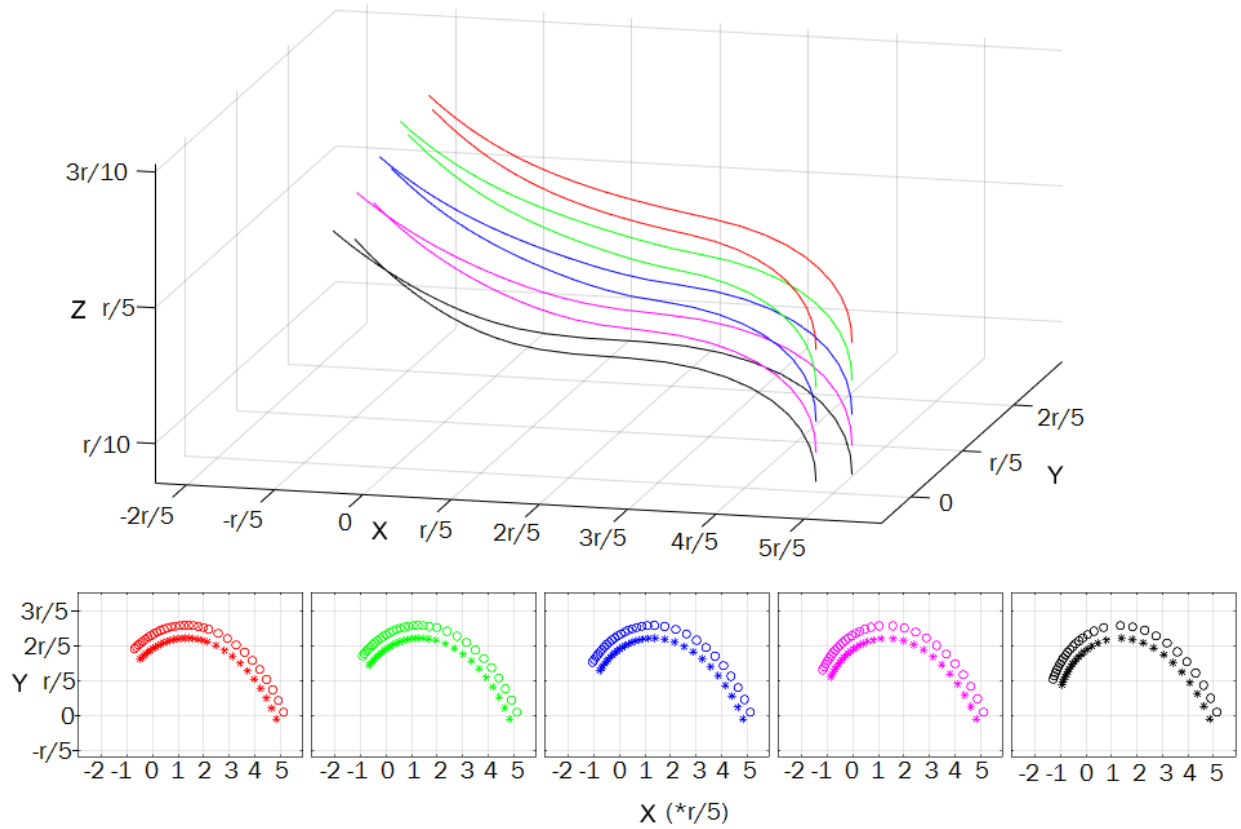

(a) Baseline blade design as calculated by the preliminary design tool. Five slices of the blade are shown together in 3D as well as being individually projected onto the x-y plane. Blade leading edges are on the left however the leading edge profile is omitted as the design in not calculated with the preliminary design tool.

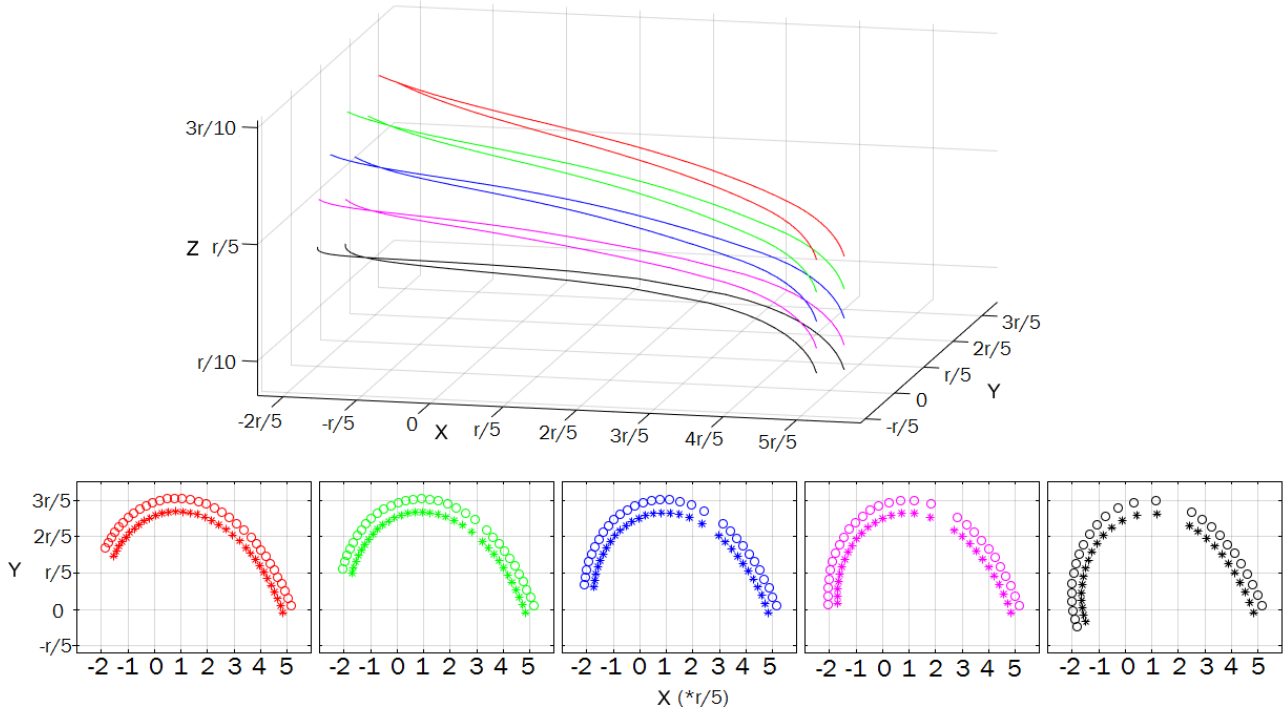

(b) Cavitation optimised blade design using the updated impeller inlet diameter equation. All other parameters are the same as in the baseline case above.

Figure 9.5: A combination plot of the three dimensional impeller blade and two dimensional sections viewed from the inlet. Five blade sections are shown from the shroud (red) to the hub (black). The difference is most obvious in the hub profile and the 3D image indicates a more gradual turn from the leading to trailing edges in the cavitation optimised design. The scales are fraction of the impeller outlet radius ***r***.

9.5 Discussion and Recommendations

Cavitation modelling of highly complex flows and cryogenic Methane was generally unsuccessful. The unconventional fluid properties of liquid Methane such as the low density ratio and strong dependence on thermal effects make many of the well defined and validated cavitation models available in the literature inapplicable for this case. Implementation of the few cryogenic specific cavitation models was hindered by the lack of data for liquid Methane required to specify the user inputs such as nucleation rate and vaporisation and condensation factors. The numerical models invariably broke down or produced unrealistic results which has been attributed to inaccurate modelling of the changing fluid properties given that the same mesh and simulation parameters produced reasonable results when water was implemented instead of Methane.

With these results in mind a number of recommendations for future work on the characterisation of cavitation within the LUMEN Methane pump have been made:

1. Conduct an experimental test of an impeller prototype to provide up to date and relevant comparison data, and to determine if further cavitation modelling is necessary.

2. Implement customised source and sink terms on a simplified mesh to more accurately model the phase transition in cryogenic fluids. Utturkar [32] and Tseng et al. [89] provide guidance on these equations.

3. If successfully implemented on a simplified mesh, revise the full pump numerical mesh to ensure uniform and structured interfaces with high resolution in the areas of expected cavitation.

4. If these fail to provide acceptable results, alternative two-phase modelling software may be required.

5. Evaluate the need to revise the impeller blade design and/or increase the supply tank pressure beyond the critical level for cavitation.

Despite these challenges a number of empirical tools for determining the pump inlet pressure required to avoid the negative implications of cavitation have also been compared. The results vary greatly and reflect the focused nature of the equations used. Despite this it was calculated that the default pump inlet pressure of 3 Bar is likely to result in cavitation within the pump at a level that will reduce the developed head by more than 3% of the non-cavitating case. This finding was supported with a very basic analysis of the low pressure regions as predicted by the full pump simulations without a cavitation model implemented. Given the lack of an inducer and relatively high rotation rate of the proposed design this result was expected and some potential changes to the impeller inlet and blade design have been developed to improve performance.

It must also be noted that the cavitation performance of the LUMEN fuel pump impeller has been discussed here without any consideration of the impact that cavitation has on rotordynamic stability. These phenomena are intrinsically linked and there is extensive literature available regarding the modelling and characterisation of the rotordynamic stability of a centrifugal pump impeller and how

cavitation influences this (the book by d'Agostino et al. is one example[39]). Of particular concern is the expectation of strong cavitation at the outlet of both hub and shroud seals which although may be beneficial for reducing leakage flow will have a negative impact on rotordynamic stability. For this reason a detailed investigation of rotordynamics within the LUMEN pump is planned at the DLR Lampoldshausen and therefore was not investigated further here.

10

Conclusion

At the outset of this thesis a number of research objectives were formulated to frame and guide the process of development and optimisation of the LUMEN fuel pump impeller. The completed work has provided sufficient evidence to support the achievement of those objectives and these are presented below along with a summary of the work completed. In addition to this a number of recommendations for improving the current design of the LUMEN fuel pump impeller are given along with recommendations for further work that will benefit, support or validate the findings presented here.

1. **Incorporate advanced loss models into a preliminary centrifugal pump design tool and optimise it for liquid rocket engine applications by analysis of the existing literature.**
   The preliminary design tool developed and used by the LUMEN team and based on the design model of Gülich was updated to account for seal geometry in a meaningful way. Inlet and outlet loss coefficients were changed from user inputs to calculated values based on other pump applications. The potential to expand this to labyrinth seals was also implemented although was not validated or tested in this thesis.

2. **Verify the accuracy of this preliminary design tool by comparison to a commercially available software package and/or relevant available experimental test data.**

   The revised preliminary design tool was validated against an experimental test campaign conducted for the development of the SSME-HPFTP annular seals and was shown to be accurate to within $\pm 15\%$ of all test data and to within $\pm 5\%$ of the most relevant test data for the LUMEN case when the predicted seal mass flow rates were compared. This is within the proposed thesis target range and was considered adequate for the intended rapid design iteration of the preliminary design tool however it was identified that some features of the flow could never be captured with empirical equations. Two numerical models were then created - a reduced segment to compare alternative seal designs and support the findings of the empirical equation validation and a full pump model to further investigate advanced

pump phenomena. Both of these models broadly supported the estimation of leakage massflow produced by the empirical equations, calculating total leakage flowrates of 15.8 and 13.8% of the nominal pump outlet flow compared to the 14.5% of the empirical equations. This places the numerical models within the target ±10% difference from the validated empirical model and provides support for the continued use of empirical equation models for centrifugal pump design in rocketry applications.

3. **Utilise the various models to analyse losses and recommend potential improvements to the existing pump design.**
   Leakage losses were the main target for reduction and several alternative designed were implemented into the reduced numerical model and compared for leakage performance. A multi step Z seal produced the best results although an investigation of the limitations of the proposed manufacturing process on surface roughness and corner radius revealed greater potential for reducing leakage. These models also suggested that cavitation is likely to occur at the exit of all seals, regardless of geometry.

   The full pump numerical model, created to reveal the asymmetry of a full pump operation provided further insights. A non-uniform loading of the clearance gaps, inlet recirculation and asymmetric leakage at the pump inlet were revealed despite the full pump model predicting relatively uniform pressure and velocity profiles through the whole pump. This model was also used to determine the performance of an alternative clearance gap and seal design which provided a further 1.2% reduction in the total massflow lost to leakage although the overall pump efficiency was predicted to decrease.

4. **Investigate the potential for prediction of cavitation performance within both the preliminary and numerical models.**
   Cavitation modelling proved to be a significant challenge and the models implemented here were generally unsuccessful. The prediction of local low pressure regions in all numerical models suggested that cavitation would be likely to occur in the LUMEN pump at all operating conditions. However the implementation of a dedicated cavitation modelling algorithm failed to produce realistic results. The complex nature of numerically modelling cavitation in a cryogenic fluid close to its boiling point as well as the limited literature relating directly to liquid Methane added to the challenge. Some simplified empirical models were implemented into the preliminary design tool and compared. These displayed great variation in their prediction of cavitation however all models suggest that cavitation is likely to degrade pump performance at the critical operating point if the current geometry and inlet conditions are unchanged.

The achievement of these objectives provides a basis for future work and innovation in the field of high speed, small scale centrifugal pumps in rocketry applications. The characterisation of leakage losses with a targeted empirical and detailed numerical models as well as the investigation of cavitation of cryogenic Methane within the same pump are both relatively novel findings in the growing field of micro-launcher scale liquid rocket engines.

10.1 Recommendations for Further Work

Due to the necessity of a limited timeframe and thesis scope as well as the nature of any research project a number of potential avenues of investigation were omitted or left incomplete in this thesis. Many of these warrant further work and are list below as recommendations for future work.

- Conduct an experimental test campaign of the proposed design to provide relevant validation data for the various numerical models in use.
- Complete a transient numerical simulation using the revised design, updated operating points and an updated mesh to capture additional flow features.
- Complete a detailed rotordynamic stability analysis on the proposed design using the full pump numerical results produced here. This will inform the potential need for further changes in the clearance gaps to counteract instabilities.
- Generate a sophisticated Methane cavitation model to determine the requirement for increased pump inlet pressure and changes to the blade design.
- Determine a complete potential operational load envelope to ensure the risk of recirculation is properly quantified.

10.2 Recommendations for Design Changes

Although the investigation detailed in this thesis represents a limited number of essential considerations for the design of a complex liquid rocket engine, the results here can provide some guidance for potential improvements of the LUMEN Methane pump impeller. It must also be noted that the inter-related nature of a rocket engine will require an assessment of the impact that these changes might have on the rest of the engine. The suggested changes are:

- Seek a method to reduce the limitation on rounded seal corner radius.
- Increase the surface roughness of the sealing faces above the hydraulically smooth limit of 0.2 μm, or alternatively implement a more complex hole-pattern or honeycomb face within the seals.
- Implement a labyrinth or multi z-step seal design for both shroud and hub annular seals, as well as pre-seal clearance gap geometry changes if the final assembly of the impeller allows for it.
- If deemed necessary, implement the proposed swirl brake design to reduce circumferential velocity within the seal.
- If deemed necessary, implement the revised blade design for improved cavitation performance.

The results presented in this thesis along with the proposed design changes and recommendations for future work take the LUMEN fuel turbopump impeller a

small step closer to successful fulfilment of its operational targets. As a demonstrator engine, the LUMEN project is also an indicator of the potential near-future of the liquid rocket powered micro-launcher industry. The findings and recommendations for future work that are noted here provide a clear pathway for other centrifugal pump designers seeking to optimise clearance gap leakage or assess the potential for cryogenic cavitation within a liquid rocket engine.

Bibliography

[1] J. Gülich. *Centrifugal Pumps - Second Edition*. Springer, 2010.

[2] J. Vernersen and N. Pedersen. Ansys CFX - Pumped: Simulation driven development increases pump efficiency - Grundfos. Ansys Advantage Magazine, 2015.

[3] S. Shah. CFD for centrifugal pumps: a review of the state-of-the-art. *Proceedings of the 3rd Nirma University International Conference*, 2012.

[4] X Gong and R Chen. Total pressure loss mechanism of centrifugal compressors. *Mechanical Engineering Research*, 2014.

[5] D. Childs. Ssme seal test program:test results for smooth, holepattern, and helically-grooved stators. *INTERIM PROGRESS REPORT NASA CONTRACT NAS8-35824*, 1988.

[6] H. Stocker. Advanced labyrinth seal design performance for high pressure ratio gas turbines. *Proceedings of the Winter Annual Meeting, American Society of Mechanical Engineers*, 1976.

[7] A Engeda. Early historical development of the centrifugal impeller. PPresented at the International Gas Turbine & Aeroengine Congress and Exhibition, 1998.

[8] Various. Facts about pumps and sustainability. Grundfos,`https://www.grundfos.com/water-energy/meet-the-water-and-energy-challenge-now/facts-about-pumps-and-sustainability.html`, 2018.

[9] Various NASA Lewis Research Center, Ohio. NASA SP-8107: Turbopump Systems for Liquid Rocket Engines. Monograph - Design Criteria Office - Chemical Propulsion, 1974.

[10] S. Dixon. *Fluid Mechanics, Thermodynamics of Turbomachinery - Fourth Edition*. Butterworth-Heinemann, 1998.

[11] G. Sutton and O Biblarz. *Rocket Propulsion Elements*. John Wiley and Sons, Hoboken, New Jersey, USA, 2010.

[12] E. Storteig. ynamic characteristics and leakage performance of liquid annular seals in centrifugal pumps. PhD Thesis - Department of Marine Engineering, Norwegian University of Science and Technology, 1999.

[13] W. Campbell and J. Farquhar. Centrifugal pumps for rocket engines. 1995.

[14] A. Stepanoff. *Centrifugal and Axial Flow Pumps - Theory, Design and Application*. John Wiley and Sons, Inc., 1957.

[15] J. D. Denton. Loss mechanisms in turbomachines. ASME 1993 International Gas Turbine and Aeroengine Congress and Exposition, 1993.

[16] R Bowerman and A Acosta. Effect of the volute on performance of a centrifugal pump impeller. *ASME transactions*, pages 1057–1069, 1957.

[17] J. Gülich. Disk friction losses of closed turbomachine impellers. *Forschung im Ingenieurwesen*, pages 87–95, 2003.

[18] K. Juckelandt, S. Bleek, and F. Wurm. Analysis of losses in centrifugal pumps with low specific speed with smooth and rough walls. *Proceedings of 11th European Conference on Turbomachinery Fluid dynamics & Thermodynamics*, pages 1–10, 2015.

[19] J. Kurokawa and T. Toyokura. Axial thrust, disc friction torque and leakage loss of radial flow turbomachinery. *Proceedings of the Pumps and Turbines Conference*, pages 1–14, 1979.

[20] C. Lei, Z. Yiyang, W. Zhengwei, X. Yexiang, and L. Ruixiang. Effect of axial clearance on the efficiency of a shrouded centrifugal pump. *Journal of Fluids Engineering*, 137, 2015.

[21] R. Uy, B. Bircumshaw, and Brennen C. Rotordynamic forces from discharge-to-suction leakage flows in centrifugal pumps : Effects of geometry. *JSME International Journal*, 41:208–213, 1998.

[22] T. Ha, Y Lee, and Kim C. Leakage and rotordynamic analysis of a high pressure floating ring seal in the turbo pump unit of a liquid rocket engine. *Tribology International*, 35:153–161, 2002.

[23] K. Soldatova. Cfd study of leakage flows in shroud cavities of a compressor impeller. *Conf. Series: Materials Science and Engineering*, 232, 2017.

[24] D. Childs. Ssme seal test program: Leakage tests for helically-grooved seals. *PROGRESS REPORT NASA CONTRACT NAS8-33716*, 1983.

[25] A. Rapisarda, A. Desanto, E. Campagnoli, and R. Taurino. Rounded fin edge and step position effects on discharge coefficient in rotating labyrinth seals. *Journal of Turbomachinery*, 138, 2016.

[26] J. Tuzon. Inlet recirculation in centrifugal pumps. *Proceedings: PERFORMANCE CHARACTERISTICS OF HYDRAULIC TURBINES & PUMPS, ASME WINTER ANNUAL MEETING*, 1983.

[27] C. Brennen. *Hydrodynamics of Pumps*. Concepts NREC and Oxford University Press, 1994.

[28] B. Ovsyannikov and B. Borovsky. *Theory and calculation of aggregate supply of liquid rocket engines (in Russian)*. Ministry of higher education, USSR, 1986.

[29] V. Chebaevsky and V. Petrov. *Cavitational characteristics of high-speed inducer-centrifugal pumps*. Mashinostroenie Publications, Moscow, 1979.

[30] Y. Viisanen, R Strey, and H. Reiss. Homogeneous nucleation rates for water. *Journal of Chemical Physics*, 99, 1993.

[31] L Sarosdy and A Acosta. Note on observations of cavitation in different fluids. *Proceedings of the Winter Annual Meeting, American Society of Mechanical Engineers*, 1960.

[32] Y. Utturkar. Computational modeling of thermodynamic effects incryogenic cavitation. PhD Thesis - UNIVERSITY OF FLORIDA, 2005.

[33] P. Limbach, T Müller, M. Blume, and R. Skoda. Numerical and experimental investigation of the cavitating flow in a low specific speed centrifugal pump and assessment of the influence of surface roughness on head prediction. *International Symposium on Transport Phenomena and Dynamics of Rotating Machinery*, 2016.

[34] K. Mani, A. Cervone, and J. Hickey. Turbulence modelling and cavitation dynamics in cryogenic turbopumps. *Space Propulsion [SP2016 3124788]*, 2016.

[35] H. Liu and H. Pan. The influence of turbulence model selection and leakage considerations on cfd simulation results for a centrifugal pump. *Advanced Materials Research*, 594-597:1940–1944, 2012.

[36] J. Hord, L. Anderson, and W. Hall. Cavitation in liquid cryogens. National Bureau of Standards, NASA Contractor Report CR-2054, 1972.

[37] I. Senocak and W. Shyy. Interfacial dynamics-based modelling of turbulent cavitating flows, part-1: Model development and steady-state computations. *INTERNATIONAL JOURNAL FOR NUMERICAL METHODS IN FLUIDS*, 2004.

[38] L. San Andres. Introduction to pump rotordynamics. Educational Notes: Design and Analysis of High Speed Pumps, 2006.

[39] Pasini A. d'Agostino, L. and D. Valentini. A reduced order model for preliminary design and performance prediction of radial turbopumps. *Proceedings of the 47th AIAA/ASME/SAE/ASEE Joint Propulsion Conference & Exhibit*, 2011.

[40] L. San Andres, Z. Yang, and D. Childs. Thermal effects in cryogenic liquid annular seals - part 2: Numerical solution and results. *Journal of Tribiology*, 115:277–284, 1993.

[41] Y. Tsujimoto. Cavitation instabilities in hydraulic machines. *Procedings of the 6th International Conference on Pumps and Fans with Compressors and Wind Turbines*, 2013.

[42] K. Brun and R. Kurz. Analysis of secondary flows in centrifugal impellers. *International Journal of Rotating Machinery*, 1:45–52, 2003.

[43] M. Atsumi, K. Yoshikawa, A. Ogawara, and T. Onga. Development of the le-x engine. *Mitsubishi Heavy Industries Technical Review*, 48-4, 2011.

[44] B. Greene. Inside the leo doghouse: The art of expander cycle engines. online, https://blogs.nasa.gov/J2X/2014/03/24/inside-the-leo-doghouse-the-art-of-expander-cycle-engines/, 2014.

[45] D. Waxenegger, R. Dos Santos-Hahn, and B. Wagner. Lumen preliminary design review tp - dlr-la-lm-tp-pdr-001. DLR - Internal Document, 2017.

[46] F. Lindemann. Evaluation and analysis of the lng centrifugal pump design for the liquid rocket engine demonstrator developed by the dlr - lumen project using ansys cfx. MSc Thesis - University of Stuttgart, 2018.

[47] L. Euler. Maximes pour arranger le plus avantageusement les machines destinées à élever de l'eau par moyen des pompes. *Memoires de l'academie des sciences de Berlin*, (8):185–232, 1754.

[48] J. Veres and T. Lavelle. Mean line pump flow model in rocket engine system simulation. NASA Technical Memorandum - 2000-210S74, Glenn Research Center, 2000.

[49] E. Cliquet, A. Iannetti, and J. Masse. Carmen, liquid propulsion systems simulation platform. *Progress in Propulsion Physics*, pages 695–706, 2011.

[50] A. Leto. Preliminary design method of a turbopump feed system for liquid rocket engine expander cycle. *71st Conference of the Italian Thermal Machines Engineering Association*, 2016.

[51] C. Xu. Design experience and considerations for centrifugal compressor development. *Proceedings of the Institution of Mechanical Engineers, Part G: Journal of Aerospace Engineering*, 221, 2007.

[52] S. Menon and P Menon. *Working Guide to Pumps and Pumping Stations*. Elsevier Inc., 2010.

[53] L. San Andres and J. Yang. The influence of inlet corner shape on the static and dynamic performance of an annular pressure seal. *Procedings of the Global Power and Propulsion Society Forum*, 2018.

[54] S. Berten, F. Tomasini, W. Maurer, and P. Dupont. Shut-off head prediction in single stage centrifugal pumps. *ASME/JSME/KSME 2015 Joint Fluids Engineering Conference*, 1, 2015.

[55] S. Kaewnai, M. Chamaoot, and S. Wongwises. Predicting performance of radial flow type impeller of centrifugal pump using cfd. *Journal of Mechanical Science and Technology*, 23-6, 2009.

[56] F. Menter. Two-equation eddy-viscosity turbulence models for engineering applications. *AIAA Journal*, 32-8, 1994.

[57] K. Mani. Turbulence modelling of cavitating flows in cryogenic turbopumps. MSc Thesis - Delft University of Technology, 2015.

[58] American Institute for Aeronautics and Astronautics. Guide for the verification and validation of computational fluid dynamics simulations (aiaa g-077-1998(2002)). AIAA, https://arc.aiaa.org/doi/book/10.2514/4.472855, 2002.

[59] E. Baskharone and S. Hensel. A finite-element perturbation approach to fluid/rotor interaction in turbomachinery elements. part 2: Application. *Journal of Fluids Engineering*, 113:362–367, 1991.

[60] Y. Wu, X. Chen, H. Dou, L. Zheng, Z. Zhu, B. Cui, and B. Khoo. Numerical simulation and analysis of flow characteristics in the front chamber of a centrifugal pump. *Journal of Mechanical Science and Technology*, pages 5131–5140, 2017.

[61] Various. Ansys CFX Online Documentation and Support. https://www.sharcnet.ca/Software/Ansys/16.2.3/en-us/help/cfx_mod/i5500692.html, 2016.

[62] P. Roache. Quantification of uncertainty in computational fluid dynamic. *Annual Review of Fluid Mechanics*, 29:123–160, 1997.

[63] T. Phillips and C. Roy. Richardson extrapolation-based discretization uncertainty estimation for computational fluid dynamics. *Journal of Fluids Engineering*, pages 1–17, 2014.

[64] T. Xing and F. Stern. Factors of safety for richardson extrapolation. *Journal of Fluids Engineering*, 132:1–13, 2010.

[65] E. Baskharone and S. Hensel. A new model for leakage prediction in shrouded-impeller turbopumps. *Journal of Fluids Engineering*, 111:118–123, 1989.

[66] G. Chaudhary. Labyrinth seal leakage analysis. MSc Thesis - Texas A&M University, 2011.

[67] J. Moore, S. Walker, and M. Kuzdzal. Rotordynamic stability measurement during full-load pressure testing of a 6000 psi reinjection centrifugal compressor. *Proceedings of the thirty-first turbomachinery symposium*, 2002.

[68] H. Benckert and J. Wachter. Flow induced spring coefficients of labyrinth seals for application in rotor dynamics. *NASA Technical Reports Server*, 1980.

[69] N/A. V-2 rocket engine turbopump cutaway. Online - `https://airandspace.si.edu/collection-objects/turbopump-v-2-cutaway`, 2019.

[70] J. Sivo, A. Acosta, C. Brennen, and T. Caughey. The influence of swirl brakes on the rotordynamic forces generated by bischarge-to-suction leakage flows in centrifugal pumps. *Transactions of the ASME*, 117:104–108, 1995.

[71] L. Baldassarre, M. Fontanna, A. Bernocchi, A. Guglielmo, and G. Masi. Optimization of swirl brake design and assessment of its stabilizing effect on compressor rotordynamic performance. *43rd Turbomachinery & 30th Pump Users Symposia*, 2014.

[72] R. Nardone. The effect of impeller back pump-out vanes on seal performance. *Sealing Technology*, 2006.

[73] B. Kye, K. Park, H. Choi, M. Lee, and J. Kim. Flow characteristics in a volute-type centrifugal pump using large eddy simulation. *International Journal of Heat and Fluid Flow*, 72:52–60, 2018.

[74] L. Veggi, J. Pauw, B. Wagner, and O. Haidn. Numerical investigation of the influence of leakage flow on the performance of the impeller for a lox turbopump. *Proceedings of the Space Propulsion Conference, Sevilla, Spain*, 2018.

[75] R. Miskovish and C. Brennen. Some unsteady fluid forces on pump impellers. *Journal of Fluids Engineering*, 1991.

[76] Engineering Toolbox. Engineering toolbox (2001).

[77] National Institute of Standards and Technology NIST. REFPROP - Reference Fluid Thermodynamic and Transport Properties Database. Online: `https://www.nist.gov/srd/refprop`, Online, Accessed October 2018.

[78] E. Goncalves. Numerical simulation of cavitating flows with different cavitation and turbulence models. Cavitation Instabilities and Rotordynamic Effects in Turbopumps and Hydroturbines - McGraw Hill, 2017.

[79] S. Shi and G. Wang. Thermal effects on cryogenic cavitating flows around an axisymmetric ogive. *International Journal of Fluid Machinery and Systems*, 3-4, 2010.

[80] H. Kim, Hy. Kim, Min D., and C. Kim. Numerical simulations of cryogenic cavitating flows. *Journal of Physics: 9th International Symposium on Cavitation*, 2015.

[81] L. Stripling and A. Acosta. Cavitation in turbo pumps-part 1. *Journal of Physics: 9th International Symposium on Cavitation*, 2015.

[82] L. Rayleigh. On the pressure developed in a liquid during the collapse of a spherical cavity. *The London, Edinburgh, and Dublin Philosophical Magazine and Journal of Science*, 1917.

[83] M. Plesset and A. Prosperetti. Bubble dynamics and cavitation. *Annual Review of Fluid Mechanics*, 1977.

[84] J. Franc. The rayleigh-plesset equation: a simple and powerful tool to understand various aspects of cavitation. Fluid Dynamics of Cavitation and Cavitating Turbopumps - Springer, 2007.

[85] Various. Cavititaion Model - Ansys CFX - User Guide. Online -`https://www.sharcnet.ca/Software/Ansys/17.0/en-us/help/cfx_thry/cfxMultInteCavi.html#i1307195`, 2019.

[86] H. Liu, J. Wang, Y. Wang, H. Zhang, and H. Huang. Influence of the empirical coefficients of cavitation model on predicting cavitating flow in the centrifugal pump. *International Journal of Naval Architechure and Ocean Engineering*, 6:119–131, 2014.

[87] D. Liuzzi. *Two-Phase Cavitation Modelling - Fully Compressible Formulation*. PhD thesis, 2012.

[88] K. Mani, A. Cervone, and J. Hickey. Turbulence modelling and cavitation dynamics in cryogenic turbopumps. *Space Propulsion*, 2016.

[89] C. Tseng and W. Shyy. Modeling for isothermal and cryogenic cavitation. *International Journal of Heat and Mass Transfer*, 53:513–525, 2009.

[90] I. Pearsall. Design of pump impellers for optimum cavitation performance. *Proceedings of the Institute of Meachanical Engineers*, 187:667–678, 1973.

Appendix A - Reproduction of NASA Turbopump Data Tables

These data tables are reproduced from *Centrifugal Pumps for Rocket Engines* by W. Campbell and J. Farquhar [13].

Table I. – Chief Features of Operational Turbopump Assemblies[1]

Engine				Turbopump Assembly				
Designation	Application	Thrust, lbf	Chamber pressure, psia	Arrangement	Efficiency, percent	Weight, lbm	Specific horsepower, hp/lbm	Start system
A-7	Redstone	78 000	318	Single shaft, turbine in middle	26.4	332	2.22	Liquid monopropellant start tank
MB-3	Thor	170 000	594	Geared turbine	46.0	562	5.40	Solid propellant start cartridge
LR87-AJ-3	Titan I, 1st stage	150 000	585	Geared turbine and pumps	45.8	720	5.11	Liquid propellant start tanks
LR91-AJ-3	Titan I, 2nd stage	80 000	682	Geared O_2 pump	34.0	204	7.25	Liquid propellant start tanks
H-1	Saturn IB	205 000	702	Geared turbine	47.0	520	7.98	Solid propellant start cartridge
MA-5 sustainer	Atlas	57 000	706	Geared turbine	35.0	229	7.27	Solid propellant start cartridge
MA-5 booster	Atlas	330 000[2]	577	Geared turbine	48.0	875	3.59	Solid propellant start cartridge
F-1	Saturn IC	1 522 000	1122	Single shaft, turbine on end	44.6	3150	16.6	Tank head
YLR81-BA-11	Agena	16 000	506	Geared turbine and pumps	20.0	60.5	5.81	Solid propellant start cartridge
YLR87-AJ-7	Gemini-Titan 1st stage	215 000	784	Geared turbine and pumps	38.1	484	10.70	Solid propellant start cartridge
YLR91-AJ-7	Gemini-Titan 2nd stage	100 000	804	Geared N_2O_4 pump	–	256	8.30	Solid propellant start cartridge
RL10A-3-3	Centaur	15 000	400	Geared O_2 pump	42.0	76.1	9.03	Tank head
J-2	Saturn S-II and S-IVB	230 000	787	Dual turbopump, series turbines	37.4 44.9	305 369	7.73 21.60	Pressurized-gas start tank
SSME (EPL*)[3] high pressure	Space Shuttle	512 300	3237	Dual turbopump, parallel turbines	56.5 58.5	555 701	50.0 108.9	Tank head

[1]Based on the best available data as of mid-1973. Numbers presented are those for a turbopump operational system.
[2]Two engines, each developing 165 000 hp.
[3]Not operational, but presented for comparative purposes. *Emergency power level.

Table II. – Chief Features of Operational Turbopumps*

Engine designation	Propellant	Propellant density, lbm/ft³[1]	Pump type	Number of stages	Discharge pressure, psia	Rated inlet pressure, psia	Head rise, ft	Weight flowrate, lbm/sec	Volume flowrate, gpm	Rotational speed, rpm	$NPSH_{min}$, ft[2]	$NPSH_{crit}$, ft[3]	Efficiency, percent	Power, hp
A-7	Oxygen	71.4	Centrifugal	1	356	49.8	616	205	1 290	4 718	18	11	72.0	320
	Alcohol[4]	56.6			464	42.5	1 139	150	1 190	4 718	40	35	70.0	418
MB-3	Oxygen	71.4			867	53.0	1 651	456	2 870	6 303	55	–	79.0	1 830
	RJ-1	53.2			913	48.0	2 337	202	1 700	6 303	34	–	72.0	1 210
LR87-AJ-3	Oxygen	71.4			798	53.0	1 510	412.7	2 600	7 949	40	–	–	–
	RP-1	50.5			1034	22.0	2 881	183.3	1 630	8 780	30	–	–	–
LR91-AJ-3	Oxygen	71.4			819	35.0	1 613	175.6	1 100	8 945	31	–	–	–
	RP-1	50.5			1097	42.0	3 024	74.1	659	25 207	100	–	–	–
H-1	Oxygen	70.8			980	65.0	1 851	537	3 410	6 680	35	25	77.8	2 340
	RP-1	50.5			1020	57.0	2 719	240	2 130	6 680	35	28	71.8	1 670
MA-5 sustainer	Oxygen	71.4			982	53.0	1 879	193.2	1 200	10 160	30	14	64.2	1 018
	RP-1	50.5			996	77.0	2 616	91.6	745	10 160	85	60	64.5	620
MA-5 booster	Oxygen	71.4			877	50.0	1 679	458	2 862	6 314	40	–	74.3	1 800
	RP-1	50.5			839	73.0	2 184	211	1 867	6 314	33	–	73.6	1 151
F-1	Oxygen	71.4			1600	65.0	3 097	4070	25 200	5 488	65	60	74.6	30 200
	RP-1	50.5			1856	45.0	5 168	1715	15 250	5 488	70	55	72.6	22 100
YLR81-BA-11	IRFNA[5]	98.2			949	24.0	1 360	39.3	180	25 389	12	–	–	352
	UDMH[6]	49.4			749	24.0	2 110	15.3	139	14 410	34	–	–	352
YLR87-AJ-7	N_2O_4	90.3			1182	84.0	1 740	550	2 700	8 382	44	–	68.0	2 560
	A-50[7]	56.1			1363	33.5	3 381	274	2 180	9 209	43	–	68.0	2 480
YLR91-AJ-7	N_2O_4	90.3	Mixed Flow		1112	41.0	1 713	207	1 010	8 405	30	–	67.4	960
	A-50	56.1	Mixed Flow		1201	44.5	2 981	115	904	23 685	100	–	57.1	1 090
RL10A-3-3	Oxygen	68.8	Centrifugal		597	60.5	1 120	28.2	184	12 100	17	–	62.9	94
	Hydrogen	4.35	Centrifugal	2	990	30.0	31 800	5.6	581	30 250	132	–	55.0	592
J-2	Oxygen	70.8	Centrifugal	1	1114	39.0	2 185	460.4	2 920	8 753	25	18	80.0	2 358
	Hydrogen	4.4	Axial	7+ inducer stage	1238	30.0	38 000	83.6	8 530	27 130	130	75	73.0	7 977
SSME (EPL)** high pressure	Oxygen	70.4	Centrifugal	1/2[8]	5174/ 8491	379/ 4940	9640/ 7100	1137/ 120	7250/ 633	31 000	(9)	(9)	78.1/ 69.6	27 400
	Hydrogen	4.38	Centrifugal	3	6981	188	193 900	160.5	16 450	37 400	(9)	(9)	74.1	76 400

*Based on the best data as of mid-1973. Numbers presented are those for a turbopump operational system.

(1) At temperature specified by the application.

(2) Contractually specified pump NPSH, maximum acceptable.

(3) NPSH at a given drop in pump discharge pressure, generally 2 percent.

(4) 75 percent alcohol, 25 percent water.

(5) Inhibited red fuming nitric acid.

(6) Unsymmetrical dimethy hydrazine, $(CH_3)_2 NNH_2$.

(7) 50 percent hydrazine and 50 percent UDMH.

(8) 10 percent of the flow goes through a second stage; numbers below slash are for second stage alone.

(9) Boost pump upstream.

**Not operational, but presented for comparative purposes.

Appendix B - Additional results from the validation of the preliminary design tool

To support the conclusions regarding the spread in the validation of the preliminary design tool with the Childs experimental data [5], two additional figures are presented. Firstly the experimental loss coefficient is plotted against the experimental differential pressure and secondly the comparison of calculated friction factor using the Gülich equation as a function of differential pressure. The first figure suggests inherent variation in the experimentally determined loss coefficient at the low end of the differential pressure range which is supported by the second figure which shows how the calculation of friction factor (which does not take the loss coefficient into account) also shows the largest variation at the lowest differential pressures.

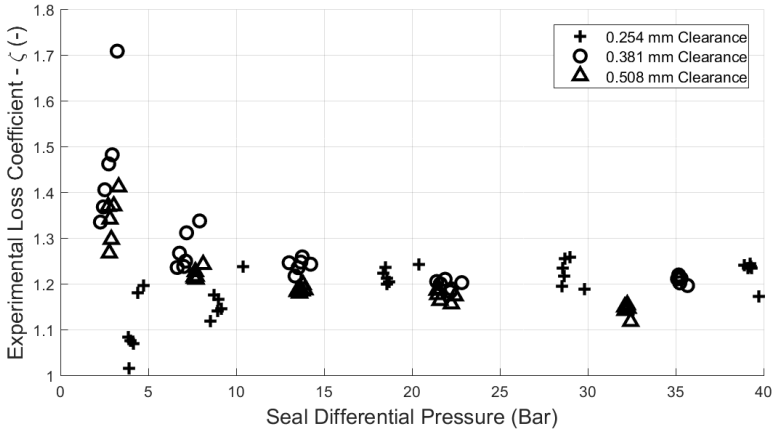

Figure B.1: A comparison of experimental loss coefficients and seal differential pressures - again note the greatest variation occurs at the lowest differential pressures. Also note here the notable difference in loss coefficient between the three clearance widths.

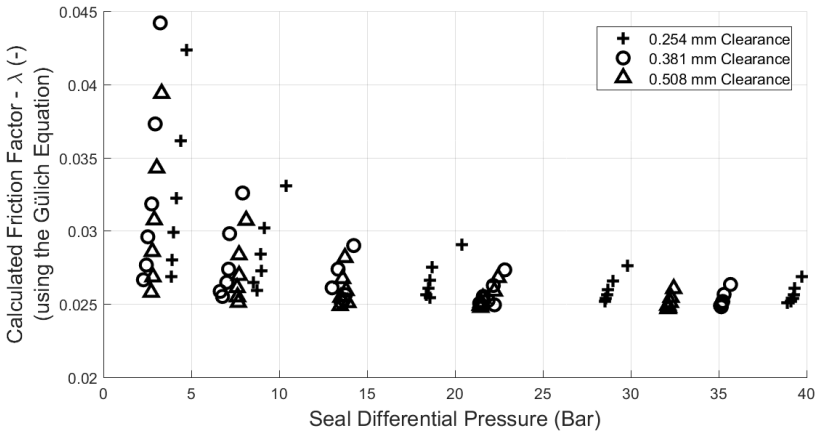

Figure B.2: The calculated friction coefficient is displayed as a function of experimental seal pressure differential - note the greatest variation occurs at low differential pressures.

The below equation is defined in the SSME experimental seal testing campaign produced by Dara Childs. It is utilised by Childs to back-calculate a value for the seal friction coefficient from the experimental results and is reproduced here to demonstrate the variation in possible methods - although this equation still relies heavily on empirical inputs.

$$\lambda = n_r {R_a}^{m_r}[1+((u_{\theta o-1})/b)^2]^{\frac{m_r+1}{2}} + n_s {R_a}^{m_s}[1+((u_{\theta o})/b)^2]^{\frac{m_s+1}{2}} \quad \text{(B.1)}$$

R_a	Axial Reynolds number
u_θ	Tangential velocity component
b	Ratio of axial to wall velocity
m_s	Experimental roughness coefficient 1 - stator
m_r	Experimental roughness coefficient 1 - rotor
n_s	Experimental roughness coefficient 2 - stator
n_r	Experimental roughness coefficient 2 - rotor

Table B.1

In this equation the friction factor λ is calculated using the inputs from Table B.1.

Appendix C - The single Z step seal model

The single z step seal was compared to various others in Chapter 6. The findings from the multi z step seal were considered adequate to describe this type of seal as the features of the pressure and velocity profiles are quite similar however the results are presented here for completeness.

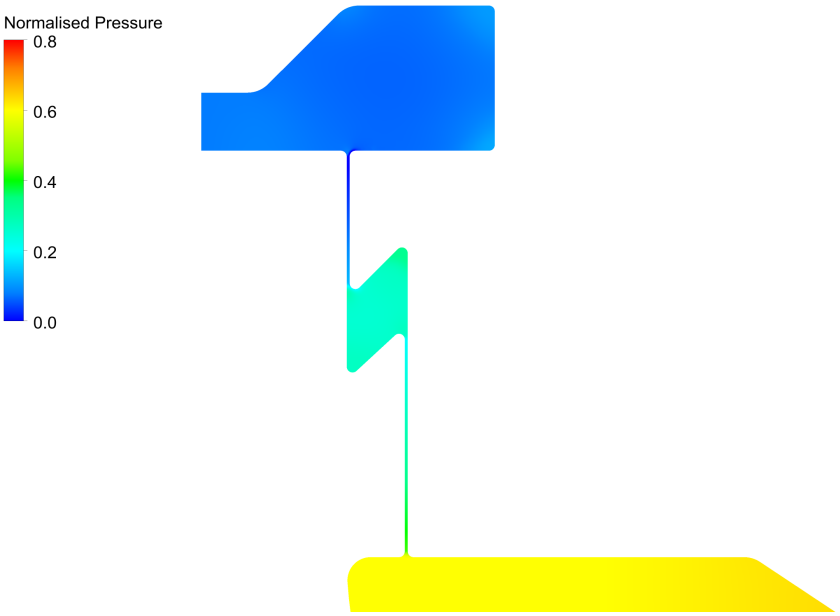

(a) Normalised pressure profile.

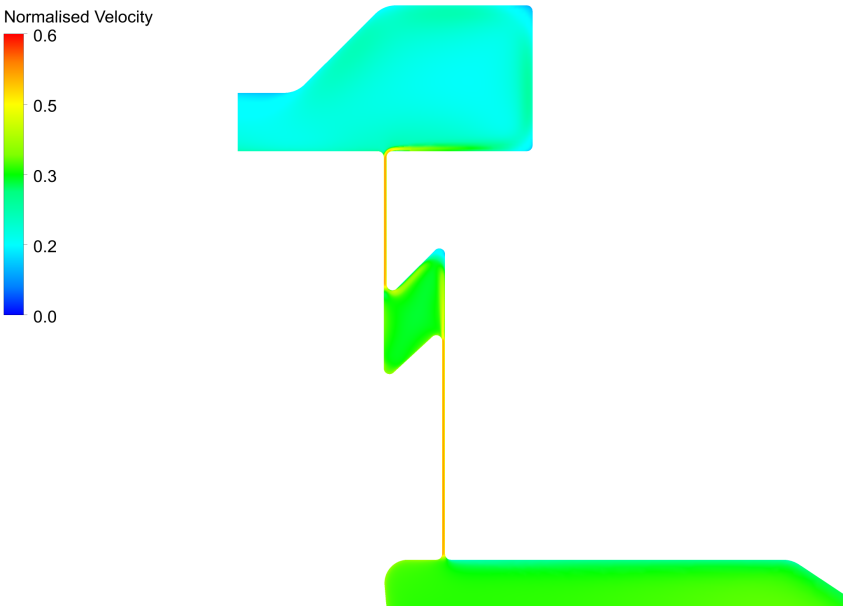

(b) Normalised velocity profile.

Figure C.1

Appendix D - The Ovsyannikov/Chebaevsky Model for Cavitation Prediction

The equations detailed by Ovsyannikov and Chebaevsky are reproduced here. These were used in Chapter 9 for the comparison of empirical cavitation models and use the following inputs.

Variable	Description	Units	Value or Recommended Range
i_{cp}	inlet angle of attack	°	4-11
b_0	Coefficient	-	0.115
$\bar{\delta}_{1cp}$	Coefficient	-	0.005 to 0.045
γ_c	Coefficient		4
$\bar{b}_{\pi.cp}$	Coefficient	-	> 2.3
τ_{cp}	Coefficient	-	3.5
z_w	Blade Number	-	7
p_v	Vapour Pressure	Pa	120000
ρ	Density	kg/m^3	425
w_{1cp}	Inlet velocity - Resultant	m/s	-
u_{cp}	Circ. velocity at Inlet (mid-span)	m/s	-
ω	Rotation Rate	RPM	52000
D_{hub}	Hub Diameter	m	-
D_{shroud}	Shroud Diameter	m	-
D_{seal}	Seal Diameter	m	-
$\dot{m}$	Mass Flowrate	kg/s	4
c_{1z}	Inlet velocity - Axial	m/s	-

Table D.1

The set of equations describe the method to determine a series of pump inlet pressures (p_{0-III}) required to avoid the corresponding level of pump inlet cavitation as noted in Figure 9.2.

$$\lambda_0 = a_o + b_0 c_{1z} \tag{D.1}$$

$$a_o = 0.043\left(\left(\frac{\gamma_{cp}}{i_{cp}}\right)^{0.25} - 1\right) + 0.21(\bar{\delta}_{1cp})^{0.5} + \frac{0.11}{(\bar{b}_{\pi.cp})^{1/6}} + 0.0027(Z_w - 2) - 0.095 \tag{D.2}$$

$$p_0 = p_v + \rho\lambda_0 w_{1cp}^2/2 \tag{D.3}$$

$$\lambda_I = (1.44 - 0.7m)\left(0.02 + \left(0.12 + \frac{sin(\beta_{w2}) - sin(\beta_{w1})}{\tau_{cp}}\right)\right) \tag{D.4}$$

$$m = \left(240\frac{\dot{Q}}{n}\right)/(\pi S(D_{seal}^2 - D_{hub}^2)) \tag{D.5}$$

$$S = tan(\beta_{w1})\pi(D_{seal} + D_{hub})/2 \tag{D.6}$$

$$p_I = p_v + \rho\lambda_I w_{1cp}^2/2 \tag{D.7}$$

$$\lambda_{II} = 0.024 + \frac{2.8}{k_{D_w}^3} \tag{D.8}$$

$$k_{D_w} = \frac{(D_{seal}^2 - D_{hub}^2)^{0.5}}{(\dot{Q}/n)^{0.33}} \tag{D.9}$$

$$p_{II} = p_v + \rho \lambda_{II} w_{1cp}^2/2 \tag{D.10}$$

$$\lambda_{III} = \frac{c_{1z}}{u_{cp}} sin(i_{cp} 2\pi/180) \tag{D.11}$$

$$p_{III} = p_v + \rho \lambda_{III} w_{1cp}^2/2 \tag{D.12}$$

Appendix E - Results from the Venturi Cavitation Simulations

As part of the failed attempt to develop a numerical cavitation model for Methane a simplified venturi nozzle simulation was created and a comparison between a water and Methane case is presented here. There is a small region of cavitation in the water case as the flow passes the nozzle throat as shown in Figure E.1. In comparison the Methane case Figure E.2 displays a full vapour stage past the nozzle throat as the model predicts a continued decrease in pressure past the nozzle throat and ultimately a very high exit velocity at the right hand edge of the model domain. This result is considered non-realistic given the literature that describes cryogenic cavitation suggests a relatively small region of cavitation should be expected. Note the model domain extends both left and right of the images shown however was removed to more clearly display the nozzle throat region.

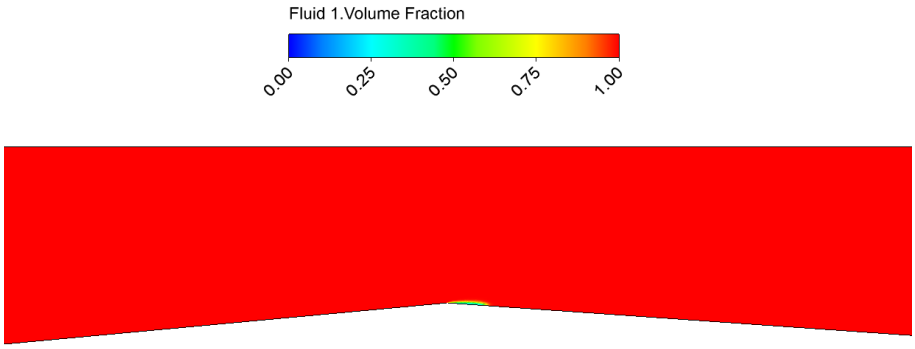

Figure E.1: Simplified Venturi nozzle cavitation model with water as the working fluid at 298 K. Note the small area of non-zero vapour phase volume fraction near the nozzle throat.

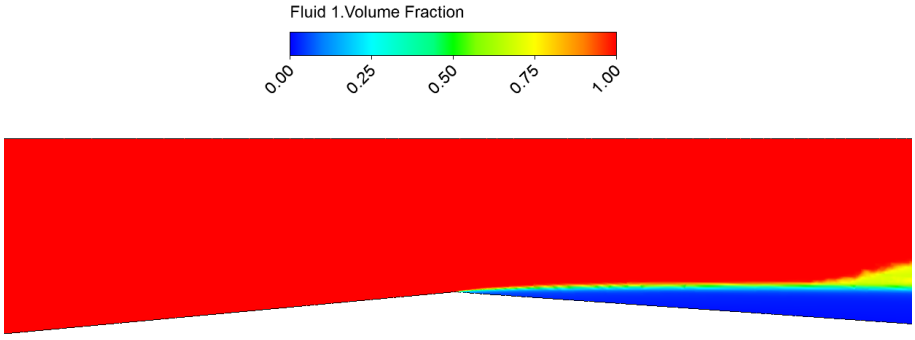

Figure E.2: Simplified Venturi nozzle cavitation model with Methane as the working fluid at 114 K. The simulation produced unrealistic results with the given boundary conditions and very few other simulations completed at all.